Object-Color Description Under Varying Illumination

by

Hamidreza Mirzaei Domabi

M.Sc., Simon Fraser University, 2011

B.Sc. (Hons.), Isfahan University of Technology, 2009

Thesis Submitted in Partial Fulfillment
of the Requirements for the Degree of

Doctor of Philosophy

in the
School of Computing Science
Faculty of Applied Sciences

SIMON FRASER UNIVERSITY
Summer 2016

APPROVAL

Name:	Hamidreza Mirzaei Domabi
Degree:	Doctor of Philosophy
Title:	Object-Color Description Under Varying Illumination

Examining Committee:

Chair: Dr. James Delgrande
Professor

Dr. Brian Funt
Senior Supervisor
Professor

Dr. Alexander Logvinenko
Supervisor
Professor

Dr. Richard Vaughn
Internal Examiner
Associate Professor

Nathan Moroney
External Examiner
Principal Scientist
HP Labs

Date Approved: August 9th, 2016

Abstract

Given a fixed and uniform illumination, metameric objects appear as the same color. However, when the illumination is altered, two metameric reflecting objects under the first illuminant may no longer produce the same color signal under the second. This situation is called metamer mismatching. Metamer mismatching poses several challenges for the camera and display industries as well as color-based computer vision technology. In light of metamer mismatching, the present study criticizes the conventional approaches to color description when the illuminant alters, and then lays a foundation to robustly describe object colors under varying illumination conditions. Later, the degree of metamer mismatching is used as a measure of the quality of lights. We demonstrate that although the common color spaces such as CIELAB and related spaces in the literature may work well for a fixed illuminant, they can lead to poor results when the illuminant is changed. In view of these problems, new descriptors for hue, lightness and chroma are presented that are based on properties of a Gaussian-like spectrum metameric to the given color tristimulus coordinates. Experiments show that the new Gaussian-based appearance descriptors correlate with different descriptors as well as the CIECAM02 appearance model does on average. Furthermore, the Gaussian-based descriptors are significantly more stable than the descriptors defined in the CIECAM02 appearance model. Afterwards, the problem of predicting how the color signal arising in response to light reflected from the surface of an object is likely to change when the lighting alters is investigated. A new method, called the Gaussian Metamer (GM) method is proposed for predicting what a color signal observed from a surface under a first light is likely to be when the same surface is lit instead by a second light. Due to metamer mismatching, there is not a unique answer for this problem. Our approach is to use one of the possible metamers that is likely to do well on average. The results outperform other state-of-the-art prediction methods.

Keywords: Object color; metamerism; metamer mismatching; color prediction; color appearance attributes; color rendering index; Gaussian

To my family for their constant support and care.

To my wife for her unconditional love and encouragement.

Acknowledgements

I would like to express my deepest gratitude to my senior supervisor Prof. Brian Funt, for his continuous support of my Ph.D study and research. He has been not only a perfect supervisor, but also a close friend of mine during these years. He has been always supportive and has given me the freedom to choose what project to pursue without any objection. I could not have asked for a better supervisor. I am also very grateful to Prof. Alexander Logvinenko for his knowledge and many insightful discussions and suggestions.

I would like to also thank the rest of my thesis committee: Prof. Richard Vaughan, and Nathan Moroney, for their ideas, encouragements, and insightful comments.

I hereby would like to acknowledge the financial support I received from Point Grey Research Inc. In particular, I owe thanks to Don Murray for his support and encouragement.

I thank my friends at SFU who are too many to be listed here. Especial thanks to Ehsan Asadi, Amin Hejazi, Hossein Khatoonabadi, Mohammadreza Mohammadnia, Mehdi Seyfi, and Moein Shaygannia, for the sleepless nights we were working together before deadlines, and for all the fun we have had in the last seven years.

Most importantly, none of this would have been possible without the support of my family. I especially thank my mom Nargess Ziaei and my dad Abbasali Mirzaei. My hard-working parents have sacrificed their lives for my sister, my brothers and myself, providing unconditional care and love for us all. My brothers Abdolreza and Ali, and my sister Fatima have supported me spiritually throughout my life, and have directed me towards this success. The best outcome from these past years is finding my soul-mate and wife, Emitis. I married the best person out there for me. My wife has been my best friend, and I love her dearly and I should thank her for unflagging love and support throughout these years. I would have not been here without her. I dedicate this thesis to them. Hopefully I have made them proud.

List of Figures

List of Tables

Contents

Chapter 1

Introduction

Colors provide computer vision systems with a lot of information to help automatic recognition. People discriminate the colors so easily they do not really think about it, but distinguishing colors in different illumination conditions is very difficult for a machine. This problem originates from the central theory in color science that the color devices differentiate colors based on trichromacy and therefore are very poor in discriminating illuminants of different spectral power distributions. Trichromacy assumes that we have only three types of cone photoreceptors. According to trichromacy, two lights may be indiscriminable when they produce an equal rate of photopigment absorption for each of the three cone types. These two equally perceived reflected lights are called metameric. The problem is that this equivalence in three channels does not generalize when scene lights are changed. Given a fixed illumination, the reflecting objects producing the same color signal (metameric reflecting objects) exhibit the same color. However, when the illumination is changed, two objects reflecting metameric light under the first illuminant may no longer produce the same color signal under the second. This situation is called metamer mismatching [5].

A change of the illumination spectrum of a scene leads to changes in the light reflected off the surfaces. If this is an extreme change it will lead to a great change in the color of each surface and cause serious problems for many applications whose main feature is the color information, such as color-based object recognition, scene understanding, image reproduction, digital photography, human-computer interaction, color feature extraction, and color appearance models [12–14]. For example, if the colors of the objects in a database are trained for illuminant A (a reddish tungsten lamp), then a color-based object recognition will likely have problems when the objects are seen under a blue illumination (e.g., blue sky).

For object recognition to work properly, the change of colors caused by illuminant changes must be within the tolerance of the system [15]. Thus the illumination must be controlled in a way i.e., determined and taken into account. The human visual system has the ability to get a relatively stable representation of colors despite changes of the illumination. This ability is called color constancy [16–19].

As an example, the focus of color balancing in Figure 1.1, where a single scene is rendered under four different illuminants, is to correct the images so that they all appear identical to the bottom-right image that is rendered under a white light source. It is generally desired to mitigate this effect on any captured image. One of the biggest challenges towards this goal is metamerism, which is studied in details in this thesis.

Metamerism is of both theoretical interest and practical importance. At a high level, research on metamer mismatching will lead to theoretical results of interest to the broad imaging and vision communities in terms of how much color constancy is possible. Although color constancy has been always taken for granted, some experiments have shown large deviations from perfect color constancy [14, 20, 21]. A critical reason for this imperfectness is metamer mismatching. Unfortunately, the seriousness of metamer mismatching is frequently neglected and most of the computational studies of color constancy implicitly assume perfect color constancy as their goal. However, metamer mismatching in its serious cases shows that the color of an object is not a stable and intrinsic feature to be used because it can disperse to many different colors under a second illuminant. An interesting research direction emerges here to check how different a color can become under different lighting and sensor sensitivity conditions. In light of metamer mismatching, Chapter 3 reports a set of experiments forming an essential foundation for a larger collaborative project with Logvinenko, Funt and Tokunaga [1] studying the consequences of metamer mismatching for color constancy. That project explores the fact that color is not an intrinsic and independent attribute of an object, but rather is an attribute of a combination of light and surface reflectance pair.

Metamer mismatch volumes are also important in the related field of lighting design. In particular, lights leading to the smallest amount of metamer mismatching are naturally expected to yield the best color rendering. All of these applications have been limited, until now, by the lack of a method for computing metamer mismatch volumes precisely. In Chapter 4 we discuss the possibility of evaluating the illuminants based on their potential metamer mismatching. Variants of metamer mismatching have been previously used as a

measure of the color rendering of lights. Most of the proposed methods are limited to the specific reflectance set they use. Whitehead et al. [22] extend this general idea by using a large number of randomly generated metameric spectra and then assessing the fraction of them that undergo a noticeable color signal change when the illuminant changes. In contrast, the method proposed here is based on measuring the size of the metamer mismatch volume, which is the volume of color signals (i.e., XYZs) induced under the second light by the set of all theoretically possible reflectances that make a metameric match under the first light.

Then we move on to object colors, where the main issue with color description is the illumination variation. We demonstrate that although the common color spaces such as CIELAB and related spaces in the literature may work well for a fixed illuminant, they can lead to unstable results when the illuminant is changed. We show that the source of this instability is that they account for the illumination via von Kries scaling, but von Kries scaling can be subject to very large errors. In addition, even the most recent color appearance models fail to resolve the instability of the appearance dimensions under different lighting conditions. In view of these problems, in Chapters 5 and 6, new descriptors for hue, lightness and chroma are presented that are based on properties of a Gaussian-like spectrum metameric to the given color tristimulus coordinates. These Gaussian functions have interesting features that include illuminant invariance and reasonable correlation with appearance attributes of color. The color of any given object can then be described in terms of this object-color space and its three main appearance dimensions. We investigate the new descriptors in terms of three fundamental issues. First, what is the gamut of colors these Gaussians can represent? Second, in comparison to CIECAM02 how well do these new descriptors correlate with the appearance attributes in different datasets. Third, in comparison to CIECAM02 how stable are the new correlates across different illuminants?

The development of a robust hue-chroma-value description of colors is followed by another line of research. In Chapter 7 the problem of predicting how the color signal (i.e., cone LMS, CIE XYZ or sRGB) arising in response to light reflected from the surface of an object changes when the lighting alters is investigated. It arises in computer vision applications such as color-based object identification and tracking, where it is important to be able to recognize the same object under different illuminants. It also arises in white balancing digital imagery, and when re-rendering printed material for viewing under a second illuminant (e.g., changing from D65 to D50). In particular, in Chapter 7 a new method, called the Gaussian Metamer (GM) method, is proposed for predicting what a color signal observed

from a surface under a first light will be when the same surface is lit instead by a second light. This method is then extended for a more limited case when we only know the color of the illuminants and not their spectral power distribution. The results outperform other state-of-the-art prediction methods.

In summary, this thesis begins by criticizing the established approaches of color description, and then laying a foundation to robustly represent the object colors under varying lights. A robust hue-chroma-value description of object colors is introduced, and novel approaches are taken to perform the prediction procedure of the colors when lighting alters.

Chapter 2 provides some fundamental background knowledge required for this research. Please note that the following published articles form the basic foundation and also most significant contributions of this thesis [1, 6, 8, 23–33]:

- Xiandou Zhang, Brian Funt, and Hamidreza Mirzaei. Metamer mismatching in practice versus theory. *JOSA A*, 33(3), A238-A247, 2016.
- Alexander Logvinenko, Brian Funt, Hamidreza Mirzaei, and Rumi Tokunaga. Rethinking colour constancy. *PLOS ONE*, 2015.
- Hamidreza Mirzaei and Brian Funt. Gaussian-based hue descriptors. *IEEE Transactions on Pattern Analysis & Machine Intelligence*, 2015.
- Hamidreza Mirzaei and Brian Funt. Robust chroma and lightness descriptors. In *Color and Imaging Conference*, 2015. Society for Imaging Science and Technology, 2015.
- Xiandou Zhang, Brian Funt, and Hamidreza Mirzaei. Metamer Mismatching and Its Consequences for Predicting How Colours Are Affected by the Illuminant. *ICCV*, Proceedings of the IEEE International Conference on Computer Vision Workshops, 2015.
- Hamidreza Mirzaei, and Brian Funt. Metamer Mismatching as a Measure of the Color Rendering of Lights. In *Proceedings of the Congress of the International Colour Association (AIC 2015)*, 2015.
- Hamidreza Mirzaei and Brian Funt. Object-color-signal prediction using wraparound gaussian metamers. *JOSA A*, 31(7):1680–1687, 2014.

- Hamidreza Mirzaei and Brian Funt. Gaussian illuminants and reflectances for colour signal prediction. In *Color and Imaging Conference*, volume 2014, pages 212–216. Society for Imaging Science and Technology, 2014.

- Brian Funt, Hamidreza Mirzaei, and Alexander Logvinenko. Metamer Mismatch Volumes of Flat Grey. In *Proceedings of Color and Imaging Conference (CIC 2014)*, 2014.

- Hamidreza Mirzaei and Brian Funt. Hue correlate stability using a gaussian versus rectangular object colour atlas. In *AIC 2013, 12th International Colour Congress, International Colour Association*, pages 1133–1136, 2013.

- Hamidreza Mirzaei and Brian Funt. A robust hue descriptor. In *Color and Imaging Conference*, volume 2013, pages 75–78. Society for Imaging Science and Technology, 2013.

- Alexander Logvinenko, Brian Funt, and Hamidreza Mirzaei. The extent of metamer mismatching. *Proc. 12th Congr. AIC*, pages 507–510, 2013.

- Hamidreza Mirzaei and Brian Funt. Gaussian-metamer-based prediction of colour signal change under illuminant change. *AIC 2011, Congress of the International Colour Association*, 2011.

- Brian Funt and Hamidreza Mirzaei. Intersecting color manifolds. In *Color and Imaging Conference*, volume 2011, pages 166–170. Society for Imaging Science and Technology, 2011.

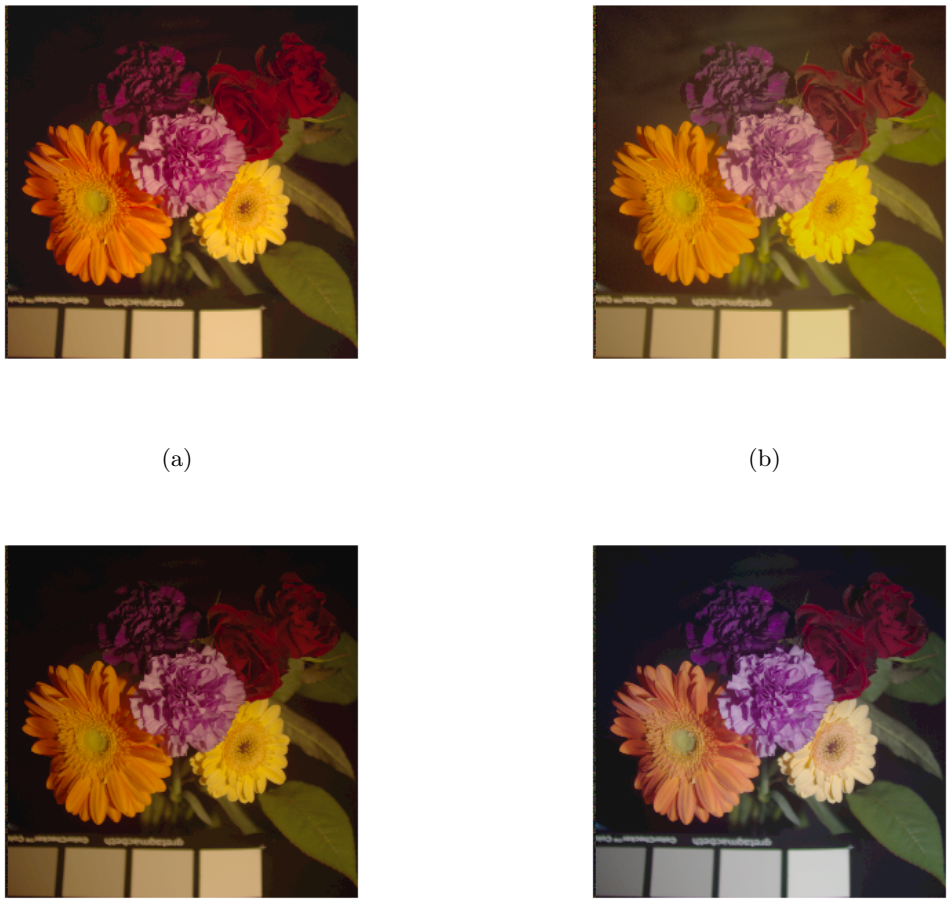

(a) (b)

(c) (d)

Figure 1.1: The sRGB rendering of the same image from Columbia dataset [2], computed under 4 different lighting conditions. (a) CIE A (b) CIE F3 (c) LED with correlated color temperature of 2900K. (d) CIE D65.

Chapter 2

Background

In what follows, we provide the background and fundamental theory of color image formation, followed by different concepts studied in this thesis.

2.1 Color formation

In this section we talk about the basic physical model of color formation. There are three important factors determining the color of a pixel recorded by a camera:

1. The illuminant spectrum
2. The surface reflectance spectrum at each pixel of the image
3. The camera's sensor-response-curve

In what comes next a brief introduction to each of these concepts is provided.

2.1.1 Illuminants

An "illuminant" or "light" is usually described by a Spectral Power Distribution (SPD) $P(\lambda)$ defining its radiant power at each wavelength of the spectrum [4]. Note that we are essentially concerned with the visible part of the radiation spectrum that the human visual system is sensitive to (approximately 380-780 nm). It is also the case for the sensors and reflectance spectra. The Commission International de L'Eclairage (CIE) [3, 4] specifies the relative spectral power distributions of typical lights e.g., different phases of daylight and

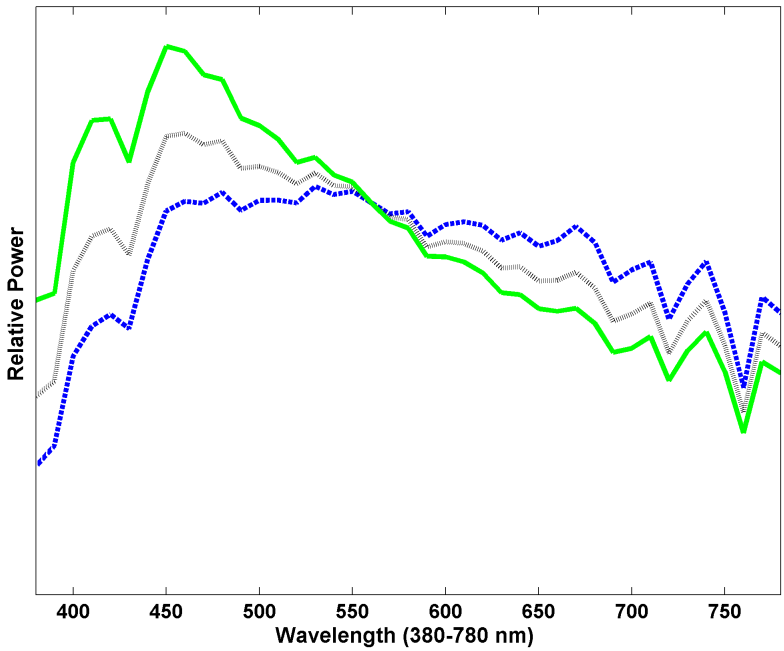

Figure 2.1: Three different phases of CIE Daylight illuminants. D55: dashed blue, D65: dotted black, D80: green curve.

fluorescent illuminants. As for daylight illuminants, they are usually called by a letter "D" for daylight, followed by two numbers indicating the corresponding correlated color temperature as the temperature of a blackbody (Planckian) radiator whose perceived color most closely matches the given color under certain viewing conditions [4]. Figure 2.1 illustrates three different phases of standard daylight illuminants, including D55 (i.e., Daylight with the CCT of 5500), D65 and D80.

The SPD of a blackbody radiator can be completely recovered from its color temperature in Kelvin (K). It is common to use the correlated color temperature (CCT) as a measure of light source color appearance defined by the proximity of the light's chromaticity coordinates with respect to the blackbody locus, as a single number. Light sources of different SPD may have identical CCTs if they have identical chromaticities.

2.1.2 Surface Reflectance

The second factor on determining the color of an object is its surface reflectance spectrum $R(\lambda)$, where it is considered to be physically realizable i.e., $0 \leq R(\lambda) \leq 1$ [34]. This function indicates, at each wavelength, the proportion of the incoming light that is reflected off the surface. The perfect reflector $R(\lambda) = 1$ reflects all the incoming light and the perfect absorber $R(\lambda) = 0$ characterizes a surface that does not reflect any of the incoming light.

2.1.3 Spectral Sensitivity Functions

In this context, a sensor is defined as an entity that reacts to light [34]. The sensitivity function $S(\lambda)$, also referred to as the sensor response curve (SRC), is defined as the human eye or camera sensor's response to the incoming radiation at each wavelength [34].

Similar to reflectances, sensors are usually considered to be physically realizable, such as CCD or CMOS photo sites or the cones in the human retina, all of which give a positive response when radiation is detected. As an example of sensor response curves, the NIKON D700 SRC and CIE 1931 2-degree standard observer color matching functions have been plotted in Figure 2.2 and Figure 2.3, respectively.

2.1.4 Color Image Formation

The image recorded from a scene is defined as a function of the light source with spectral power distribution $P(\lambda)$, the surface reflectance $R(\lambda, x)$, and the camera sensitivity function $S_k(\lambda)$ is given by:

$$\begin{aligned} \Phi_k(x) =& m_b \int_w R(\lambda, x) P(\lambda) S_k(\lambda) d\lambda + m_s \int_w R(\lambda, x) P(\lambda) S_k(\lambda) d\lambda \\ & k = 1, 2, 3. \end{aligned} \tag{2.1}$$

where w is the visible spectrum (e.g., $[380nm - 780nm]$), x is the spatial location of the pixel in the image, and m_b and m_s are scale factors of body and specular reflectance that contribute to the overall light reflected at location x [35]. Assuming fully Lambertian non-specular surface reflectances we have:

$$\Phi_k(x) = \int_w R(\lambda, x) P(\lambda) S_k(\lambda) d\lambda \qquad k = 1, 2, 3 \tag{2.2}$$

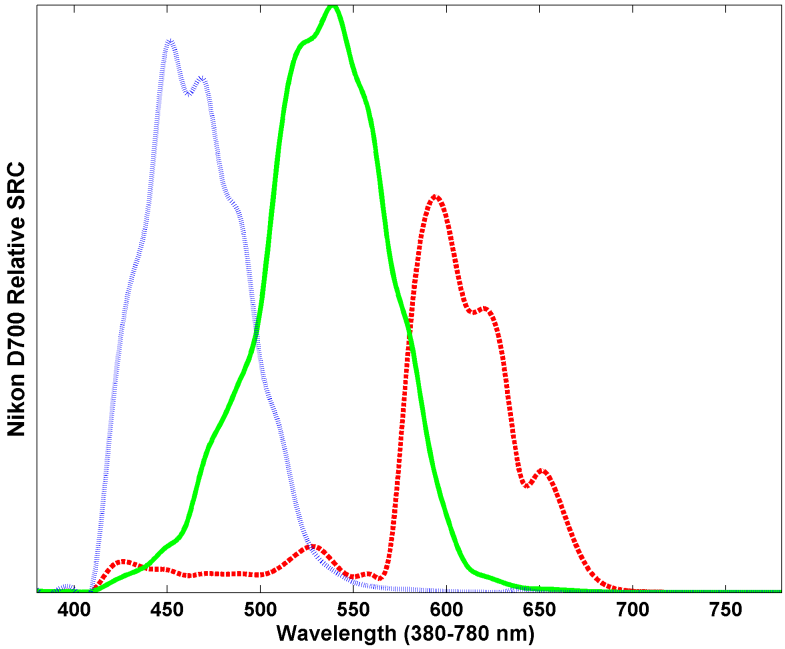

Figure 2.2: The sensor response curves of the Nikon D700 camera.

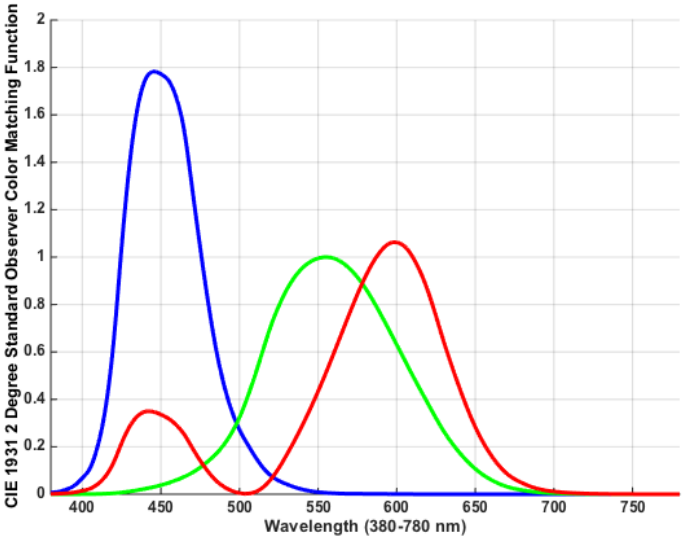

Figure 2.3: The *CIE* 1931 $\overline{x}\,\overline{y}\,\overline{z}$ color matching functions for standard 2-degree observer defined by CIE [3, 4].

It is generally assumed that the scene is observed under one single light source. The color of any given illuminant depends only on the SPD of the light source $P(\lambda)$ as well as the camera sensitivity function $S_k(\lambda)$:

$$e_k = \int_w P(\lambda) S_k(\lambda) d\lambda \qquad k = 1, 2, 3 \tag{2.3}$$

It is desired to separate P out of the integral in equation 2.1. Without prior knowledge, both P and R are unknown, and hence, this task is an under-constrained problem that cannot be solved without further assumptions. Therefore, in practice, the proposed theories usually make assumptions about the world such as the maxima obtained from each color channel represents the illumination color [36], there is a specularity [35], there are no specularities [37] in every scene and so on. A general assumption also is that the color of the illuminant is constant through the scene. There are also other assumptions such as restricted gamuts (limited number of image colors which can be observed under a specific illuminant), the distribution of colors that are present in an image (e.g., white patch, gray world, etc.), and the set of possible light sources.

In the next sections we will study in more details the limits of the color changes that might be perceived under illumination change (the so called metamer mismatching effect), discuss different ways to predict these changes, and present an object-color space that is more stable under illuminant changes.

2.2 Metamer Mismatching

2.2.1 What is Metamerism?

Although color constancy has received a lot of attention in the digital color imaging community, previous studies have not shown whether perfect color constancy is possible, nor how constant the colors humans perceive really are. Many experiments have shown significant deviations from color constancy [20]. One of the underlying problems is the phenomenon called metamerism. Metamerism poses important challenges for the computer vision and digital camera industries. One such challenge is metamer mismatching, which refers to the circumstance in which two objects having the identical color under one illumination have different colors under a second illumination [38].

2.2.2 Literature Review

A tristimulus value under one light (called source illuminant) may be dispersed into several different tristimulus values under a different light (called target illuminant). The question is how large the range of possible colors that might be observed under the second light is? For instance, given a color value under CIE illuminant D65, what is the set of all possible colors that could be invoked under CIE illuminant A? This set of colors constructs a convex volume [39], which is known as the metamer mismatch volume (MMV) or sometimes gamut [38, 40, 41]. The convexity of the metamer set was first studied by Schmitt [41].

Many methods in the literature have tried to characterize the MMV. There are several works that derive the metamer set in a framework of linear models of surface reflectances [40, 42, 43]. Wyszecki has employed the concept of metameric black. He first decomposes a reflectance into two parts: one part that is a particular solution and results in the actual tristimulus, and a part that results in a tristimulus of zeros, the metameric black. See Equation 2.4. In this framework, the metameric black part represents the variation between metameric answers. The answers are then computed by adding the fundamental metameric solution to a linear combination of metameric black components.

$$\begin{aligned} \Phi_k = &\int_w R_{fundamental}(\lambda, x)P(\lambda)S_k(\lambda)d\lambda + \int R_0(\lambda, x)P(\lambda)S_k(\lambda)d\lambda \\ &k = 1, 2, 3. \end{aligned} \tag{2.4}$$

Finlayson [40] uses the original framework of Wyszecki [42], but also tries to enforce more constraints on the reflectances to make them physically realizable. Cohen and Kappauf [44] employed Wyszecki's decomposition [42], but solved it using linear algebra and their matrix based method called matrix-R theory. This was later extended for multiple illuminants by Berns et al. [45].

There are some other methods that find a basis of the entire set of metameric reflectances and color signals (called simple metamers [41]), as opposed to finding a fundamental answer plus metameric blacks. Any metamer is then defined as a convex combination of the simple metamers. All of the mentioned attempts have in common that they provide a model to continuously express all the metamers.

On the other hand, there are some discrete solutions that characterize only a subset of metamers that are of particular interest. These methods are usually called discrete solutions

[40]. These approaches define a set of constraints that form the set of solutions. Different methods differ in the way they create the constraints and properties that best characterize surface reflectances. Takahama et al. [46, 47] work based on a given tristimulus ϕ^* and a set of N reflectances $R_i(\lambda)$ resulting in tristimulus values $\phi_i, i = 1, .., N$. N metameric reflectances $R_i^*(\lambda)$ are found such that a minimal change from the original reflectance occurs:

$$\int_w R_i^*(\lambda, x)P(\lambda)S(\lambda)d\lambda = \phi^* \tag{2.5}$$

and

$$\min_{R_i^*(\lambda)} \int_\omega [R_i(\lambda) - R_i^*(\lambda)]^2 d\lambda. \tag{2.6}$$

In [47] a similar strategy is used, however, reflectances are constrained to be in the [0,1] range. According to [40], both these methods have the problem that the final metamers depend significantly on the initializations. The set of initial N reflectances, $R_i(\lambda)$, if selected badly, could be such that the resulting final metamers, $R_i^*(\lambda)$, are all the same.

These methods usually don't provide a systematic way to generate metamers, and also, essentially, depend on the initialization. In addition, most of them are based on finding metameric reflectances under the source illuminant and then computing their corresponding tristimulus values under the target illuminant. There is not a clear understanding of where exactly these metamers fall within the mismatch volume. Therefore they do not accurately specify the metamer mismatch volume. On the other hand, it is not possible to find out the accuracy of these approximations because there is no precise boundary of the mismatch volume as the ground truth. This problem may arise more seriously specially in the methods such as [40, 48] where the sampling is done only from a finite-dimensional subset of the infinite-dimensional set of all the reflectances.

In view of this issue, a recent method proposed by Logvinenko et al. [5], computes only the metamer mismatch volume boundary. This boundary, which is sufficient to specify the whole convex volume, is of more interest in this thesis. This method is applicable for any reflectance and strictly positive illuminant. Note that metamer mismatching also happens in case of a change in the sensor sensitivities (called observer-induced metamer mismatching). In this context, this phenomenon is essentially analogous to an illuminant change (called illuminant-induced metamer mismatching). Logvinenko et al. refer to the set of illuminant

and sensor as a color mechanism [5] and provide a general solution for metamer mismatching that arises under a change of the color mechanism.

2.2.2.1 Logvinenko's Metamer Mismatching Theory

Logvinenko et al. investigate the boundary of the metamer mismatch volume from the formal point of view and then provide an algorithm for computing the metamer mismatch volumes for arbitrary, strictly positive illuminants and strictly positive sensor sensitivity functions, without placing any restrictions on the reflectances. Specifying the boundary of the mismatching can fully describe this convex volume.

Consider a set of sensors $\Phi = (\phi_1, ..., \phi_n)$, the response of each of which to a reflecting object with spectral reflectance function $R(\lambda)$ illuminated by a light with spectral power distribution $P(\lambda)$ is given by:

$$\begin{aligned} \phi_k &= \int_w R(\lambda)P(\lambda)S_k(\lambda)d\lambda \\ &(k = 1, ..., n). \end{aligned} \tag{2.7}$$

where w is the visible spectrum interval, and $S_k(\lambda)$ is the sensitivity of the k^{th} sensor. Note that this is a general formulation for a vision system with n sensors. The vector $\Phi = (\phi_1(x), ..., \phi_n(x))$ of the sensor responses is referred to as the *color signal* produced by the sensor set Φ in response to $R(\lambda)$ illuminated by $P(\lambda)$. In the case of trichromatic human color vision, $n = 3$ and $S_1(\lambda)$, $S_2(\lambda)$, and $S_3(\lambda)$ are the CIE 1931 2-degree standard observer color matching functions. Note that $S_1(\lambda)$, $S_2(\lambda)$, and $S_3(\lambda)$ can be sensors' spectral sensitivity functions of a digital camera.

In this context, the reflectances mapping to the MMV boundary are called optimal [38]. The goal is not to solve for all the optimal reflectances directly because the set of possible optimal reflectances is infinite. However, for different directions from the center of the MMV, reflectance functions with a particular parameterization specifying the boundary points can be found [39, 49]. The possibility of such parameterization emerges from the fact that the optimal reflectances are step-like functions that can be characterized by a finite number of transition wavelengths. There is an accepted assumption, first proposed by Schrodinger [50], that the optimal spectral reflectance functions only take two values: either 0 or 1.

In order to find the metameric members on the boundary of MMV, an either 0 or 1 step-like function with 5 transitions is defined: $x_5(\lambda; \lambda_1, ..., \lambda_5)$. As in related works [39, 49, 51],

the elementary step-like functions are defined with x_m as type 1:

$$x_m = (\lambda; \lambda_1, ..., \lambda_m) = \sum_{i=1}^{m} (-1)^{i-1} x_1(\lambda; \lambda_i) \tag{2.8}$$

and $1 - x_m$ as type 2:

$$1 - x_m(\lambda; \lambda_1, ..., \lambda_m) \tag{2.9}$$

where

$$x_1 = (\lambda; \lambda_1) = \begin{cases} 0 & if\ \lambda < \lambda_1 \\ 1 & otherwise; \end{cases} \tag{2.10}$$

and $\lambda_{min} < \lambda_1 < \lambda_2 < ... < \lambda_m < \lambda_{max}$. In this context λ_1, λ_2,... and $< \lambda_m$ are called the transition wavelengths of the step-like elementary function $x_m = (\lambda; \lambda_1, ..., \lambda_m)$. It is shown that these elementary steplike functions with $m = 5$ map to the boundary of the metamer mismatch volume under the second illuminant. Therefore, finding the boundary points in enough number of directions in the color space will specify the MMV. The detailed implementation of the method is available in "Metamer Mismatching," authored by Logvinenko, Funt, and Godau [5].

To gain some more intuition into metamer mismatch volumes consider the simple one-dimensional case of a pair of color mechanisms. As shown in Figure 2.4 (directly taken from [5]), the object-color solid (i.e., the whole set of possible colors that can be observed under the second illuminant) becomes a convex region in 2 dimensions. In the trichromatic case, the object-color solid is the set of all possible XYZ that can arise for all possible reflectance functions $R(\lambda)$ (i.e., $0 \leq R(\lambda) \leq 1, 380 \leq \lambda \leq 780nm$). For this figure, the $CIE1931\ \overline{x}(\lambda)$ color matching function has been used as the single underlying sensor. Under CIE illuminants D65 and A, with spectral power distributions $P_{D65}(\lambda)$ and $P_A(\lambda)$, the spectral weighting functions of the corresponding color mechanisms are $P_{D65}(\lambda)\overline{x}(\lambda)$, and $P_A(\lambda)\overline{x}(\lambda)$. As can be seen from the figure, the color signal $CIE\ X = 35$ under D65 could potentially become any value in the range $CIE\ X = [20.5, 58]$ under A.

Figure 2.6 shows an example of the metamer mismatch volume for the XYZ of flat grey for a change in illuminant from a 2900K LED to CIE D65, the spectra of which are shown in

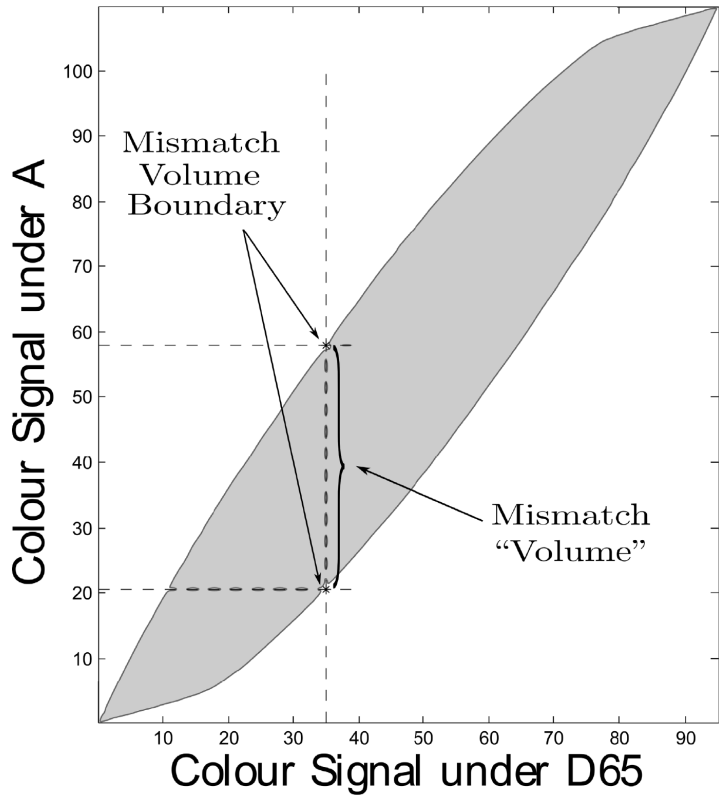

Figure 2.4: Metamer mismatch volume for a monochromatic color device with sensitivity function $CIE1931\ \overline{x}(\lambda)$. The CIE X obtained under CIE illuminant D65 are plotted along the horizontal axis, and under CIE A along the vertical axis. The shaded area indicates the set of all CIE X pairs arising under D65 and A from all possible object reflectances. The metamer mismatch volume for color signal value $X = 35$ under D65 is obtained from the projection shaded area at X=35 onto the vertical axis. The color signal $CIE\ X = 35$ under D65 could, under A, potentially become any value in the range $CIE\ X = [20.5, 58]$. This figure is directly taken from [5].

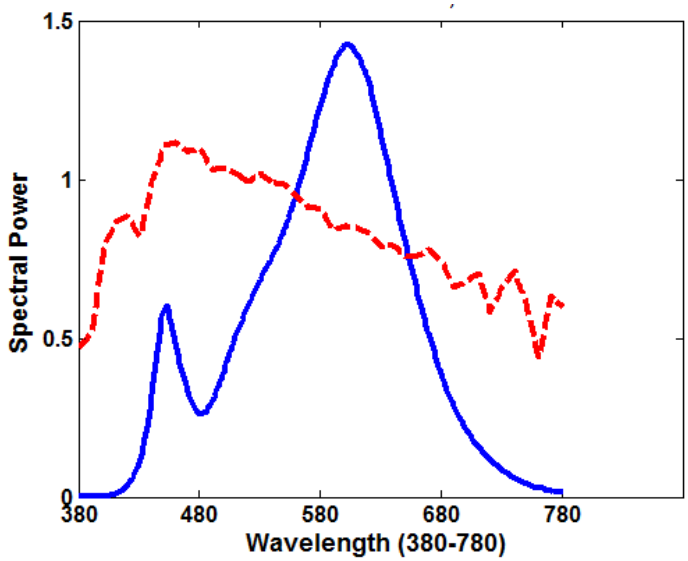

Figure 2.5: Spectra of a 2900K LED (blue) and that of CIE D65 (dashed red).

Figure 2.5. Even though the two illuminants are of the same CCT the metamer mismatch volume is quite large: it fills a sizable fraction of the entire object-color solid. This means that a single color under 2900K LED light, can be possibly dispersed into a large portion of all the possible colors under CIE D65. Therefore, it is not reasonable to ignore the huge impact of metamer mismatching on color science, especially the problem of estimation of the reflectance spectrum that could possibly produce a given color under a given illuminant.

Digital camera companies are becoming interested in metamerism issues in camera design. As well, the issue of metamerism is important in the design of new energy efficient light fixtures. In Chapters 3 and 4 we discuss two important implications of metamer mismatch volumes.

2.3 Reflectance Based Object-Color Space

Common color spaces such as CIE 1931 [4] and its derivatives are more appropriate for representing the colors of self-luminous than reflecting objects. The main problem in using them to specify object colors is that their coordinates depend on the illumination. CIELAB adjusts for the illumination using a von Kries type transformation, but this adjustment compensates only partially for the illumination. In view of this problem, Logvinenko introduced a new object-color atlas that is invariant to illumination [49, 52]. Logvinenko bases

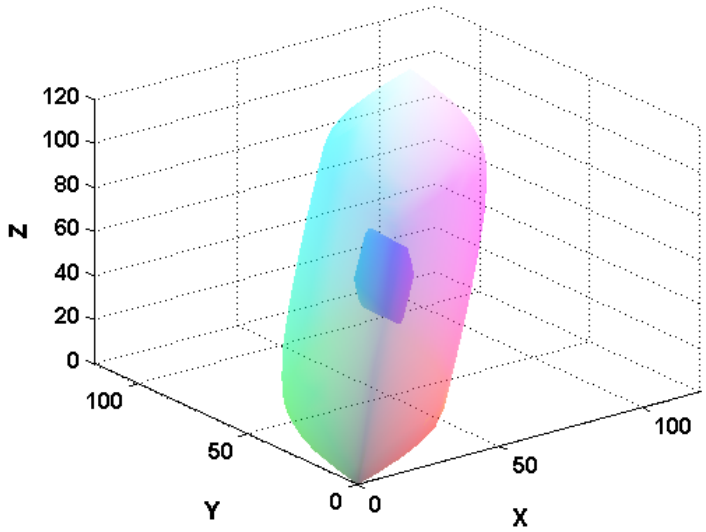

Figure 2.6: Metamer mismatch volume (for the XYZ of flat grey lit by a 2900K LED) shown inside the object-color solid of the CIE D65 for the case when the illuminant is changed from the LED to D65. Coordinates are the CIE 1931 XYZ space.

his color atlas on 'optimal reflectance' spectra that take on only the values 0 or 1 and make no more than two transitions between 0 and 1 over the visible spectrum [49]. The optimal reflectances generate color stimuli on the surface of the object-color solid, which is the set of all possible colors from reflecting objects under a given illuminant. The spectral locus must be convex in order for the two-transition property to hold. It has been shown that for the CIE color matching functions, the points on the boundary of the object-color solid are unique. In particular, they can be uniquely specified by their two transition wavelengths, λ_1 and λ_2 [49]. In Logvinenko's theory, the color atlas is based on object reflectances that are rectangular functions [49] formed as a mixture of the flat grey spectral reflectance function (0.5 across the visible spectrum) and an optimal reflectance. Given λ_1 and λ_2 as transition wavelengths, the optimal reflectance functions can be expressed equivalently by their central wavelength $\lambda = (\lambda_1 + \lambda_2)/2$ and spectral bandwidth $\sigma = \lambda_2 - \lambda_1$. The relative weighting of the grey and rectangular components is controlled by a parameter α called the chromatic amplitude. Each triple of these components $\alpha\delta\lambda$ therefore specifies a unique rectangular reflectance. The set of all such reflectances constitutes the elements of the color atlas. The coordinates of an arbitrary object under a given illumination creating color signal XYZ are the $\alpha\delta\lambda$ coordinates of the rectangular reflectance generating the same color signal XYZ. In

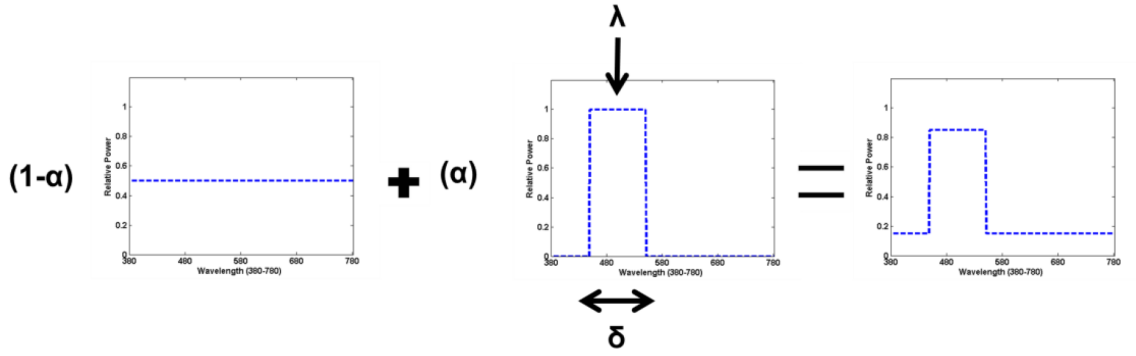

Figure 2.7: The composition of a rectangular reflectance spectrum.

other words, the atlas coordinates are those of the rectangular reflectance that is metameric to the object under the given illumination.

Figure 2.7 illustrates an example of a rectangular spectra generated as a mixture of a flat grey (left panel), and an optimal rectangular spectra (middle panel) via parameter α.

Logvinenko's object color atlas has several interesting features including:

- illuminant invariance (i.e., the elements of the atlas do not change with the illuminant);
- reasonable correlation between two of its coordinate axes and the perceptual dimensions of hue and chroma;
- the possibility of predicting the effects of a change in illuminant.

Another favorable property is that the $\alpha\delta\lambda$ coordinates are somewhat independent of the spectral sensitivity of the sensors. In particular, under any linear transformation of the sensitivity functions they remain completely unchanged.

2.3.1 Other Representations

The color atlas that has been defined above consists of rectangle spectral reflectance functions. The issue with these reflectances is that they cannot be implemented in practice. Logvinenko approaches this problem by trying to use physically implementable objects to model an object color atlas that is suitable not for all the objects but only for a limited subset of them [52].

In one of his alternatives, Logvinenko suggests a parameterization of his color atlas based on "wraparound Gaussian" reflectance functions as defined in section 2.3.1.1. Gaussians are smooth by definition and have been used in modeling objects and lights [53–55]. They can represent the whole object color solid, but only if some functions that are not physical reflectance functions are included. Specifically, functions are required with 'reflectance' values exceeding 1.

2.3.1.1 Gaussian parameterization

Consider a three-parameter set of spectral reflectance functions which are Gaussian-like functions where k, $1/\sqrt{\theta}$, and μ indicate the height, standard deviation and center (peak wavelength) of the Gaussian. These functions are not strictly Gaussians, but rather are defined on a finite wavelength interval and in some cases wraparound at the ends of the interval, hence the name "wraparound Gaussians"[52]. Wraparound Gaussians are defined by the following equations:

If $\mu_m \leq (\lambda_{min} + \lambda_{max})/2$ we have two cases:

1. For $\mu_m \leq \lambda \leq \mu_m + \Lambda/2$:

$$g_m(\lambda; k_m, \theta_m, \mu_m) = k_m \; exp[-\theta_m(\lambda - \mu_m)^2] \tag{2.11}$$

2. For $\mu_m + (\Lambda/2) \leq \lambda \leq \lambda_{max}$:

$$g_m(\lambda; k_m, \theta_m, \mu_m) = k_m \; exp[-\theta_m(\lambda - \mu_m - \Lambda)^2] \tag{2.12}$$

where $\Lambda = \lambda_{max} - \lambda_{min}$.

On the other hand when $\mu_m > (\lambda_{min} + \lambda_{max})/2$, again we have two cases:

1. For $\lambda_{min} \leq \lambda \leq \mu_m + \Lambda/2$:

$$g_m(\lambda; k_m, \theta_m, \mu_m) = k_m \; exp[-\theta_m(\lambda - \mu_m - \Lambda)^2] \tag{2.13}$$

2. For $\mu_m - (\Lambda/2) \leq \lambda \leq \lambda_{max}$:

$$g_m(\lambda; k_m, \theta_m, \mu_m) = k_m \; exp[-\theta_m(\lambda - \mu_m)^2] \tag{2.14}$$

Then, for $0 \leq K_m \leq 1$, $\lambda_{min} \leq \lambda_m \leq \lambda_{max}$ and positive θ_m, we have a Gaussian reflectance spectrum. In this representation, the roles of μ and θ are analogous to those of central wavelength λ and spectral bandwidth δ defined in the Logvinenko's original [49] $\alpha\delta\lambda$ coordinate system.

We will refer to triples $k\sigma\mu$ as KSM coordinates. Figure 2.8 shows an example of a wraparound Gaussian metamer for the spectral reflectance of Munsell paper 5 YR 5/6 under D65.

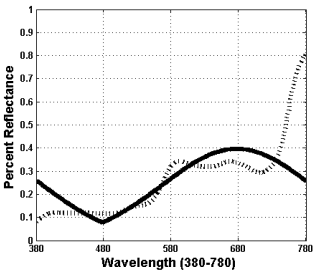

Figure 2.8: The spectral reflectance of Munsell 7.5 PB 5/8 (dashed black) and its metameric wraparound Gaussian (solid black). Figure is copied from [6].

In this thesis, such Gaussian-like reflectances have been used to describe the appearance attributes of object-colors in Chapters 5 and 6. Due to their interesting properties, they have been also employed as a tool for predicting how a color signal (i.e., cone response triple) changes with a change in illumination as explained in Chapter 7 [8, 27].

2.4 Appearance Dimensions of Color

The development of color science research in the literature can be divided into three main directions: color specification, color difference measurement and color appearance modelling [56]. The first component deals with the need to specify and convey the color information via numbers. The CIE recommended a set of standards for a color specification system in 1931 that include standard colorimetric observers, or color matching functions ($CIE\ \overline{x}, \overline{y}, \overline{z}$), standard illuminants such as daylight illuminants, and standard viewing conditions. The typical colorimetric measures are the tristimulus value (X,Y,Z) and chromaticity coordinates (x,y).

The second component deals with the need of having a uniform color space and a color difference formula. The CIE XYZ and xy chromaticity coordinates are not uniform spaces.

Therefore, CIELAB and CIELUV were recommended by CIE in order to providing uniformity and calculating color differences. Later on, CIE recommended the CIEDE2000 [57] for evaluating color differences.

The next important aspect of color science deals with color appearance models. Although conventional colorimetry has existed for a long while, it is limited to the local signals coming from each single object. However, the colors humans perceive depend on the relationship and integration of signals across the whole visual scene. The question of how these light signals are playing their role in generating the perceived colors has been an object of research for understanding color vision. In addition, conventional colorimetry can be used only under quite limited and standardized viewing conditions and contexts. For example it does not consider background and surrounding objects, and reference white in the scene. Recent developments in color technology and the need to match the appearance of a color across different platforms, for example a camera, a display or a printed paper, have heightened the importance of color appearance models. The main challenge for a color appearance model is its capability to predict the appearance attributes across different viewing conditions. The color of any given object can be described in terms of three main appearance dimensions:

1. Hue
2. Chroma
3. Lightness

Different color spaces employ different definitions for each of these appearance correlates. The attributes were originally defined on regular color spaces such as CIELAB too, but later received considerable critical attention in color appearance models. The first appearance model, titled CIECAM97s, was proposed and recommended by CIE in 1997 [58]. After a few years of evaluation by different researchers, it was improved and revised. A simpler and more accurate model, called CIECAM02, was recommended by CIE in 2002 [59]. CIECAM02 provides the prediction of a range of different color appearance attributes, among which, we pay more attention to hue, chroma, and lightness.

2.4.1 Illumination Effect

When a color appearance attribute is calculated under a target illuminant, a color appearance model such as CIECAM02 [59] containing a chromatic adaptation transform (CAT)

is used. A CAT is a transformation that converts the input colors captured under a first illuminant to the corresponding output colors under the second illuminant. In this case, the CAT maps the color values under the given light source to the predicted color values under the canonical target light source. All these color appearance models and other color spaces are under the von Kries rule limitations.

The change of illumination can significantly affect the color appearance attributes. Colored illuminants will neutralize and darken surfaces of complementary-colors. It will also increase the relative lightness of all surfaces that reflect wavelengths present in the light. The surface hues also shift towards the dominant wavelength of the light. In addition, the range of colors seen under a white illuminant is always wider than that seen under a colored illuminant. To achieve robustness with respect to illuminants, the appearance dimensions of object color have been studied in more detail and new hue, chroma and lightness descriptors have been developed in Chapters 5 and 6 of this thesis.

2.5 Mitigating the Illumination Effects

It is usually desired to simulate the ability of the human visual system to preserve an approximate color of an object under different lighting conditions. The human visual system has a mechanism to identify objects across different illumination conditions. But this ability for a computational model is difficult to maintain. In order to illustrate the concept, consider, for example, the Munsell chips Logvinenko and Tokunaga used in their experiments [7], as shown in Figure 2.9. Figure 2.10 graphically depicts the change of object colors when the illuminant is changed from a Neutral to a Blue illuminant. Each reflectance sample (Munsell chip) under a source illuminant can be described in terms of its $CIE\ XYZ$ coordinates i.e., $XYZ_{reference}$. Changing the illuminant will lead to different $CIE\ XYZ$ values i.e., XYZ_{target}. These plots compare the $CIE\ xy$ chromaticity coordinates of the actual papers under the first (shown by blue curve) and second (shown by black curve) illuminants and the asymmetric color matches made by observers in Logvinenko & Tokunaga's experiment (shown by red curve). The average matches chosen by human subjects are fairly close to the ground truth papers. It means that they have been able to identify the correct paper in each of the 20 cases based on its color under the second illuminant quite well.

In the literature, the fact that color is not an intrinsic and independent attribute of an object, but rather is an attribute of a combination of light and surface reflectance pair, has

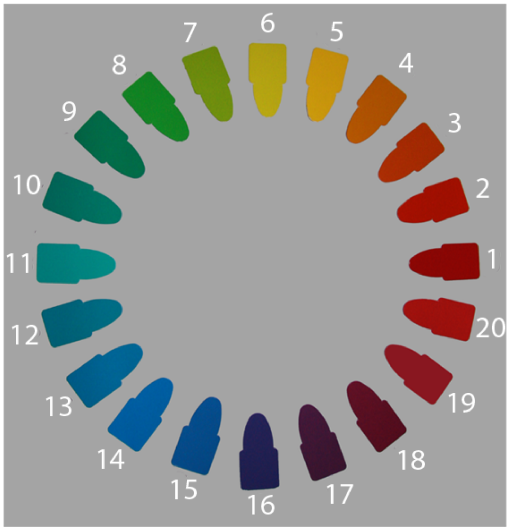

Figure 2.9: Photograph giving a general indication of the colors of the 20 chromatic stimulus papers used in Logvinenko & Tokunaga's experiment. To evaluate the colors correctly requires viewing the actual Munsell papers. Their Munsell notations starting from 1 are: 10 RP 5/14, 5 R 4/14, 10 R 5/16, 5 YR 7/14, 10 YR 7/14, 5 Y 8/14, 10 Y 8.5/12, 5 GY 7/12, 10 GY 6/12, 5 G 5/10, 10 G 5/10, 5 BG 6/10, 10 BG 5/10, 5 B 5/10, 10 B 5/12, 5 PB 5/12, 10 PB 4/12, 5 P 4/12, 10 P 4/12, 5 RP 5/12.

been often neglected. Therefore, the goal of computational methods have been to model the mapping from $XYZ_{reference}$ to XYZ_{target} values. This mapping, usually referred to as a chromatic adaptation transform (CAT), has fundamental issues.

2.5.1 Chromatic Adaptation

In this section, we discuss different chromatic adaptation transforms, most of which are based on the model proposed by Johannes von Kries [60], the first who attempted to describe this phenomenon with a mathematical model. In his model, each color channel is independently scaled by the ratio of the color signals obtained from an ideal reflector under the two illuminants. It can be implemented as a diagonal-matrix that maps a color response matrix under one illuminant to a corresponding color response matrix under a second illuminant. Despite its simplicity, von Kries model is a generally accepted color correction model [61–64]

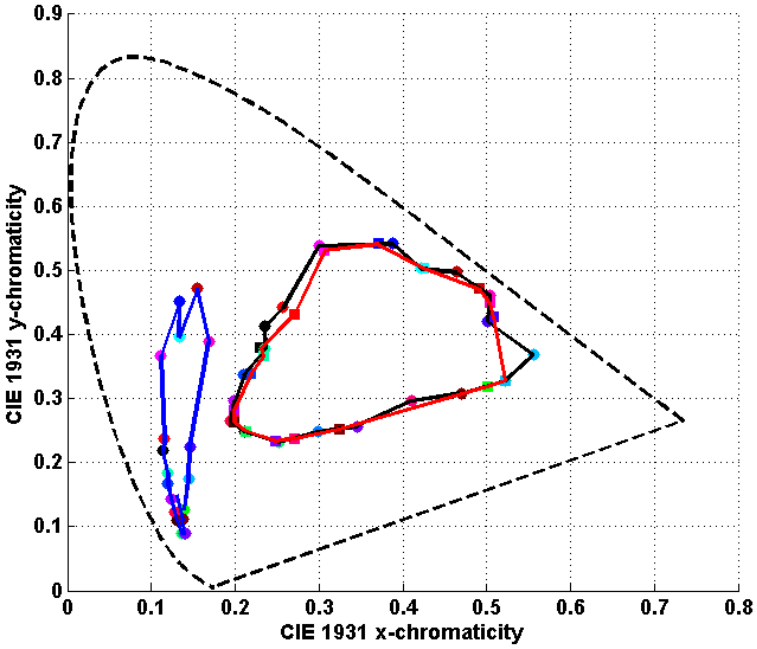

Figure 2.10: The asymmetric color matching (blue to neutral) [7] done by different observers for 20 Munsell papers shown in Figure 2.9. Circular dots connected by the black lines stand for the stimulus papers under the Neutral illuminant. The squares connected by the red lines represent the averaged observer matches. Circular dots connected by the blue lines stand for the stimulus papers under the Blue illuminant. The dashed line is a segment of the spectrum locus. The detailed analysis is presented in Chapter 3.

used to transform the images from the estimated illuminant color to the so called illuminant-invariant descriptors under a perfect white light, i.e.,[1,1,1].

It is well known that von Kries rule performs poorly if applied on $CIE\ XYZ$ and this transform must be applied in a cone space. The Hunt-Pointer-Estevez matrix (M_{HPE}) is a transformation originally used to convert the XYZ values into LMS cone space that is more compatible with the von Kries transform method, and is therefore also called von Kries transformation matrix ($M_{vonKries}$):

$$\begin{bmatrix} L \\ M \\ S \end{bmatrix} = M_{HPE} \begin{bmatrix} X \\ Y \\ Z \end{bmatrix} \tag{2.15}$$

$$M_{HPE} = \begin{bmatrix} 0.3897 & 0.6890 & -0.0787 \\ -0.2298 & 1.1834 & 0.0464 \\ 0 & 0 & 1 \end{bmatrix} \tag{2.16}$$

Although von Kries model has been elaborated during the past years, the essential idea has not been changed much. In a number of studies [64–66], West, Worthey, and Brill analyzed the factors that limit this model and found that sensor sensitivity breadth and overlap affect von Kries based color constancy significantly and cause imperfect constancy. Later, Finlayson, Drew, and Funt [63, 67–69] showed that von Kries can be successfully employed on tri-stimulus values if they are prepared by transforming to a space of more concentrated and sharper sensors. In particular, they showed that if reflectances can be accurately modelled by 3 basis functions and illuminants by 2 basis functions, then there exists a set of new sensors as linear combinations of the fixed cone sensitivity functions that guarantees diagonal color constancy [70]. Therefore, the color values must be first transformed to a space of sharpened sensor sensitivities. This transformation can be done via a linear 3x3 matrix (M). The diagonal von Kries transform matrix can then be applied.

There are different versions of von Kries in the literature that work based on transformation to a sharpened space [71–73], among which, Bradford and CAT02 are more popular. CAT02 is implemented in CIECAM02, the most recent color appearance model approved by CIE. Given a set of $CIE\ XYZ$ values, the corresponding sharpened LMS values given by CAT02 are given by the following transform:

$$M_{CAT02} = \begin{bmatrix} 0.7328 & 0.4296 & -0.1624 \\ -0.7036 & 1.6975 & 0.0061 \\ 0.0030 & 0.0136 & 0.9834 \end{bmatrix} \tag{2.17}$$

The other popular transform, the Bradford transformation matrix, works best with a modified von Kries transform that has a small non-linearity in the blue channel. However, this is often neglected and a linear von Kries in all channels is used with the Bradford transformation matrix.

$$M_{BFD} = \begin{bmatrix} 0.8951 & 0.2664 & 0.1614 \\ -0.7502 & 1.7135 & 0.0367 \\ 0.0389 & -0.0685 & 1.0296 \end{bmatrix} \tag{2.18}$$

2.5.2 Other Illuminant Invariant Spaces

Another line of research, not pursued in this report, focuses on the invariance that can be obtained by applying other transformations, sometimes also referred to as color constancy [74–77]. Such methods often present different forms of invariance, like invariance to highlights or shadows, but do not result in output images that have any visual similarity to the original input image. The shadow removal methods proposed by Finlayson and Drew fall into this category [74, 76, 77]. There are some assumptions such as Lambertian surfaces and Planckian lights in order for the model to hold. Although it is not always the case for the sensors, narrow-band sensors better follow the requirements of the invariant model. There have been also some sharpening methods proposed to better remove the shadows using a 3x3 sensor sharpening matrix and fulfill the requirements of the model. The key step of these algorithms is to find an angle to project the log-log chromaticities into a 1D illuminant-invariant space. This is obtained by finding a projection that minimizes the entropy. The obtained intrinsic image is claimed to represent the reflectance property of the image pixels and is independent of lighting condition. Once the invariant image is obtained, one can reintegrate this image back into the original image preserving the original colors and removing the shadows and other effects of illumination [74]. One can find two edge maps, one from the original image, and one for the invariant image. Comparison of edges in these two images gives the required information to detect the shadows.

In Chapter 7 of this thesis, we have proposed novel approaches that map the input colors that are viewed under the source illuminant to the desired colors under the canonical illuminant.

Chapter 3

Implications of Metamer Mismatching

3.1 Summary

This chapter describes the experiments that form the underlying results of the joint project with Logvinenko, Funt, and Tokunaga, titled "Rethinking Colour Constancy" [1] where the implications of metamer mismatching on color constancy are discussed. Metamer mismatching refers to the fact that two objects reflecting metameric light under one illumination may no longer reflect metameric light under a second light. Therefore two objects appearing as having the same color under one illuminant may appear as having different colors under a second. This phenomenon is a serious obstacle towards perfect color constancy but the deviations from perfect color constancy reported in experiments have been typically thought to be small enough that they do not controvert the concept of color constancy.

The question is whether this imperfectness is because of the imperfectness of illuminant estimation or there is perhaps some other fundamental underlying problem. One important source of color inconstancy is metamer mismatching problem. Therefore, it is important to determine how the deviations from color constancy relate to the limits metamer mismatching imposes on constancy. This has been limited, until now, by the lack of a method for computing metamer mismatch volumes precisely.

Employing the method for calculating the exact boundaries of metamer mismatch volume [5], the experiments described in the next sections show how serious metamer mismatching

can be. The variation in object colors under illumination changes is large enough so as to confirm that color is not an independent, intrinsic attribute of an object, but rather an attribute of an object/light pair. In its stead, Logvinenko suggests a definition of color in terms of object/light pairs (called material color [1, 52]). The findings of this chapter have led to publications in PLOS ONE, 2015, JOSA A, 2016, proceedings of the IEEE International Conference on Computer Vision (ICCV) Workshops, 2015, proceedings of Color and Imaging Conference (CIC), 2014, and proceedings of the 12th Congress of the International Colour Association (AIC), 2013 [1, 23, 26, 28, 31].

3.2 Method and Materials

The goal of this section is to investigate the metamer mismatch volumes in different lighting conditions. These volumes can be used for defining the limits of both human and machine-based color constancy. Since the metamer mismatch volumes are convex bodies, they have been determined by their boundary surfaces computed using the recent algorithm proposed by Logvinenko et al. [78].

As an example output of this method, Fig. 3.1 illustrates a metamer mismatch volume computed for a point produced by the flat spectral reflectance function (0.5 across the visible spectrum) for the case of a change from illuminant CIE D65 to CIE A.

In this study metamer mismatch volumes were also computed for the color stimuli and illuminants used in Logvinenko & Tokunaga's color matching experiments [9]. For each metamer mismatch body evaluated in this thesis, 1000 5-transition reflectances that map to the metamer mismatch boundary have been computed. All these reflectances are, in fact, metameric under the first illuminant, but disperse to a 3D volume under the second. As a double check, any point found to be more than 0.01% away from the mean (of the 1000 values) for at least one of the three tristimulus values (i.e., X, Y or Z) was discarded as an outlier. A complete database of the 5-transition reflectance functions for all the metamer mismatch volumes is available on-line from http://www.cs.sfu.ca/∼color/data/. The reader may easily compute the XYZ tristimulus values of the reflectances under any illuminant. In particular, they all lead to equal XYZ values under the source light of the metamer mismatching condition.

Logvinenko & Tokunaga employed 20 chromatic Munsell papers as shown in Fig. 2.9 along with a grey (N5/) and a black (N1/) paper, and six different chromatic lights that

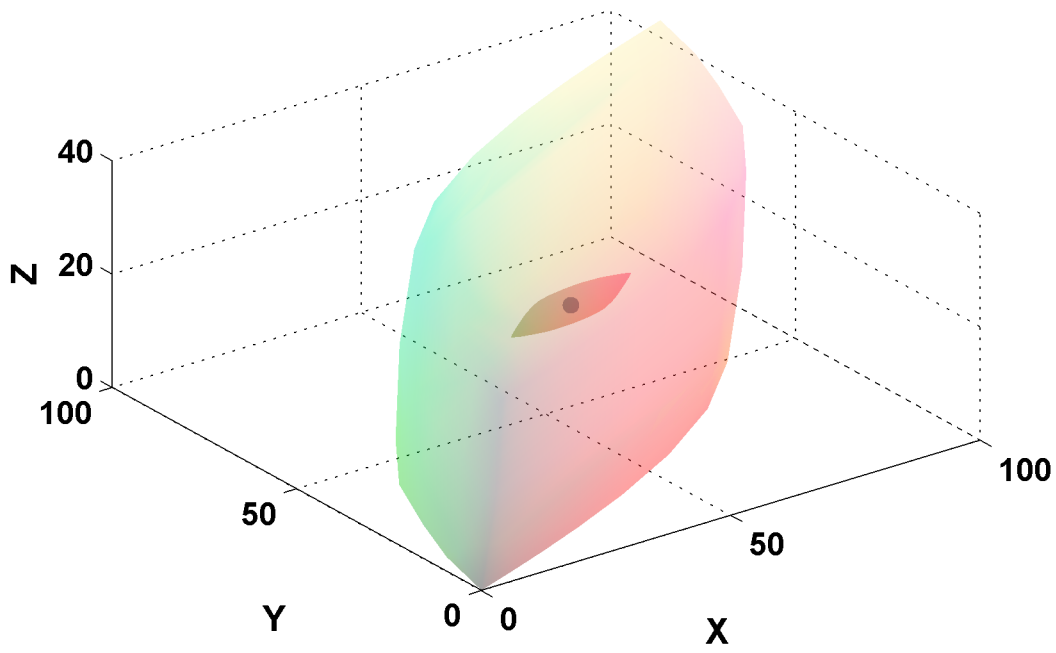

Figure 3.1: Metamer mismatch volume for the flat grey spectral reflectance function (i.e., 0.5 across the visible spectrum) when the illuminant changes from CIE D65 to CIE A is shown inside the object-color solid for CIE D65. The coordinates are XYZ in the CIE 1931 colorimetric space. The grey dot indicates the location of the color signal corresponding to the flat grey reflectance. It is located at the centre of the object color solid and also at the centre of the metamer mismatch volume.

were used to illuminate the papers: neutral (N), yellow (Y), blue (B), green (G), and two reds (R1 and R2). Their spectral power distributions are plotted in Fig. 3.2. Fig. 3.3 presents the CIE 1931 chromaticity coordinates of the stimulus papers under different lights excluding R2, which is rather similar to R1. In the rest of this thesis, results for R2 are not included and R1 will be referred to as R. The next section investigates the extent of metamer mismatching for these chromatic illuminants.

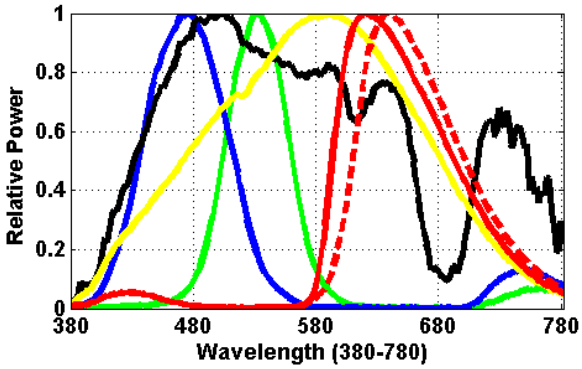

Figure 3.2: Spectral power distribution of the illuminants employed in Logvinenko & Tokunaga's experiment. The line color indicates the color of the light each line represents. The R2 light is represented by the dashed red line and the neutral light by the black line.

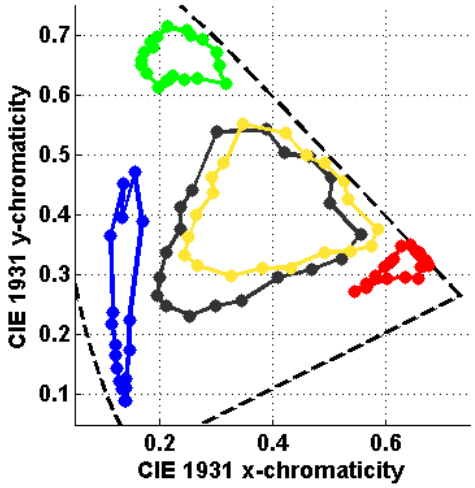

Figure 3.3: The CIE 1931 xy chromaticity coordinates of the light reflected from the stimulus papers under the lights used in Logvinenko & Tokunaga's experiment shown in Fig. 2.9 and 3.2. The marker color indicates the color of the corresponding light.

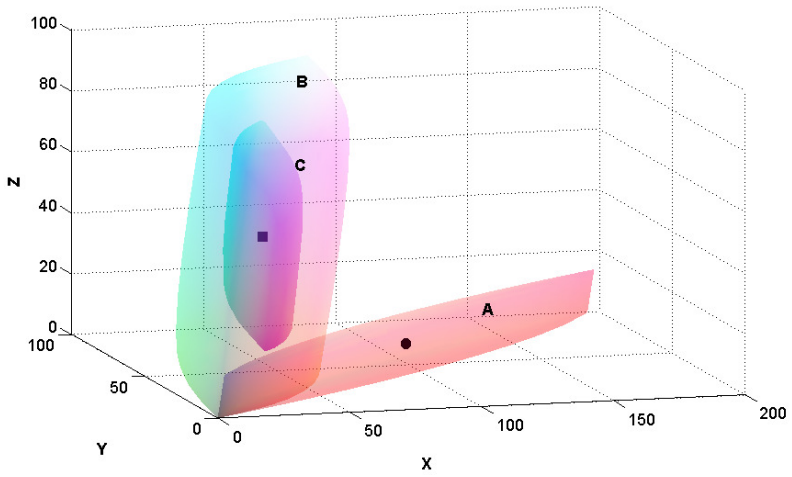

Figure 3.4: Label A indicates the object color solid under red light. Label B indicates the object color solid under neutral light. The black dot indicates the XYZ of flat grey under red. The black square shows its XYZ under neutral. C indicates the metamer mismatch volume of the flat grey for a change in illumination from red to neutral.

3.3 Extent of Metamer Mismatching for Chromatic Illuminants

The metamer mismatch boundary surfaces were computed for the chromatic Munsell papers depicted in Fig. 2.9 under all 8 pairs of illuminants that include the neutral. A pair of illuminants, for example N and Y, will be referred to as an illumination condition and written as NY. All computation was done using the CIE 1931 color matching functions [38]. Fig. 3.4 shows an example MMV for the case of a change from the red illuminant to the neutral (RN). It is surprising that such a large fraction of the object color solid is occupied by the metamer mismatch volume.

The overlap between multiple mismatch volumes makes it hard to have them in a 3D plot. Alternatively, we will plot 2D projections of the volumes in the CIE 1931 xy chromaticity diagram. The area covered in the CIE xy chromaticity plane, produced by the projection of the points in a metamer mismatch volume will be referred to as the *chromaticity mismatch area (CMA)*. This area shows how much the initial chromaticity is dispersed as a result

of metamer mismatching. Fig. 3.5 depicts the chromaticity mismatch area corresponding to the metamer mismatch volume for the flat grey from Fig. 3.1, where the illuminant has changed from CIE D65 to A .

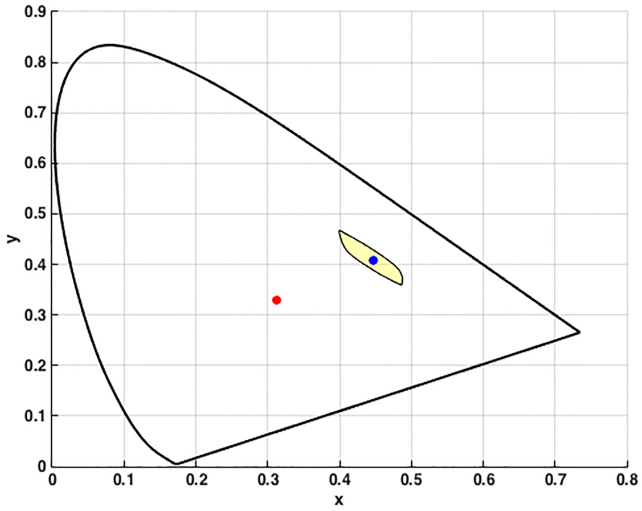

Figure 3.5: Chromaticity mismatch area (yellow area) for the flat grey reflectance $R(\lambda) = 0.5$ when CIE illuminant D65 is replaced by CIE illuminant A. The red dot indicates the chromaticity of the flat grey under CIE A and the blue dot the corresponding chromaticity under CIE D65 lying inside the metamer mismatch area.

Figs. 3.6 and 3.7 show the chromaticity mismatch areas for the different Munsell papers from Fig. 2.9 under NY and NB illumination conditions (i.e., resulting from changes from the neutral illuminant to the yellow and to the blue illuminants). On the other hand, Figs. 3.8 and 3.9 depict the NG and NR illumination conditions (i.e., for the shift from the neutral to the green and red illuminants). Note that, for each of these four illumination conditions, to avoid cluttered and confusing plots, the chromaticity mismatch areas are shown for 10 odd-numbered Munsell papers from Fig. 2.9 as a representative sample set. As it can be seen from the figures, the chromaticity mismatch areas are large, even for the NY illumination condition, for which the source and target illuminants are quite close.

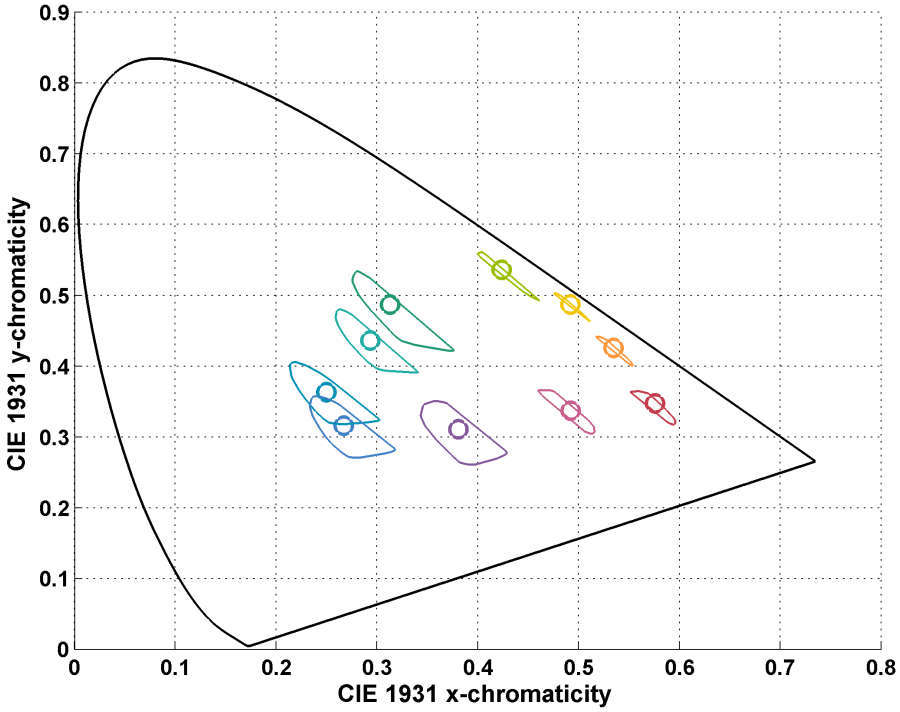

Figure 3.6: Chromaticity mismatch areas for shifts from the neutral illuminant (N) to the yellow (Y). The circles are the chromaticities of the 10 odd-numbered Munsell papers from Fig. 2.9 under the second illuminant in each case. The closed contours indicate the boundaries of the chromaticity mismatch areas. The color of the circles and boundaries of the metamer mismatch areas correspond to one another, and very roughly indicate the colors of the Munsell papers.

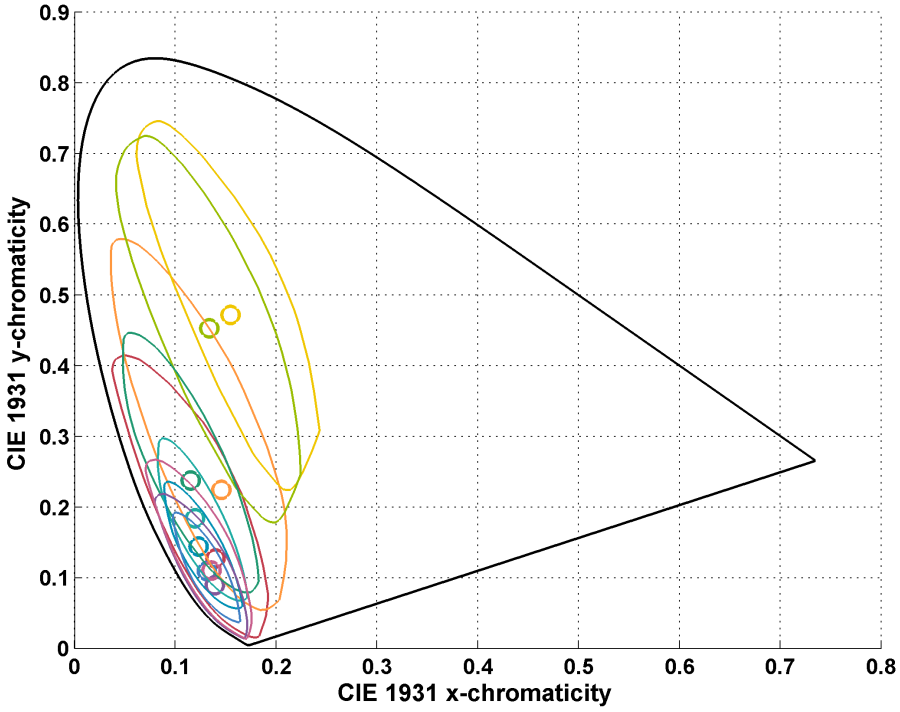

Figure 3.7: Chromaticity mismatch areas for shifts from the neutral illuminant (N) to the blue illuminant (B). The circles are the chromaticities of the 10 odd-numbered Munsell papers from Fig. 2.9 under the second illuminant in each case.

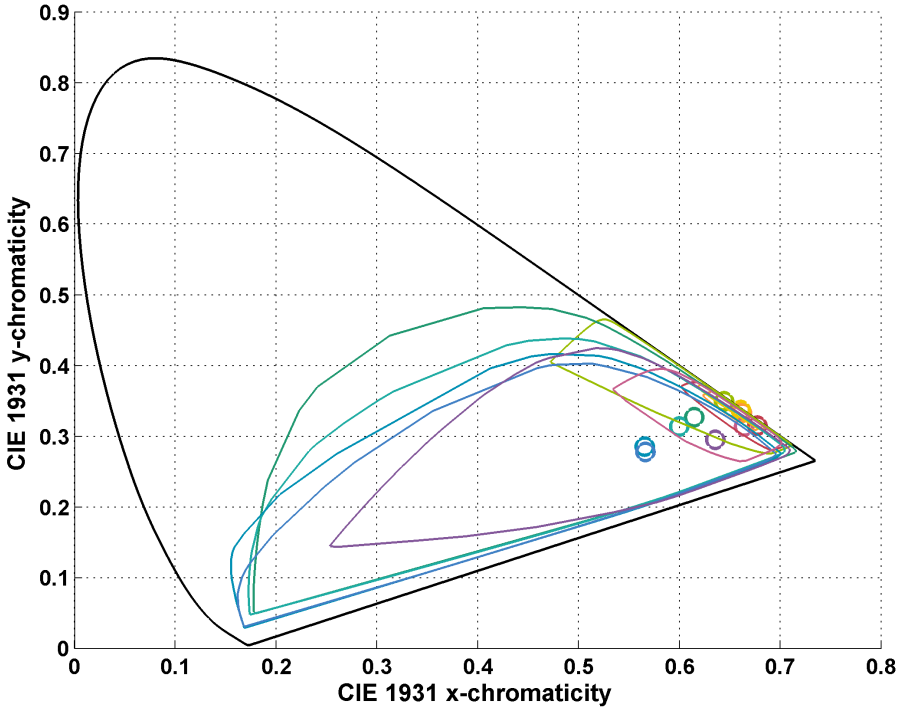

Figure 3.8: Chromaticity mismatch areas for the shifts from the neutral illuminant (N) to the green (G) illuminant. The circles are the chromaticities of the 10 odd-numbered Munsell papers from Fig. 2.9 under the second illuminant in each case.

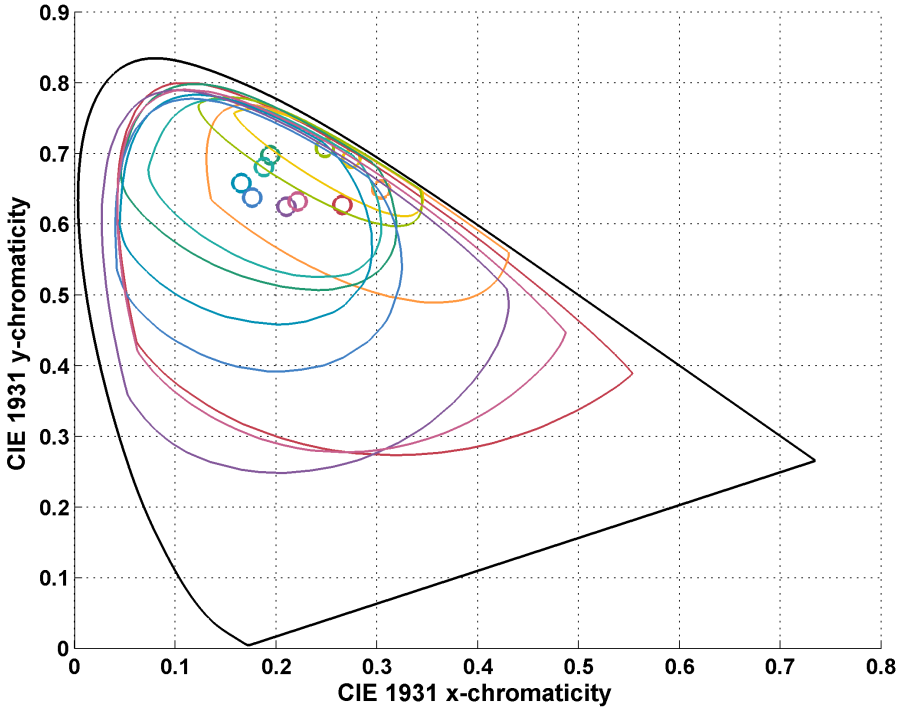

Figure 3.9: Chromaticity mismatch areas for the shifts from the neutral illuminant (N) to the red (R) illuminant. The circles are the chromaticities of the 10 odd-numbered Munsell papers from Fig. 2.9 under the second illuminant in each case.

3.3.1 Quantitative Assessment of Metamer Mismatch Volumes

In addition to the figures, it seems necessary here to clarify exactly how large the mismatching effect is. In order to assess the mismatching effect quantitatively, we computed the *metamer mismatch index* as suggested by Logvinenko et al. in Eq. 15 of [78], where it is defined as the ratio of the metamer mismatch volume to that of the object color solid.

In particular, let $\mathcal{R}$ denote the complete set of all spectral reflectance functions (i.e., $\mathcal{R} = \{0 \leq R(\lambda) \leq 1\}$). When $R(\lambda)$ changes over $\mathcal{R}$ the obtained color signals (i.e., $\Phi(\mathcal{R})$) form a convex volume in the colour signal space, which is referred to as the *object-color solid* [38].

For a point z in $\Phi_{p_1}(\mathcal{R})$ (i.e., the object color solid under illuminant p_1) that under illuminant p_2 disperses into a metamer mismatch volume $\rho(z; p_1, p_2)$ in $\Phi_{p_2}(\mathcal{R})$, the metamer mismatch index [5] is:

$$i_{mm}(z; p_1, p_2) = \frac{v(\rho(z; p_1, p_2))}{v(\Phi_{p_2}(\mathcal{R}))} \tag{3.1}$$

where $v(\rho(z; p_1, p_2))$ is the volume of $\rho(z; p_1, p_2)$, and $v(\Phi_{p_2}(\mathcal{R}))$ is the volume of the $\Phi_{p_2}(\mathcal{R})$ object-color solid.

The metamer mismatch indices in percent for different illumination conditions and Munsell papers are presented in Table 3.1. Note that also the metamer mismatch index of a Grey paper has been added into the last row of the table. Also, to make the results easier to follow, Fig. 5.17 graphically illustrates the trend of metamer mismatch indices for the shift from the neutral to other illuminants. As an example, the first entry in the table (i.e., 0.32%) stands for $i_{mm}(z_1; N, G)$, where z_1 is the CIE tristimulus values for Munsell paper #1 (Fig. 2.9) under the neutral (N) illuminant (Fig. 3.3).

As can be observed from the figures, the least amount of metamer mismatching occurs for NY and YN illuminant conditions, for which the metamer mismatch index averaged across all papers (excluding flat grey) is just 0.008%. On the other hand, the largest amount of mismatching is observed for the red illuminant for which the average metamer mismatch indices are 9% and 11% for the NR and RN conditions, respectively.

Note that, in 2D figures (Figs. 3.6, 3.7, 3.8, and 3.9), the mismatching effect looks much more serious than the numbers tabulated in Table 3.1. The first reason for this impression is that the metamer mismatch index is defined as a measure in 3D volume space, not in 2D or linear space. For example a hypothetical metamer mismatch volume having the same shape as the object color solid but 25% its size (in each dimension) would have a metamer

Munsell Paper	Illumination Condition							
	NG	NB	NY	NR	GN	BN	YN	RN
1	0.32	0.14	0.0024	5.4	1.1	0.69	0.0023	9.3
2	0.55	0.10	0.0019	6.3	1.2	0.53	0.0019	7.2
3	3.4	0.55	0.0064	7.5	4.1	1.3	0.0059	9.1
4	3.0	0.13	0.0047	5.0	2.3	0.54	0.0026	5.5
5	4.2	0.23	0.0048	5.4	3.9	0.70	0.0042	5.9
6	5.9	0.77	0.0088	11	5.7	1.4	0.0082	9.6
7	6.3	0.37	0.0056	8.5	4.9	0.86	0.0051	6.6
8	5.5	0.96	0.0072	5.6	6.1	1.3	0.0068	6.9
9	4.3	1.5	0.0089	6.1	6.3	1.9	0.0086	9.8
10	4.2	1.9	0.0090	6.3	6.7	2.1	0.0097	11
11	7.5	3.4	0.016	14	8.4	2.8	0.017	14
12	3.9	2.6	0.0102	7.0	6.8	2.5	0.011	13
13	3.6	2.9	0.0105	7.0	6.7	2.7	0.011	13
14	3.7	2.9	0.0110	7.5	6.9	2.8	0.012	14
15	3.5	2.8	0.0117	9.2	6.5	3.0	0.013	15
16	1.4	1.5	0.0075	7.8	4.0	2.0	0.0083	15
17	1.2	1.2	0.0074	9.9	3.4	1.9	0.0079	15
18	0.81	0.84	0.0064	10	2.7	1.6	0.0066	14
19	2.0	1.29	0.0078	22	4.0	1.9	0.0074	16
20	0.98	0.65	0.0051	15	2.9	1.4	0.0054	13
Flat Grey	13	4.1	0.021	47	9.7	3.1	0.018	20
Average Excluding Flat Grey	3.3	1.3	0.0077	8.8	4.7	1.7	0.0077	11.1
Average Including Flat Grey	3.8	1.5	0.0083	10.6	5.0	1.8	0.0082	11.6

Table 3.1: Metamer-mismatch indices in percent. Rows correspond to papers that are numbered as in Fig. 2.9. Columns correspond to illumination conditions.

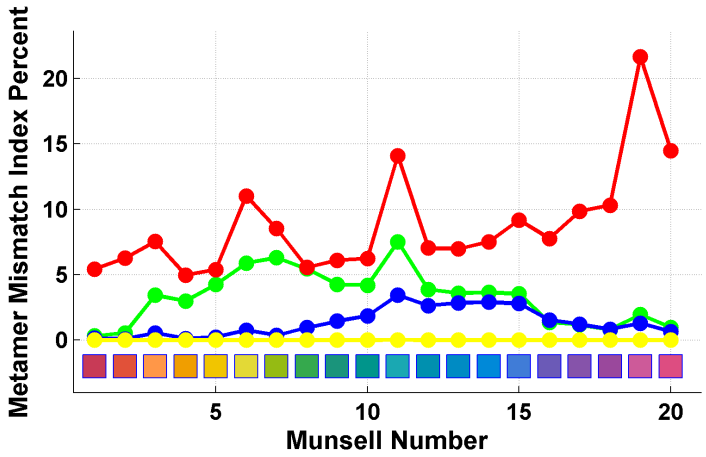

Figure 3.10: Metamer mismatch indices in percent (from Table 3.1) for the shift from the neutral to colored illuminants. The marker color indicates the color of illuminant. The abscissa is the number of the corresponding Munsell paper from Fig. 2.9. The color of squares on abscissa roughly represents each paper's color.

.

mismatch index of $(1/4)^3 \times 100 = 1.6\%$. If the ratios were measured in 2D, the index would have been $(1/4)^2 \times 100 = 6.25\%$. The other reason is that the metamer mismatch volumes might be thin in the luminance dimension and wide when projected in the chromaticity plane.

An important conclusion emerges here. The large size of metamer mismatch volumes and chromaticity mismatch areas shows that finding a correspondence between an object color seen under the first illuminant to when it is seen under the second is impossible.

In addition, the significantly large size of chromaticity mismatch areas leads to another interesting observation that is the chromaticity mismatch area for a single paper covers the chromaticities of many other papers. For example, for the blue illuminant, the metamer mismatch area of paper #2 covers the chromaticities of 18 of the 20 Munsell papers. For the green and red illuminants, some of metamer mismatch areas cover the entire set of 20 Munsell papers. This emphasizes the extent of metamer mismatching even more seriously.

The next section moves on to discuss the performance of human subjects on the same color matching experiment.

3.4 Analysis of Logvinenko & Tokunaga's Experiments and Prediction of the Results

The data used here originates from the color matching experiment performed by Logvinenko & Tokunaga [9]. They have provided an interesting investigation of human observers' performance but not in light of metamer mismatching. In this thesis, their results are analyzed in the context of metamer mismatching and a comparison of our findings with the von Kries adaptation transform is provided.

In Logvinenko & Tokunaga's experiment [9], for each paper seen under each of the illuminants, four observers were asked to find the matching paper (least dissimilar) seen under each of the six lights. Each observer repeats this task three times for each paper and illuminant pair. Throughout this thesis, for a given test Munsell paper, the average chromaticity of the matches taken over four observers and three repetitions is considered as the indicator of the observers' match.

Figs. 3.11, 3.12, 3.13, 3.14, 3.15, 3.16, 3.17, and 3.18 illustrate the asymmetric color matching experiment data in terms of the following items for different pairs of illuminants:

- The chromaticities of the 20 Munsell stimulus papers (Fig. 2.9) under the target lights (Fig. 3.2) indicated by circular dots connected by black lines;
- The averaged matches indicated by squares connected by red lines;
- The mismatch centroid chromaticities given the illumination condition indicated by asterisks connected by green lines;
- The von-Kries-coefficient-rule-based prediction for the given illumination condition indicated by diamonds connected by blue lines.

When a circle and square of the same color are close it means that for that test paper the observers (on average) have chosen a closely matching paper. On the other hand, a circle close to a square of a different color indicates a mismatch i.e., the observers chose a different Munsell paper under the matching illumination than the given test paper. Generally the corresponding circle and squares (the ones having the same color) must be overlapped in case of an exact match (i.e., perfect color constancy).

We computed the centroids of the metamer mismatch volumes and projected them onto the chromaticity diagrams. We will refer to these projected points as *mismatch centroid chromaticities* and approach the centroids as a possible vehicle for color prediction. Predictions were also made using the von Kries [79] coefficient-rule-based model of color constancy. Since the CIE 1931 color matching functions $\overline{x}(\lambda), \overline{y}(\lambda)$, and $\overline{z}(\lambda)$ are used as the color matching functions, the color signal is represented initially in CIE XYZ coordinates. In order to make predictions of a von Kries type, the XYZ are first transformed to a new set of primaries using the Hunt-Pointer-Estevez transformation as described by Hunt [80, 81]. This transformation is used, for example, as a component of the RLAB color appearance model [82]. The plots compare matches made by observers to predicted matches based on the mismatch centroid chromaticities and on the von Kries coefficient rule under 4 different illumination conditions.

Figs. 3.11 and 3.12 depict the asymmetric color matches made by observers in Logvinenko & Tokunaga's experiment as well as the predicted matches based on the mismatch centroid chromaticities and on the von Kries coefficient rule for the Neutral/Yellow and Yellow/Neutral conditions.

In particular, Fig. 3.11 demonstrates the NY condition: (i) The chromaticities of the papers under the yellow light indicated by circles connected by the black lines; (ii) The averaged matches indicated by squares connected by the red lines; (iii) The mismatch centroid chromaticities for the neutral/yellow (NY) illumination condition indicated by asterisks connected by the green lines; and (iv) The von-Kries-coefficient-rule-based prediction for the neutral/yellow (NY) illumination condition indicated by diamonds connected by the blue lines.

Similarly, Fig. 3.12 shows the analogous results for the yellow/neutral (YN) illumination condition. Note that all the data in Fig. 3.12 are from an entirely separate, though related, experiment than for Fig. 3.11. In Fig. 3.11 the squares connected by red lines indicate the matches made under the yellow illuminant when the stimulus papers are lit by the neutral illuminant. In Fig. 3.12 it is the other way around: matches are made under the neutral illuminant when the stimulus papers are lit by the yellow illuminant. Similarly, in Fig. 3.11 the mismatch centroid chromaticities and the von-Kries-based predictions are calculated for the NY condition, while in Fig. 3.12 they are calculated for the YN condition.

For the conditions involving the yellow illuminant, most of the circles and squares of the same color are either overlapped or quite close together. To assess the accuracy of the

Illuminant Condition	Neutral	Yellow
Neutral	92	77
Yellow	80	93

Table 3.2: The average exact match rates (i.e., percentage of cases when the same paper was chosen as the match) of symmetric and asymmetric illumination conditions involving Yellow and Neutral illuminants in Logvinenko & Tokunaga's experiment [9]. Rows and columns correspond to source and target illumination conditions.

matching quantitatively, for each illumination condition, the average exact match rate (i.e., percentage of cases when the same paper was chosen as the match) was also calculated. The average exact match rate for neutral-neutral and yellow-yellow, and neutral-yellow and yellow-neutral cases have been tabulated in Table 3.3. The rates for the asymmetric illumination conditions in this case are only slightly less than under symmetric illumination conditions, whether neutral-neutral or yellow-yellow. Both of the figures and the table are a good illustration of rather good color constancy in these cases, even when one illuminant was neutral and the other yellow.

Figs. 3.11 and 3.12 also show that for the NY and YN illumination conditions the observers' matches are generally more accurate than those provided by the von Kries prediction method or mismatch centroid chromaticities. But still, the predictions, are not too far from the observers' matches for both the NY and YN cases.

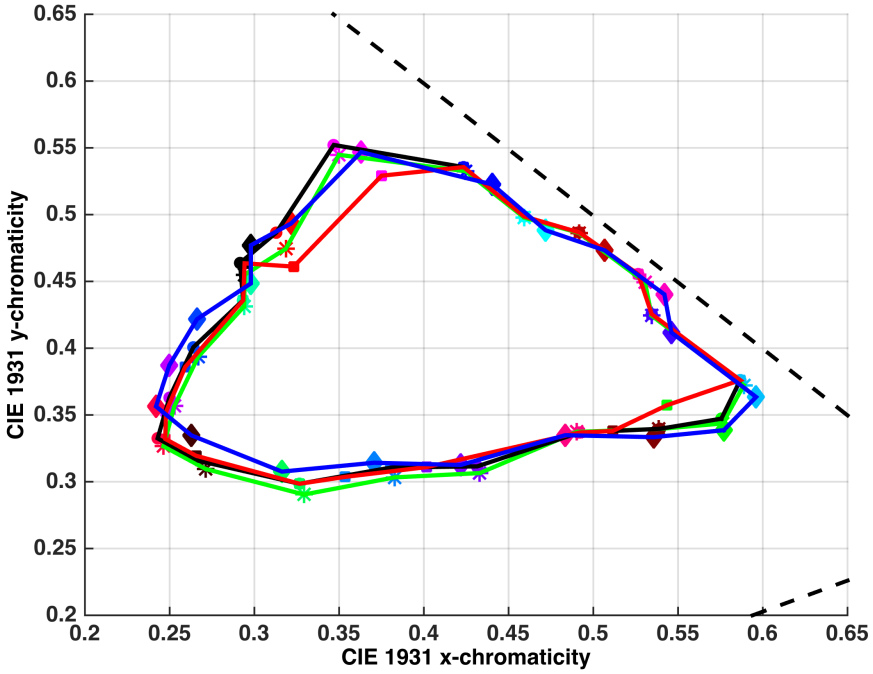

Figure 3.11: Comparison of asymmetric color matches made by observers in Logvinenko & Tokunaga's experiment to predicted matches based on the mismatch centroid chromaticities and on the von Kries coefficient rule for the Neutral/Yellow asymmetric color matching (see Figs. 3.12 through 3.18 for more). Circular dots connected by the black lines stand for the stimulus papers. The squares connected by the red lines represent the averaged observer matches. Asterisks connected by the green lines stand for the mismatch centroid chromaticities. Squares connected by the blue lines indicate the von Kries prediction. The dashed line is a segment of the spectrum locus.

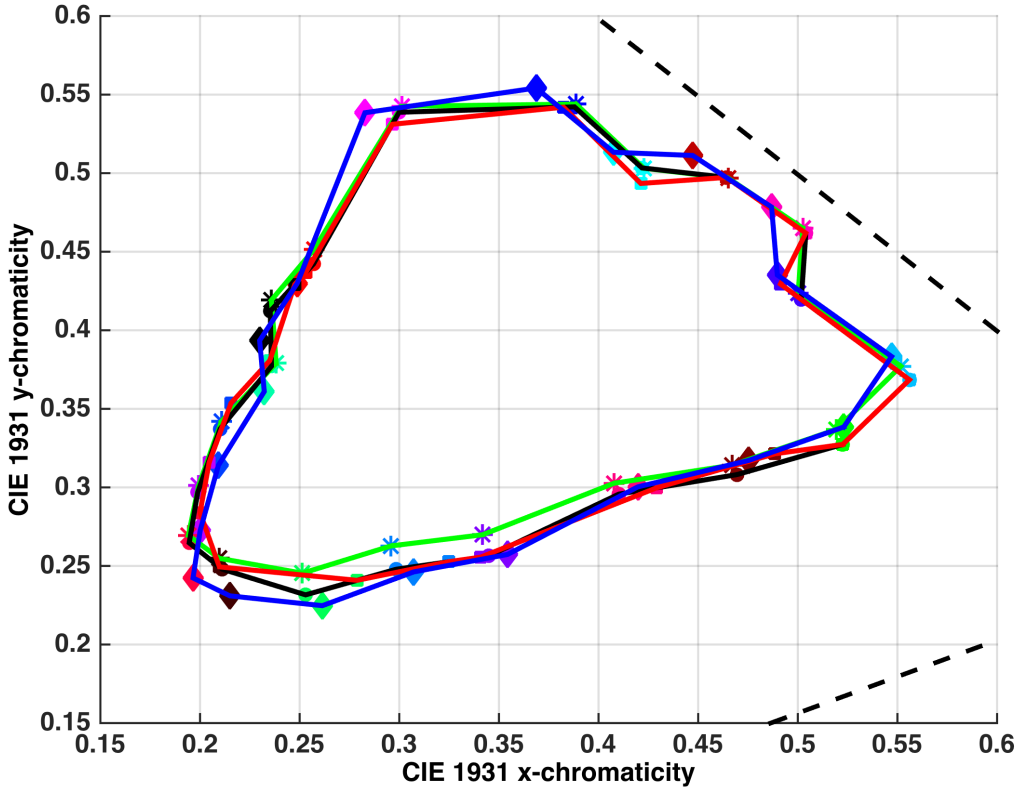

Figure 3.12: Continuation of the comparisons in Fig. 3.11. Yellow/Neutral asymmetric color matching. Note, however, that in here the squares connected by red lines indicate matches made under the neutral illuminant, whereas in Fig. 3.11 the matches were under a yellow illuminant and so forth.

In Figs. 3.13 through 3.18 that correspond to other illumination conditions it is evident that the accuracy of the predictions is much worse than the observers' matches. The von Kries predictions are especially bad because they are not guaranteed to be in the metamer set. It is somewhat surprising that this leads to the von Kries coefficient rule even predicting points falling outside the chromaticity diagram (i.e., it predicts non-existent lights). The mismatch centre chromaticities make reasonable predictions only for the NB and NG illumination conditions.

Section 3.4.1 studies the metamer mismatch volumes of flat grey under chromatic illuminants. This section presents more surprising results.

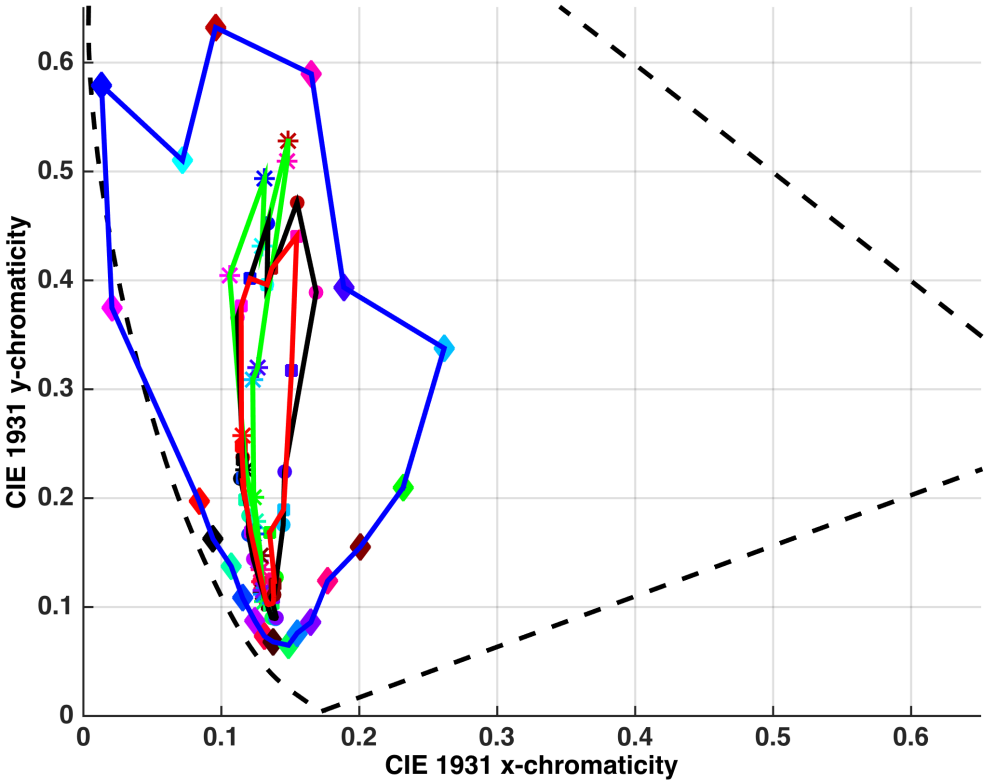

Figure 3.13: Continuation of the comparisons in Fig. 3.11. Neutral/Blue asymmetric color matching. Note that some of the von Kries predictions (blue curve) in fact fall outside the spectrum locus.

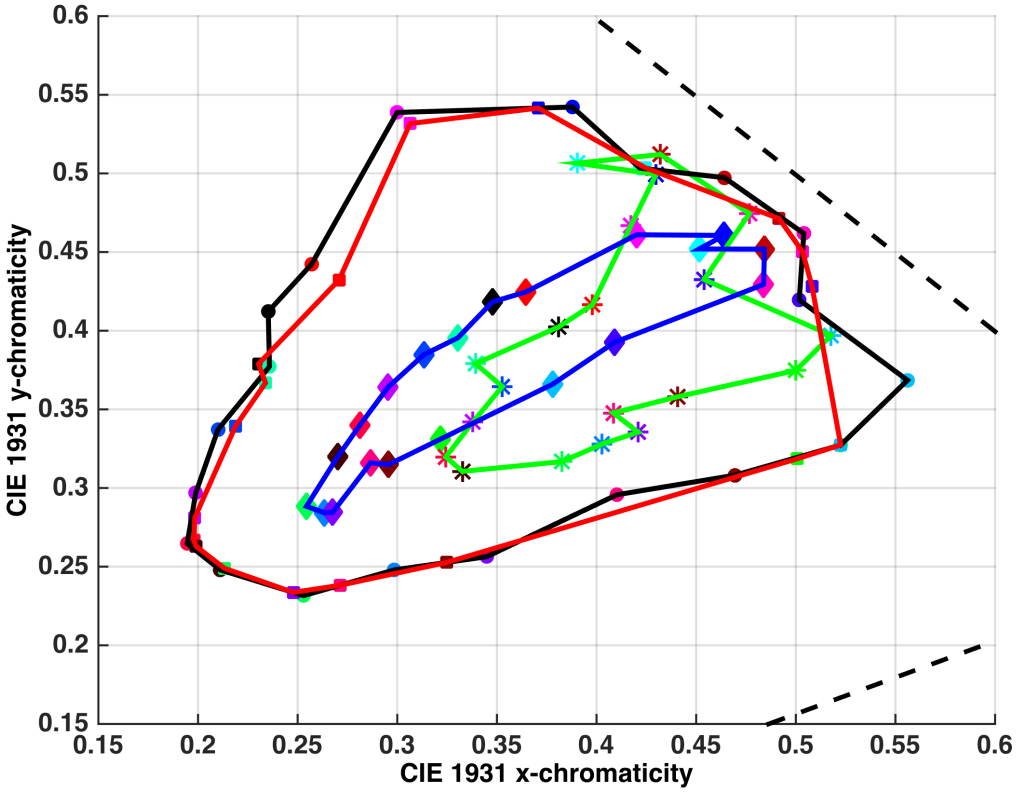

Figure 3.14: Continuation of the comparisons in Fig. 3.11. Blue/Neutral asymmetric color matching.

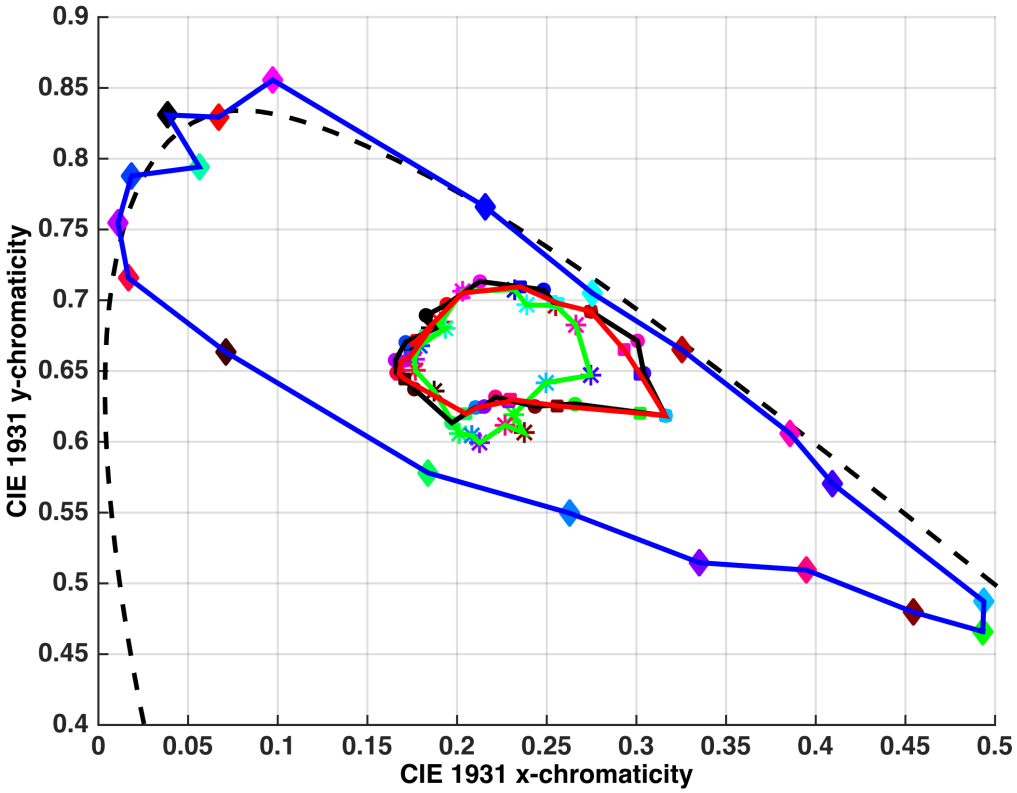

Figure 3.15: Continuation of the comparisons in Fig. 3.11. Neutral/Green asymmetric color matching where again some of the von Kries predictions (blue curve) fall outside the spectrum locus.

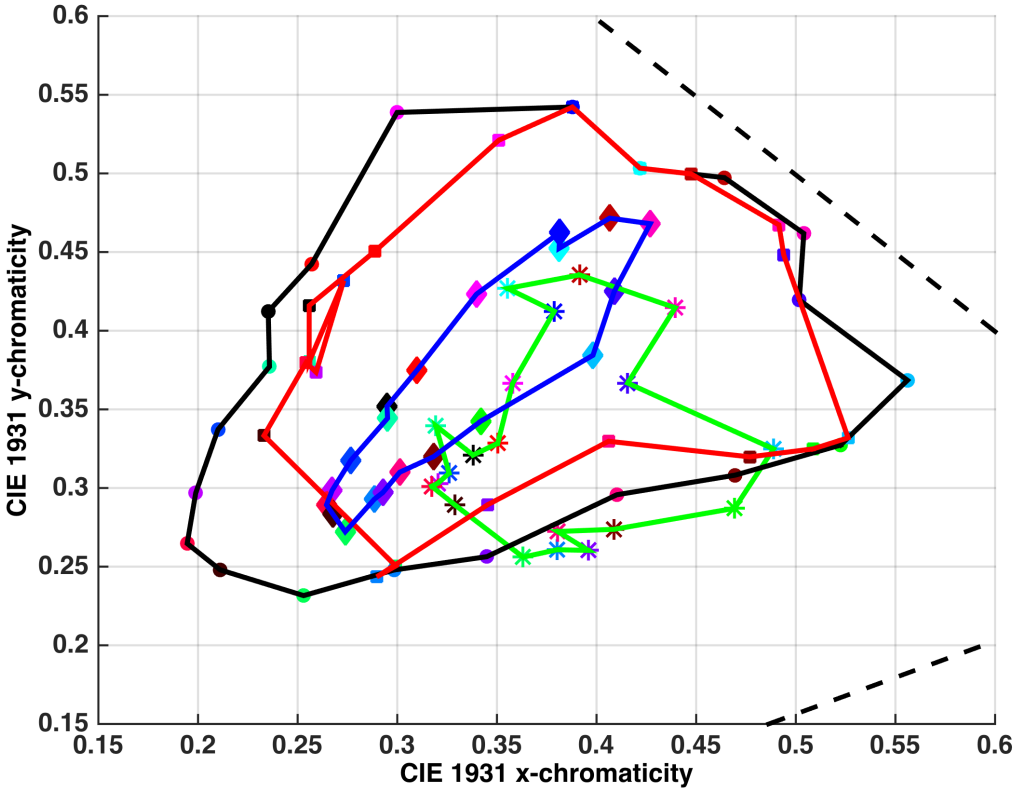

Figure 3.16: Continuation of the comparisons in Fig. 3.11. Green/Neutral asymmetric color matching.

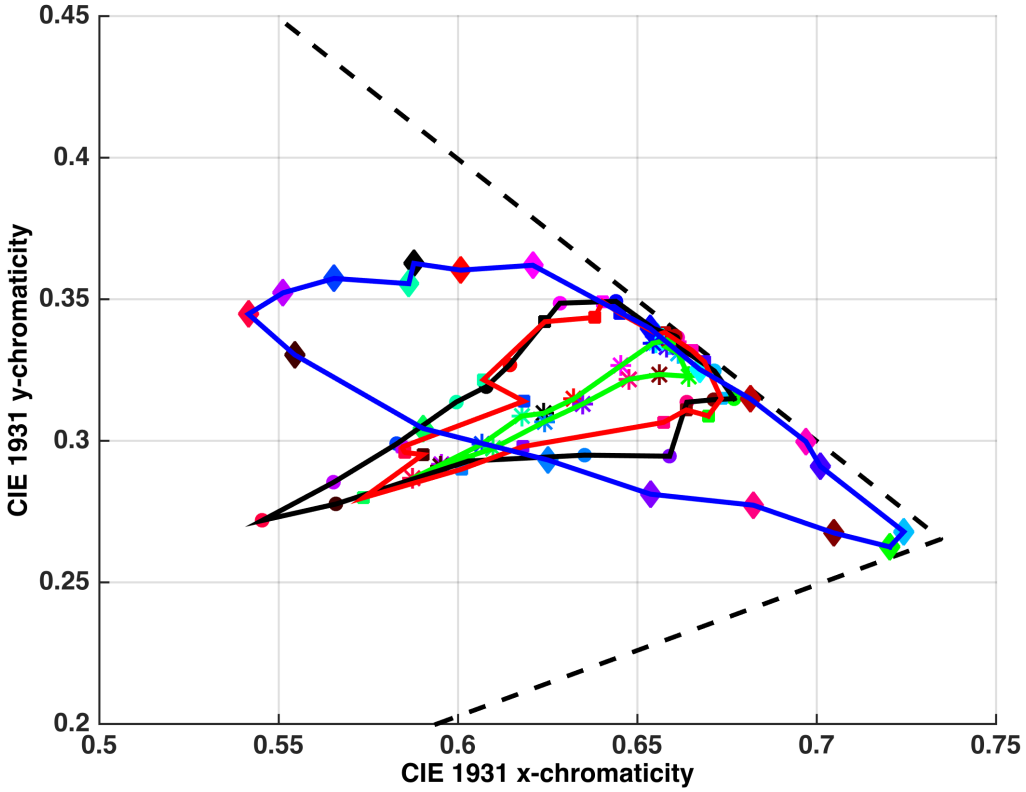

(a)

Figure 3.17: Continuation of the comparisons in Fig. 3.11. Neutral/Red asymmetric color matching.

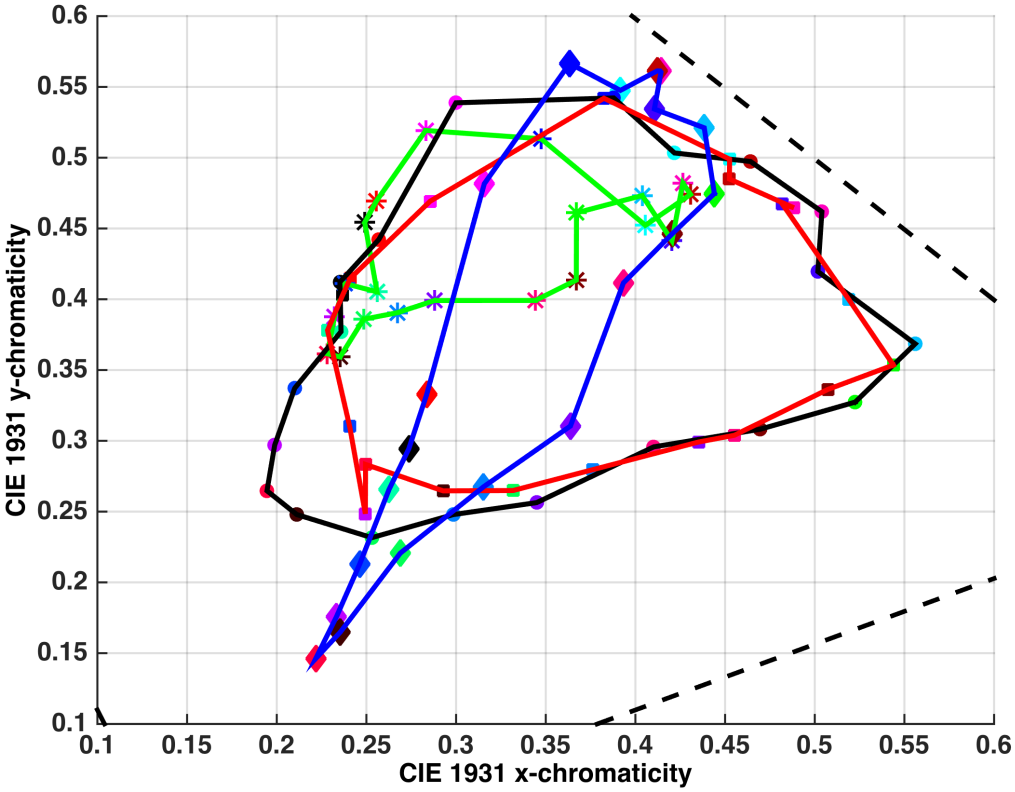

(a)

Figure 3.18: Continuation of the comparisons in Fig. 3.11. Red/Neutral asymmetric color matching.

3.4.1 Color Dispersion of Grey Patch

In this section we talk about the metamer mismatch volume that arises for the flat grey (i.e., $R(\lambda) = 0.5$) under different illuminant pairs. Fig. 3.19 demonstrates the seriousness of the problem for the GN illumination condition. This figure illustrates the object-color solids for the green and neutral illuminants (normalized to CIE Y=100), and the metamer mismatch volume for the flat grey (i.e., for the object-color solid centre) inside the latter. It is large with a metamer mismatch index of 9.7%. The corresponding chromaticity mismatch area is presented in Fig. 3.20.

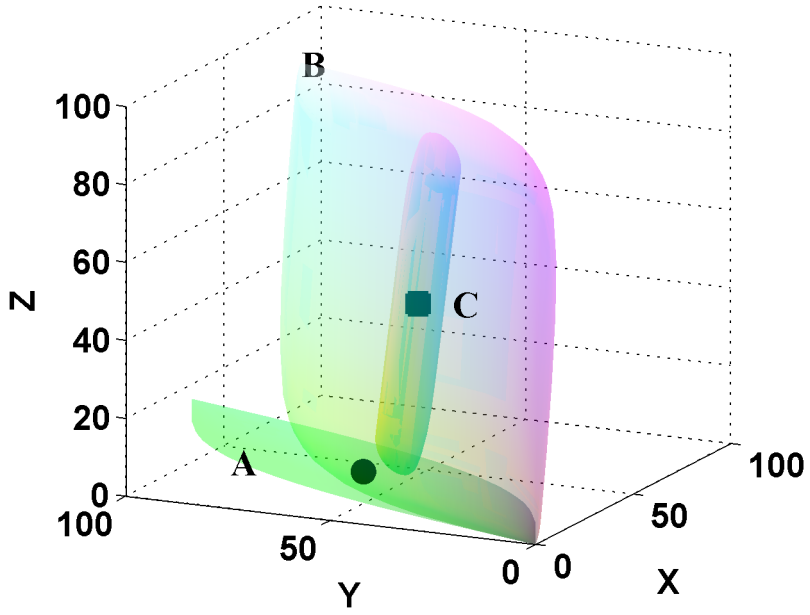

Figure 3.19: Label A indicates the object color solid under the green (G) illumination. B indicates the object color solid under neutral (N). The black dot indicates the XYZ of flat grey under G. The black square shows its XYZ under N. C indicates the metamer mismatch volume of the flat grey for a change in illumination from G to N.

Let us inspect this case in more detail. It is the metamer mismatch volume for the flat grey. It means that for each point inside this volume there exists a reflecting object such that, under the green illumination condition, it induces the same CIE XYZ tristimulus values as the flat grey, while, under the neutral illumination, it induces different CIE XYZ

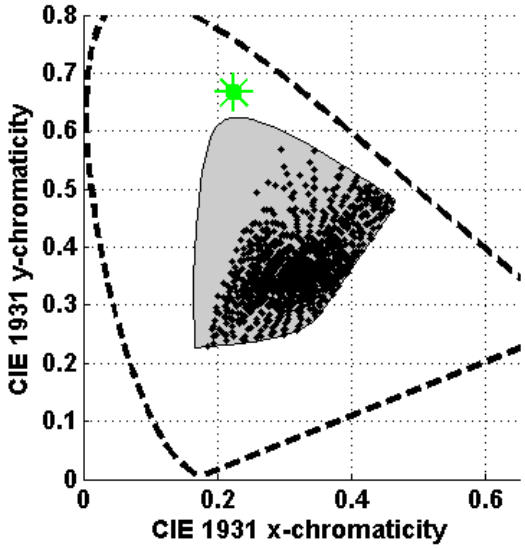

Figure 3.20: Chromaticity mismatch area (grey region) of the flat grey for the GN illumination condition. The green asterisk indicates the chromaticity of the flat grey reflectance under G. The black squares are the chromaticities of the Munsells falling inside the metamer mismatch area under N.

tristimulus values from the flat grey.

Given its large size, it would be interesting to know how different the color of the metamers of the grey sample can become under the neutral light. In other words, the goal is to compute the range of colors that a flat grey could lead to under the neutral light. To solve this problem we determined which of the 1600 Munsells papers from the complete Munsell glossy set [83] fall inside the metamer mismatch volume of flat grey under the GN condition presented in Fig. 3.19. In this figure, under the neutral light, 14% of the 1600 Munsell papers lead to CIE XYZ tristimulus values that fall into the metamer mismatch volume. These Munsell chips give an indication as to the range of colors the flat grey reflectance might become. Note that these Munsell chips themselves are not necessarily metameric to the flat grey under the green illumination, but indicate the colors that a potential metamer to the flat grey under the green light can become under the neutral light.

Fig. 3.21 renders a series of 20 Munsell papers from every other page of the Munsell book of color that were all found to lie inside the metamer mismatch volume for flat grey.

Note the high Munsell Chroma of these, which is 8 or higher for 14 or the 20 papers.

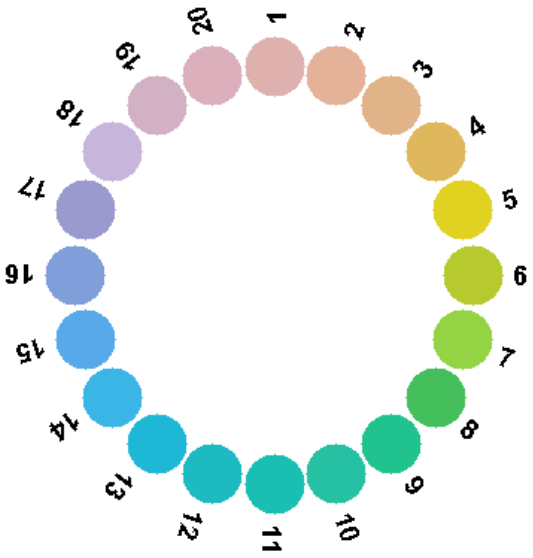

Figure 3.21: Pictorial representation of the 20 Munsell papers lying inside the metamer mismatch volume of flat grey for the GN illumination condition. The colors in the figure only approximate those of the actual Munsell papers. For the correct colors refer to the actual Munsell papers, which starting from 1 are: 5R 8/6, 10R 8/6, 5YR 8/6, 10YR 8/8, 5Y 8.5/12, 10Y 8/10, 5GY 8/10, 10GY 7/10, 5G 7/10, 10G 7/8, 5BG 7/8, 10BG 7/8, 5B 7/8, 10B 7/8, 5PB 7/8, 10PB 7/8, 5P 7/8, 10P 8/6, 5RP 8/6, and 10RP 8/6.

Therefore metamer mismatching results in a set of objects appearing as having the same color under one light, but a wide range of different colors under another light. In particular, it is shown that there exist 20 reflecting objects that, under the green illumination, all induce the same color as flat grey, but, under the neutral illumination, become the set of different saturated colors making a hue circle as in Fig. 3.21. This finding is surprising and suggests that the very concept of color constancy understood in its conventional terms cannot exist.

Generally, when talking about color constancy, the question to solve is whether the color of an object stays constant under a change to another illuminant. This is clearly an ill-posed problem, because this color depends on which object arises that color under the given two illuminants. Therefore, the concept of constancy can apply only to objects, not to colors. Fig. 3.21 shows that when the illumination is changed from green to neutral, the colors of

	Illumination condition			
	GN	BN	YN	RN
MMV	223 (13.9%)	71 (4.4%)	1 (0.001%)	452 (28%)
CMA	1293 (80.8%)	1132 (70.8%)	122 (7.6%)	1311 (81.9%)

Table 3.3: The number and percentage of Munsell papers falling within the metamer mismatch volume (MMV) and chromaticity mismatch areas (CMA) of flat grey for four illumination conditions involving N.

the objects that are all the same under the green illumination disperse into a wide range of colors. From a theoretical point of view, there is an infinite subspace of colors from which the carrier of the color must be chosen. Therefore the color signals under different illuminations cannot be unambiguously be related to another.

Contrary to expectations, 81% of Munsell papers fall into the chromaticity mismatch area (for the GN illumination condition). This proportion for Munsell papers falling into the metamer mismatch volume is 14%. The papers falling outside the metamer mismatch volume but within the chromaticity mismatch area differ from the corresponding objects only in luminance. This is a surprising finding that, if one ignores the color appearance variation induced by the luminance change, then one can claim that grey under the green light can turn into 81% of the possible colors from Munsell collection. Surprisingly, a very close proportion was found for the RN illumination condition(82%). Percentages for the other illuminants can be found in Table 3.3. The BN and RN cases have been illustrated in Figs. 3.22 - 3.23).

3.4.2 Color Dispersion of Chromatic Papers

Even for the NY illumination condition and the high-chroma papers used by Logvinenko & Tokunaga (Fig. 3.6) the chromaticity mismatch areas overlap and, for example, two of the papers, #15 and #14, fall inside the metamer mismatch volume of paper #15. In Logvinenko & Tokunaga's experiment, the asymmetric NY match for paper #14 was #14, and for #15 it was #15 i.e., the true papers.

The situation is even more extreme for other illuminant pairs. For instance, for the NR illumination condition the metamer mismatch volume of paper #10 covers 11 of the papers (#8 to #18).

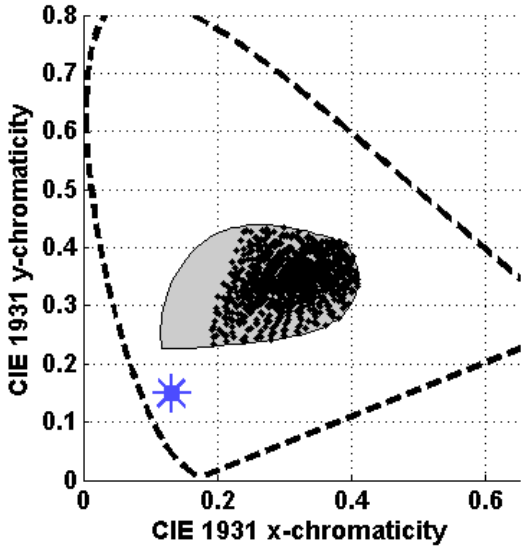

Figure 3.22: Chromaticity mismatch area (grey region) of the flat grey for the BN illumination condition. The green asterisk indicates the chromaticity of the flat grey reflectance under B. The black squares are the chromaticities of the Munsells falling inside the metamer mismatch area under N.

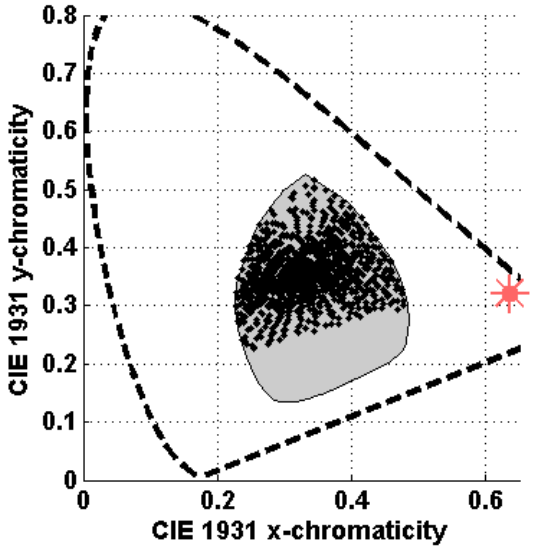

Figure 3.23: Chromaticity mismatch area (grey region) of the flat grey for the RN illumination condition. The green asterisk indicates the chromaticity of the flat grey reflectance under R. The black squares are the chromaticities of the Munsells falling inside the metamer mismatch area under N.

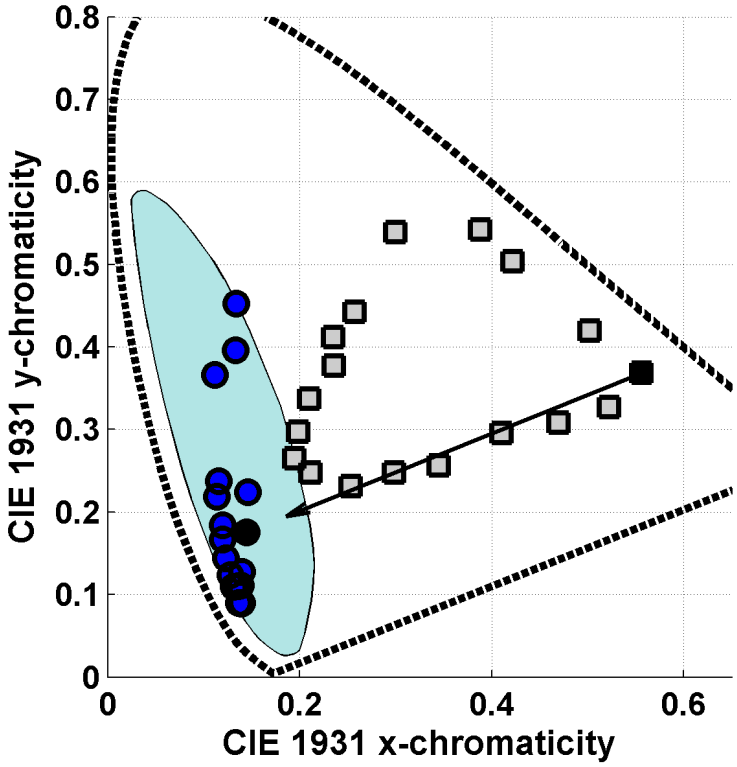

Figure 3.24: Chromaticity mismatch area for Munsell paper #2 for the NB condition. It covers the chromaticities of 18 of the 20 Munsell papers. Squares indicate chromaticities of Munsell papers under N. Dots indicate chromaticities of the papers under B. The black square and black dot correspond to paper #2.

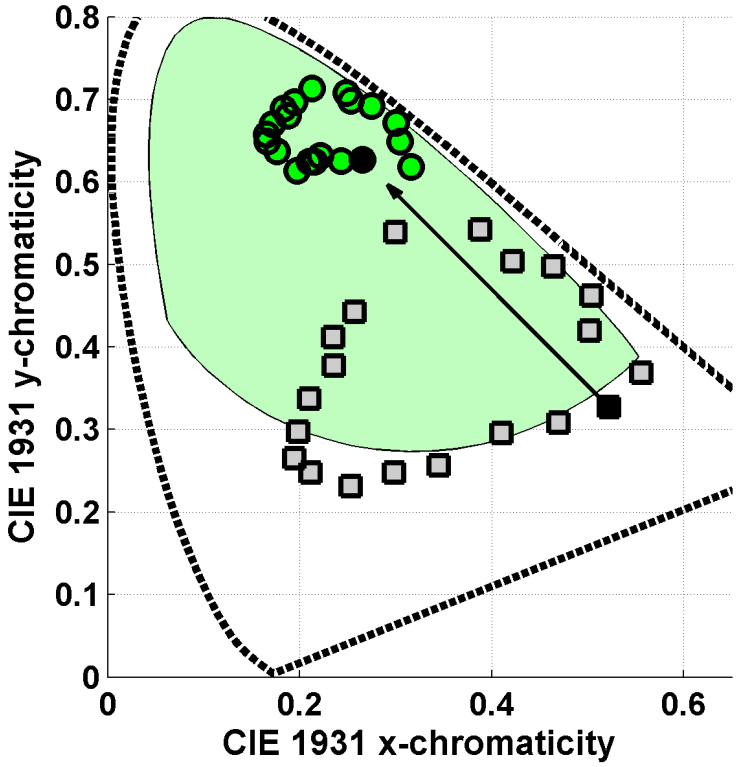

Figure 3.25: Chromaticity mismatch area for Munsell paper #1 for the NG condition. It covers the chromaticities of 20 of the 20 Munsell papers. Squares indicate chromaticities of Munsell papers under N. Dots indicate chromaticities of the papers under B. The black square and black dot correspond to paper #1.

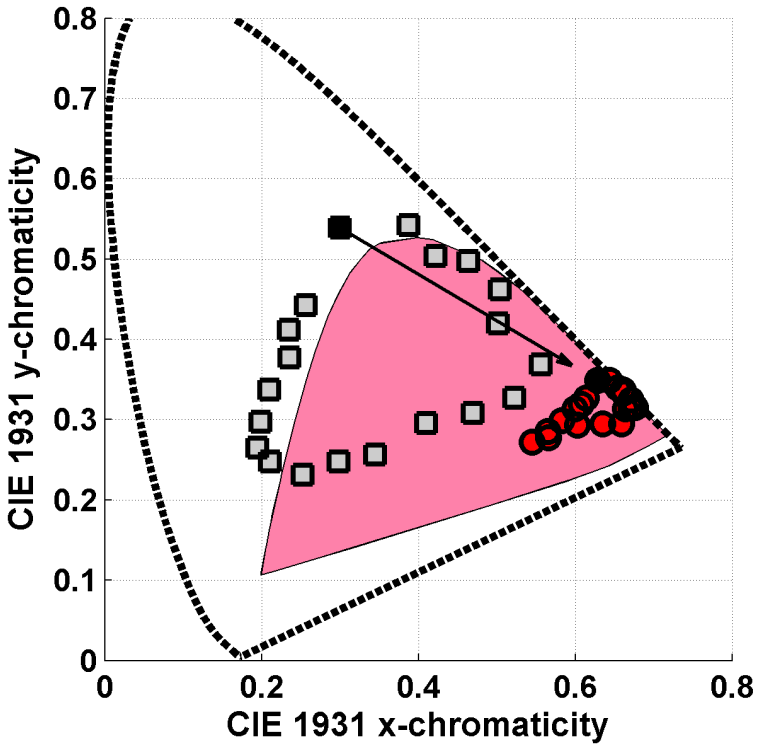

Figure 3.26: Chromaticity mismatch area for Munsell paper #8 for the NR condition. It covers the chromaticities of 20 of the 20 Munsell papers. Squares indicate chromaticities of Munsell papers under N. Dots indicate chromaticities of the papers under B. The black square and black dot correspond to paper #8.

The above analysis was in terms of 3D metamer mismatch volumes. However the mismatching is even more extensive in the 2D chromaticity plane as the metamer mismatch volumes turn out to be rather thin along the luminance axis.

Some of the metamer mismatch areas contain the chromaticities of nearly all 20 Munsell papers. For example, under the blue light, paper #2 disperses into a chromaticity mismatch area that covers 18 of the 20 Munsell papers shown in Fig. 3.24. Paper #1 under the green light (Fig. 3.25) and paper #8 under the red light (Fig. 3.26) disperse into chromaticity mismatch areas covering all 20 Munsell papers.

Therefore, ignoring the luminance dimension, the color inconstancy problem is more severe. Because one can select 20 objects of identical color when lit by the neutral light that will be dispersed into 20 different colors lying on a hue circle when lit by the red (or green) light that will differ from those depicted in Fig. 2.9 only in that some colors will have a different luminance factor.

3.5 Conclusion

A set of experiments on metamer mismatching was done forming an essential part of the joint project with Logvinenko, Funt, and Tokunaga [1], that tries to reconsider the concept of color constancy due to the extreme degree of metamer mismatching. Metamer mismatching was shown to be extremely large and result in a set of objects appearing as having the same color under one light, but a wide range of different colors under another. In addition to the large size of metamer mismatch volumes for different Munsell papers under chromatic illuminants, an interesting scenario originally suggested by Logvinenko was found: In some illumination conditions, there exist 20 *natural* reflecting objects that, under the first illumination, all induce the same color as flat grey, but, under the second illumination, become a complete set of different saturated colors *making a full hue circle*.

In other words, there can be several objects resulting in the color seen under the first light. The essential question is: which object is the actual carrier of that color? From a theoretical point of view, there is an infinite subspace of colors from which the carrier of the color must be chosen. Therefore the color signals under different illuminations cannot be unambiguously related to another. This finding is rather surprising and suggests that the very concept of color constancy understood in its conventional terms needs to be reconsidered.

Chapter 4

Metamer Mismatching as a Measure of the Color Rendering of Lights

4.1 Summary

We propose a new method for evaluating the color rendering properties of lights. The new method uses the degree of metamer mismatching for the CIE XYZ corresponding to flat grey (constant reflectance of 0.5) quantified in terms of the metamer mismatch volume index proposed by Logvinenko et al. [5]. A major advantage of this method is that unlike many previous color rendering indices it does not depend on the properties of a chosen set of representative test objects. A version of this chapter has been published in proceedings of the Congress of the International Colour Association (AIC 2015) [25].

4.2 Introduction

Evaluating the color rendering properties of lights is an important issue in the lighting industry. It is well known that the colors of objects viewed under lights of identical correlated color temperature may look very different under the different lights. Several color rendering indices have been used in the past. Perhaps the most widely used is the CIE color rendering index CIE Ra [84], which is based on computing the average color difference induced by the

illuminant for a fixed set of reflectances. The CIE Ra is a color fidelity measure. There have also been preference-based measures such as Judd's flattery index [85] and Thornton's color preference index [86], in which the focus is more on the subjective preferability of lights. More recently Smet et al. [10, 87] have suggested a memory-color-similarity measures, Sa and Rm (a non-linear scaling of Sa), based on how a light affects the colors of a sample set of familiar objects (green apple, banana, orange, lavender, Smurf, strawberry yoghurt, sliced cucumber, cauliflower, Caucasian skin, sphere painted Munsell N4 grey) in comparison to the average subjects memory of the colors of those objects as determined by psychophysical experiments.

The CIE Ra is defined in terms of a reference illuminant and the test light being evaluated. For test lights of CCT less than 5000K the reference illuminant is chosen to be the ideal blackbody radiator of the same CCT. For test lights with CCT of 5000K or greater, the reference light is chosen to be the standard CIE daylight D-series illuminant of the same CCT. There are 8 test color samples (Munsell papers) whose color differences, after an adjustment for chromatic adaptation, under the test and reference lights are evaluated.

The CIE Ra has been widely criticized, especially for the evaluation of LED lights. One of the key problems with it is that it is based on measuring the color differences that arise across a small sample of 8 (sometimes generalized to 14) colored papers. Not only may such a sample not represent what the color differences for all other possible surface reflectances may be, it also gives manufacturers the opportunity to tune the spectra of their lights to perform well on the standard sample.

Variants of metamer mismatching have been previously used as a measure of the color rendering of daylight simulators. In particular, the CIE Metamerism index is a measure based on calculating the average color difference between each of a set of reflectance pairs that are initially metameric matches under the reference light but not necessarily metameric matches under the target light. However, this method is limited to the specific reflectances used. Whitehead et al. [22] extend this general idea by using a large number of randomly generated metameric spectra and then assessing the fraction of them that noticeably change color when the illuminant changes. In contrast, the method proposed here is based on measuring the size of the metamer mismatch volume, which is the volume of color signals (i.e., XYZs) induced under the second light by the set of all theoretically possible reflectances that make a metameric match under the first light.

4.3 Metamer Mismatch Index

The background for the proposed measure of color rendering is the concept of metamer mismatching. Consider a color signal XYZ (in CIE standard coordinates) observed under a first light. Metamer mismatching refers to the fact that the possible XYZ that might be observed under a second light is only constrained to lie within a convex volume of possible XYZ values. The size of the volume depends on the XYZ and the lights involved; however, the volume for the XYZ of flat grey is the largest. The metamer mismatch volume represents the range of possible XYZ that can arise under the second light and so provides a measure of how varied the XYZ under the second light can be–the less the variation, the better the color rendering.

The boundary of the metamer mismatch volume can be calculated using the code of Logvinenko et al. [5], which finds the maximum amount of metamer mismatching that can occur for any given XYZ and pair of lights. Fig. 4.1 shows an example of the metamer mismatch volume for the XYZ of flat grey for a change in illuminant from an ideal 2900K blackbody radiator to a 2900K LED. Even though the two illuminants are of the same CCT the metamer mismatch volume is quite large: it fills a sizable fraction of the entire object-color solid. The object-color solid is the set of all possible XYZ that can arise for all possible reflectance functions $R(\lambda)$ (i.e., $0 \leq R(\lambda) \leq 1, 380 \leq \lambda \leq 780nm$). The metamer mismatch volume depicted is the set of all possible XYZ that could arise under the second illuminant for any reflectance that is metameric to flat grey under the first illuminant.

Since both the object color solid and the metamer mismatch volume change with the second illuminant, we consider size of the metamer mismatch volume relative to the size of the object color solid it generates. In particular, both scale with the intensity of the second illuminant. Hence, the metamer mismatch volume index (MMVI) (see equation 3.1 on page 39 for a formal definition) for a given XYZ and a pair of illuminants is defined as the ratio:

$$MMVI = \frac{volume\ of\ the\ metamer\ mismatch\ volume\ for\ the\ given\ illuminant\ pair}{volume\ of\ the\ object\ color\ solid\ under\ the\ second\ illuminant} \tag{4.1}$$

Note that this ratio is also independent of any linear transformation of the color coordinate space and so will be the same for any LMS space obtained as a linear transform of CIE XYZ as for CIE XYZ itself.

In terms of color rendering, the larger the MMVI, the poorer the color rendering of the

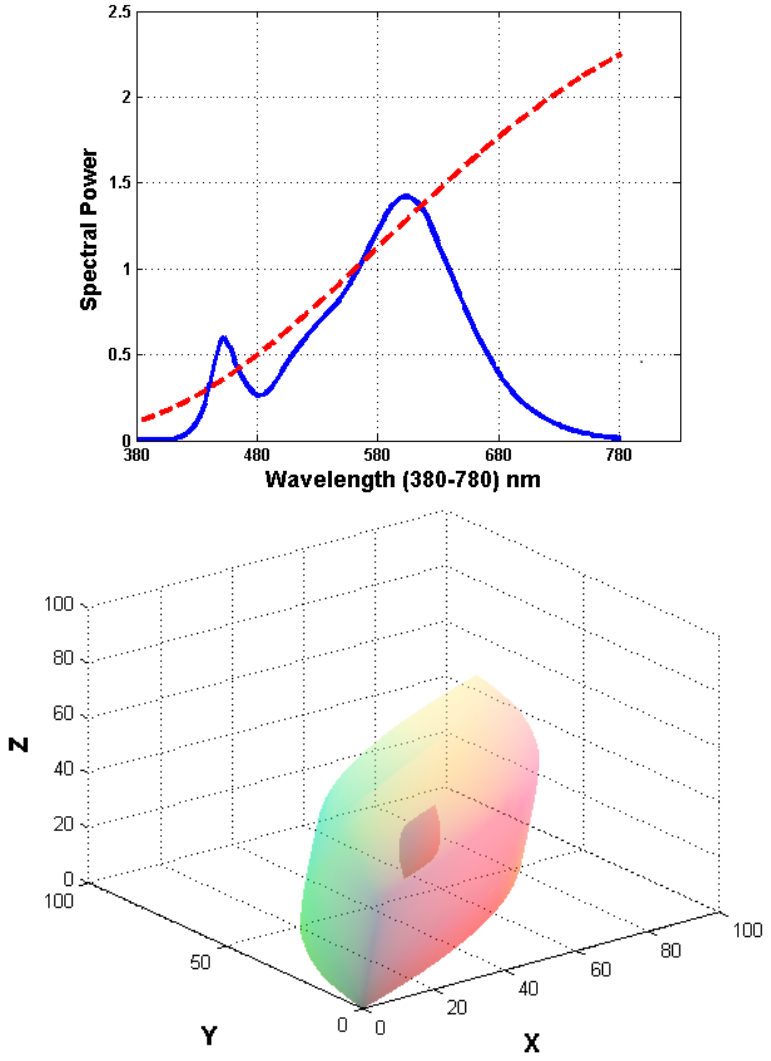

Figure 4.1: Top: Spectra of a 2900K LED (blue) and that of an ideal 2900K blackbody radiator (dashed red). Bottom: Metamer mismatch volume (for the XYZ of flat grey lit by a 2900K blackbody) shown inside the object-color solid of the 2900K LED for the case when the illuminant is changed from the blackbody to the LED. Coordinates are the CIE 1931 XYZ space.

second light relative to the first light is likely to be. Since the MMVI is volume based, we find it more intuitive to consider $MMVI^{(1/3)}$. The Metamer Mismatching color Rendering Index (MMCRI) is then defined as:

$$MMCRI = (1 - \sqrt[3]{MMVI}) \times 100 \tag{4.2}$$

where the MMVI is for that of the XYZ of flat grey under the first illuminant. The scaling by 100 is simply to make its range match that of the CIE CRI Ra.

4.4 Comparison to Other Color Rendering Indices

The MMCRI can be computed for any pair of illuminants as a measure of the color rendering properties of the second light relative to the first. However, the CIE CRI Ra for a light L is defined relative to an ideal illuminant (blackbody or D-series) of the same CCT as L. For comparison with Ra we use the same choice of ideal illuminant as the first illuminant when computing the MMCRI of L.

We have computed the MMCRI and CIE Ra for several light spectra across a range of CCTs and technologies and compared them. In particular, we measured the spectra of several commercially available LED lights and also used the spectra of the CIE standard illuminants. When plotted as in Fig. 4.2 we see a good correlation between the two indices– an indication that the MMCRI behaves reasonably–but with notable differences for some illuminants. It is exactly such differences that the proposed new method is intended to reveal. In particular, we note that F11 and F12 have a high CIE Ra but a low MMCRI. Since F11 and F12 are both dominated by three narrowband peaks, it seems unlikely that their color rendering properties are very good, and this is confirmed by the MMCRI.

As second test, we make use of the set of lights Smet et al. included in their paired comparison experiment [10]. Smet's set contains: a halogen lamp (H), a fluorescent lamp approximating CIE F4 (F4), a Neodymium incandescent lamp (Nd), a Philips Fortimo LED module with a green filter (FG), an RGB LED lamp (RGB) and a LED cluster (LC) optimized to obtain a high Sa, all of which are plotted in Fig. 4.3 The various color rendering measures are compared in Table 4.1.

The results in Table 1 show a general agreement in ranking across all the methods in that the same lights are given ranks 3 (FG), 5 (F4), and 6 (RGB). Ra and CQSa rankings for all six lights are identical. MMCRI agrees with Ra and CQSa on 4 of the rankings, but

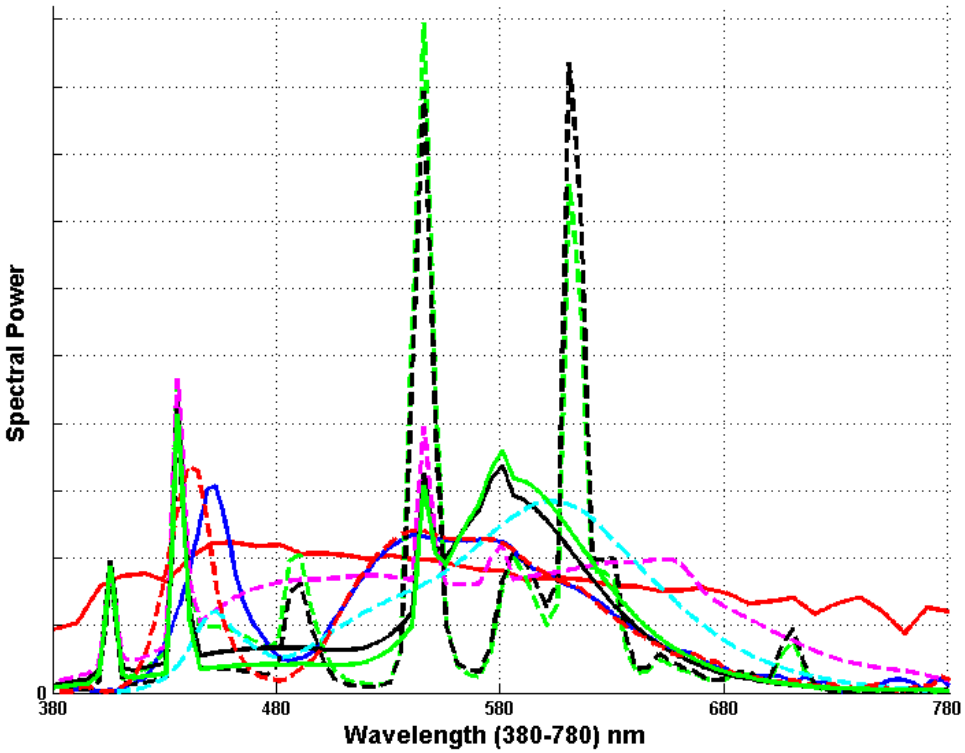

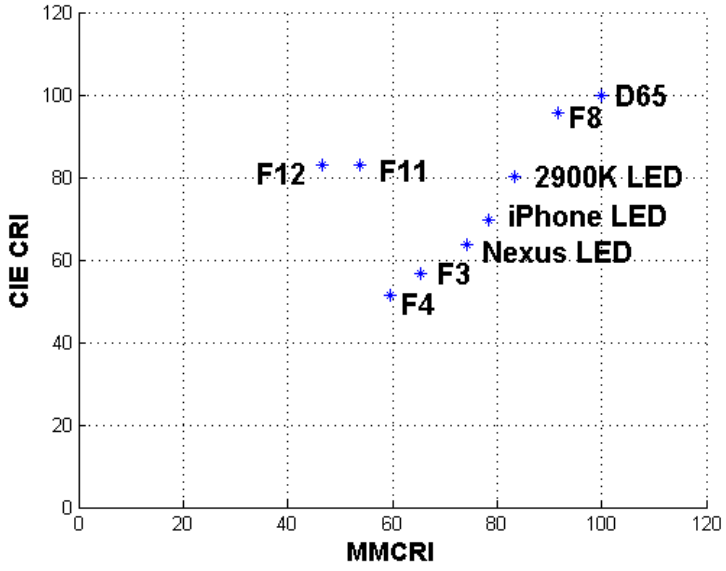

Figure 4.2: (2a) The illuminant spectra used for testing: D65 (red), F3 (black), F4 (dashed green), F8 (dashed magenta), F11 (dashed green), F12 (dashed black), 2900K LED (dashed cyan), Nexus LED (dashed red) and iPhone LED (blue). (2b) CIE CRI versus MMCRI

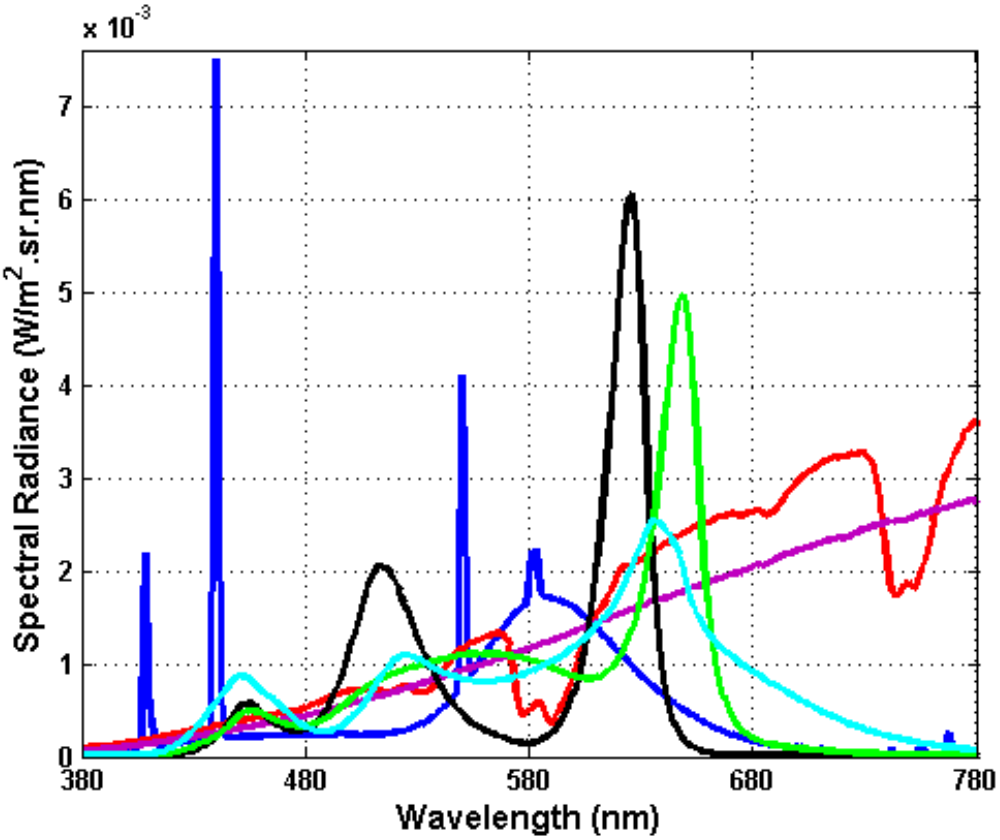

Figure 4.3: The spectral power distributions of the six light sources (provided by Smet) and used for the comparison of the color rendering measures listed in Table 1. The lights (see text) are F4 (blue curve), FG (green), Nd (red), LC (cyan), H (purple) and RGB (black).

Light source	Sa		CIE Ra		NIST CQSa		MMCRI	
	Sa	Rank	Ra	Rank	CQSa	Rank	MMCRI (Grey)	Rank
F4	0.6672	5	52.8	5	53.9	5	55.53	5
FG	0.7787	3	80.6	3	87.2	3	83.99	3
Nd	0.7841	2	73.7	4	87.0	4	89.46	2
LC	0.7899	1	81.0	2	89.0	2	74.95	4
H	0.7662	4	99.6	1	97.2	1	99.64	1
RGB	0.6548	6	31.9	6	50.5	6	49.30	6

Table 4.1: Comparison of Color Rendering Measures. Measures include: Sa, memory color similarity [10], Ra (CIE CRI), NIST CQSa Color Quality Scale [11], and MMCRI (proposed metamer mismatch index). The data reported in the table for Sa, CIE CRI Ra and NIST CQSa are quoted from Table 2 of Smet et al. ([10], page 26235). The MMCRI results were computed based on the MMVs for a change from the blackbody radiator having the CCT of the given illuminant to the given illuminant. The lights were approximately equal illuminance ranging from 239 to 251 lux, and CCT ranging from 2640 to 2878. The spectra of the lights are plotted in Fig. 4.3.

swaps the rankings of Nd and LC, ranking Nd 2nd, in agreement with Sa and the reported popularity of Neodymium lights in terms of their sales. Since LC is an LED cluster designed to optimize Sa, it is not surprising that it is ranked first by Sa. Similarly, since H is a halogen light closely approximating a blackbody radiator, it is also not surprising that MMCRI, Ra and CQSa all rank it first since they assume that a blackbody is the ideal light source in terms of color rendering. This is an assumption that Smet et al. [88] challenge, but as yet no general alternative has been proposed.

It should be noted that the Sa rankings in Table 1 do agree with the preference and fidelity rankings reported in Table 3 of Smet et al. ([10], page 26237). However, one problem Table 1 reveals about the Sa measure is that it ranks many of the lights almost identically. In particular, FG, Nd, LC and H all have Sa values of 0.778 +/- 0.012. Effectively, Sa divides the lights into just two groups: (FG, Nd, LC, H) and (F4, RGB). In comparison, with MMCRI there are clear differences in the scores such that there are four distinct groups: (F4, RGB), (LC), (FG, Nd) and (H).

4.5 Conclusion

A new measure of the color rendering properties of lights is proposed based on the general concept of metamer mismatching. The amount of metamer mismatching–effectively the range of theoretically possible color signals arising under a second light–is taken as an indicator of the difference in the color rendering properties of the second light relative to the first. The greater the degree of metamer mismatching, the poorer the color rendering is considered to be. Previous color rendering indices have been based on a fixed selection of object reflectances. Although there have been attempts to optimize the set of test reflectances [89] a finite set will always remain the source of some bias. In comparison, the proposed method, through the calculation of the metamer mismatch volume, takes into account all theoretically possible reflectances [1].

[1]The author wishes to thank Kevin Smet for providing his spectral data.

Chapter 5

Towards a new Object-Color Space

5.1 Summary

A robust and accurate hue descriptor that is useful in modeling human color perception and for computer vision applications is explored. The hue descriptor is based on the peak wavelength of a Gaussian-like function (called a wraparound Gaussian) and is shown to correlate as well as CIECAM02 hue to the hue designators of papers from the Munsell and Natural Color System color atlases and to the hue names found in Moroney's Color Thesaurus. The new hue descriptor is also shown to be significantly more stable under a variety of illuminants than CIECAM02. The use of wraparound Gaussians as a hue model is similar in spirit to the use of subtractive Gaussians proposed by Mizokami et al., but overcomes many of their limitations. This chapter has led to publications in the IEEE Transactions on Pattern Analysis and Machine Intelligence, 2015, Color and Imaging Conference, Society for Imaging Science and Technology, 2013, and 12th International Colour Congress, International Colour Association, 2013 [24, 29, 30].

5.2 Introduction

Hue is an important component of color appearance. We explore [24, 29, 30] a representation of hue for object colors in which, for a given color stimulus arising from the light reflected by an object, its hue is represented in terms of the peak wavelength of a Gaussian-like reflectance function metameric to that stimulus. Conventionally, hue is represented in terms of the angular component of the polar representation of a color in an opponent color space

such as CIELAB in which two of the axes are roughly orthogonal to lightness [4]. Although these color spaces may work well for a fixed illuminant, they can lead to unstable results when the illuminant is changed. The source of this instability is that CIELAB and related spaces account for the illumination via von Kries scaling, but von Kries scaling can be subject to very large errors [1]. This is a serious problem even when the scaling is applied in a 'sharpened' [67] basis as in CIECAM02 [59].

To overcome this problem, we explore [24, 29, 30] basing hue on the peak wavelength of a metameric Gaussian-like reflectance from Logvinenko's pseudo-color atlas as the representation of hue.

Similar, but somewhat different, Gaussian-based representations of hue have been proposed previously by Mizokami et al. [54, 90] and further explored by O'Neil et al. [91] and shown to explain the class of hue shifts known as the Abney effect. As well, Mizokami et al. have shown that Gaussian-like functions can be used to provide reasonable 3-dimensional models of reflectance spectra.

The tests reported below demonstrate that the proposed hue descriptor correlates well with the hue designators for the 1600 glossy Munsell papers and the Natural Color System samples. It also correlates well with the hue names used in Moroney's Color Thesaurus. In addition, to correlating well with the hue categories in these datasets, we find that it is considerably more consistent under different illuminants than CIECAM02 hue. Given these features, we show that it is also useful for automatic hue classification in digital images.

5.3 Background

The Gaussian-like representation for hue used here has its roots in Logvinenko's illumination-invariant object-color atlas[49, 52]. Logvinenko [52] defines a set of Gaussian-like spectral reflectance functions defined in terms of their scaling, k_m, standard deviation, σ_m, and peak wavelength, μ_m. The functions are defined in equations 2.11, 2.12, 2.13, and 2.14, in page 20. Although the equations defining them are piecewise and a bit complex, intuitively they simply describe a Gaussian centered at μ_m on the hue circle.

Note that Logvinenko's wraparound Gaussians are neither the same as the "inverse Gaussians" defined by Golz [55] nor the same as the "subtractive Gaussians" defined by Mizokami [54] or others [53]. In the inverse Gaussian representation, illuminant and reflectance spectra are characterized by three parameters: the spectral centroid, spectral curvature, and

scaling factor. The inverse Gaussian spectrum $P(\lambda)$ is defined as:

$$P(\lambda) = \gamma . e^{-C(\lambda - T)^2} \tag{5.1}$$

where γ is the scaling factor, C is the curvature and T is the centroid. Note that depending on the sign of the quadratic term these functions are either Gaussians or the reciprocals of Gaussians.

In another Gaussian model, Mizokami et al. [54] investigate reflectance spectra defined by varying the amplitude α, ϕ (peak), and standard deviation σ of the function:

$$S(\lambda) = \begin{cases} \alpha e^{-0.5\left(\frac{\lambda - \phi}{\sigma}\right)^2} & for\ \alpha \geq 0 \\ 1 + \alpha e^{-0.5\left(\frac{\lambda - \phi}{\sigma}\right)^2} & for\ \alpha < 0 \end{cases} \tag{5.2}$$

We will refer to these two cases as Gaussians of type G^+ and type G^-, respectively.

Note that Logvinenko's wraparound Gaussians are neither the same as the "inverse Gaussians" defined by Golz [55] nor the same as the "subtractive Gaussians" defined by Mizokami [54] or others [53].

5.3.1 Comparison to other Gaussian Representations

Figure 5.1 shows an example of an inverse Gaussian, a subtractive Gaussian, a wraparound Gaussian metamer and a rectangular metamer for the spectral reflectance of Munsell paper 7.5 PB 5/8.

The gamuts of chromaticities in the CIE 1931 XYZ tri-stimulus space for subtractive Gaussians, inverse Gaussians, and wraparound Gaussians under illuminant CIE D65 are compared in Figs. 5.2, 5.3, and 5.4. To compute the gamut for the wraparound Gaussians, we simply set the scaling factor$k = 1$ and stepped through all the possible standard deviations, σ, in steps of 10nm, and central wavelength, μ, in steps of 2nm, and computed the CIE1931 xy-chromaticities arising under CIE D65. In the case of wraparound Gaussians, there is no need to consider scaling factors $k < 1$ since the chromaticity for a given kμ does not depend on k. In computing the gamut for subtractive Gaussians there are two main cases. For the $\alpha > 0$ case, $\alpha = 1$ is used since for $\alpha > 0$ the chromaticity is independent of

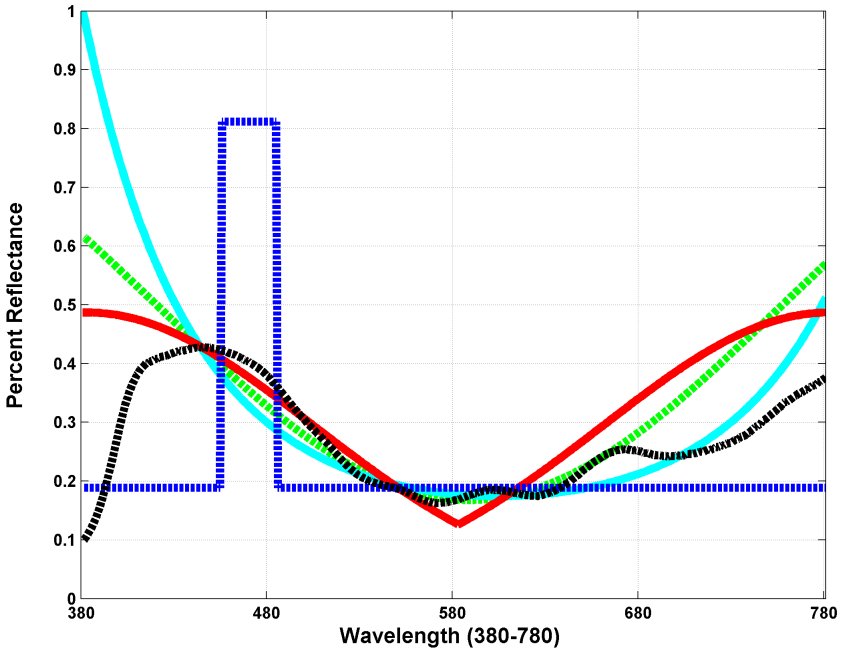

Figure 5.1: The spectral reflectance of Munsell 7.5 PB 5/8 (dashed black) illuminated by D65 and metameric inverse Gaussian (solid cyan), subtractive Gaussian (dashed green), rectangular (dashed blue), and wraparound Gaussian (solid red) spectra. Figure is copied from [8].

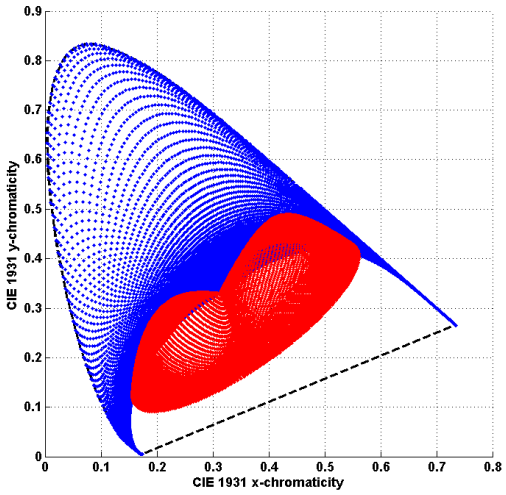

Figure 5.2: The gamut of chromaticities obtained using only true reflectance functions (i.e., all values in [0,1] across the visible spectrum) for all subtractive Gaussian reflectance functions forming either peaks (blue) or troughs (red).

α. For the $\alpha < 0$ case, chromaticity does depend on α so values $-1 < \alpha < 0$ are sampled, but any resulting reflectance with values not in [0, 1] is excluded. Similarly, for inverse Gaussians the gamut is computed by stepping through its parameters. For positive curvatures ($C > 0$) the chromaticity is independent of γ so γ was fixed to $\gamma = 1$. However, for negative curvatures ($C < 0$) we regularly sample γ and exclude all reflectances that are not physically realizable.

The chromaticity gamut of the subtractive Gaussians is shown in Fig. 5.2, where it is clear that the gamut does not fill the entire chromaticity space. To reach these missing chromaticities requires subtractive Gaussians having negative values. Similarly, for inverse Gaussians Fig. 5.3 reveals two gaps in the gamut of chromaticities. The gamut of the wraparound Gaussians, however, includes the entire chromaticity space, as shown in Fig. 5.4.

In summary, the gamuts of chromaticities in the CIE 1931 XYZ tri-stimulus space for subtractive Gaussians, inverse Gaussians, and wraparound Gaussians show that neither subtractive Gaussians nor inverse Gaussians can cover the entire chromaticity gamut when the functions are restricted to being reflectance functions (i.e., all values in [0,1]). On the other hand, wraparound Gaussians do cover the entire chromaticity gamut.

Given an XYZ, the parameters of the subtractive and wraparound Gaussians can be

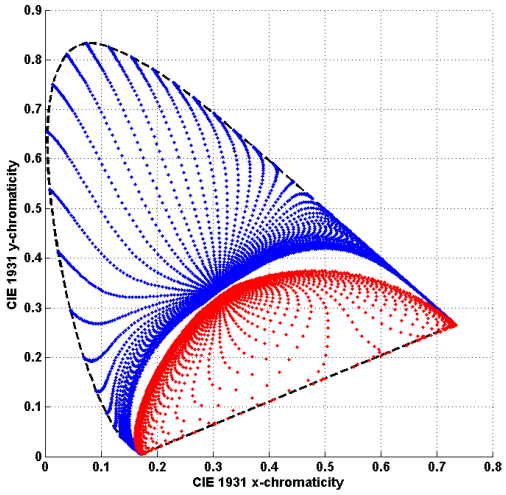

Figure 5.3: The gamut of chromaticities obtained using only true reflectance functions (i.e., all values in [0,1] across the visible spectrum) for all inverse Gaussian reflectance functions with positive curvature (blue) or negative curvature (red).

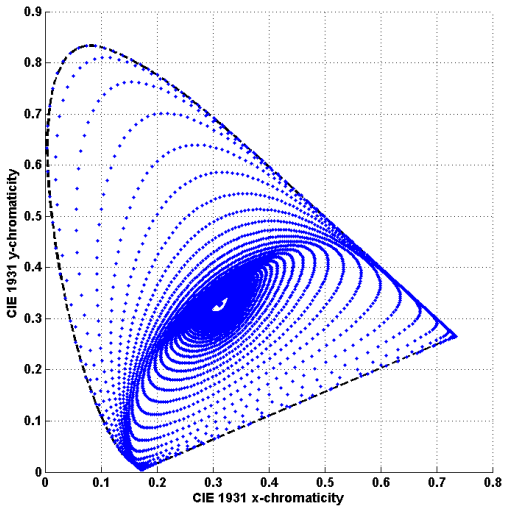

Figure 5.4: The gamut of chromaticities obtained using only true reflectance functions (i.e., all values in [0,1] across the visible spectrum) for all wraparound Gaussian reflectance functions.

found via a two-parameter optimization, explained in the next section, that is independent of the scaling parameter; however, in the case of inverse Gaussians such a decomposition is not possible, so a much more difficult, three-parameter optimization is required. Given that inverse Gaussians are more difficult to compute and do not cover the chromaticity gamut, we do not consider them further here.

5.3.2 Other Gaussian Hue Descriptors

The work of Mizokami et al. [54, 90] and O'Neil et al. [91] has shown that Gaussian spectra may provide a good model of hue in the case of lights. However, there are some difficulties that arise in applying Gaussians of the subtractive type as a descriptor of hue for objects. In particular, the G^+ and G^- chromaticity gamuts overlap (see Fig. 5.2) quite significantly. For the wraparound Gaussian, however, there is no such overlap (see Fig. 5.4). The overlap for the subtractive Gaussians implies that for a given XYZ we might find metameric Gaussians of both type G^+ and G^-. Searching for just such a case, we easily found the example shown in Fig. 5.5. The fact that there are two metameric (up to 4-digit precision) subtractive Gaussians differing significantly in their peak wavelengths (380nm versus 621nm) poses a serious impediment to using them as a hue correlate. A similar search of the space of wraparound Gaussians found no two different sets of KSM parameters resulting in metameric wraparound Gaussians. Note that this is excluding 'white' and 'black' reflectances, where there is a well-known singularity–What is the hue of black, grey or white? Of course, not finding such a case does not mean that it might still not exist, so we are not claiming that the wraparound Gaussians are better than subtractive Gaussians in this regard, only that there clearly is a problem with subtractive Gaussians.

Another difficulty with subtractive Gaussians is that the scaling parameter affects the chromaticity of the resulting Gaussian differently depending on the type. In the case of type G^+ changing has no effect on the resulting chromaticity; however, for type G^- changing α results in a different chromaticity. Gaussians of type G^- of the same chromaticity will differ in their ϕ and σ. Fig. 5.6 shows an example. Whether it is preferable for a hue descriptor to remain the same for all XYZ of the same chromaticity or instead differ with the scaling can be debated, but it makes little sense for it to do both. In the case of wraparound Gaussians, all XYZ of the same chromaticity are always represented by Gaussians of the same σ and μ.

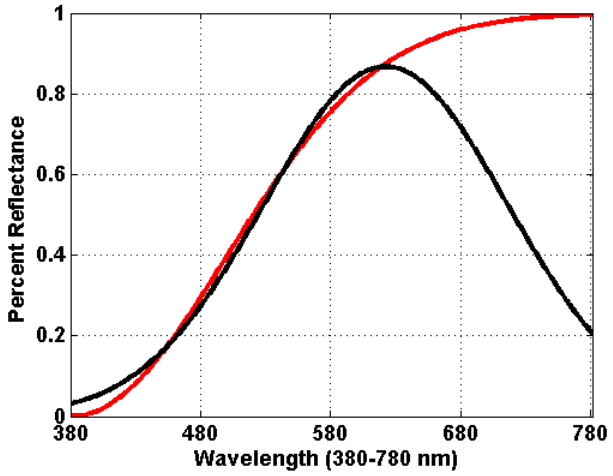

Figure 5.5: Two metameric subtractive Gaussian functions, one of type G^+ (black) and type G^- (red). Under D65, both these reflectances have CIE XYZ values (63.69, 64.97, 20.95). Parameters (α, σ, ϕ) defining these G^+ and G^- spectra are (0.8670, 93.5557, 621.1427) and (-1.0000, 118.4952, 380.0106), respectively.

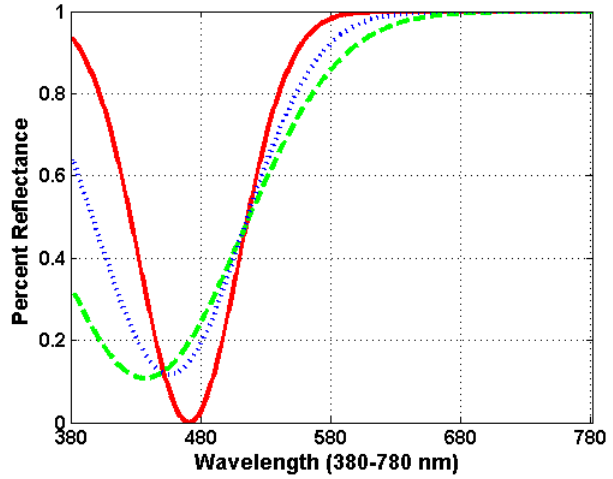

Figure 5.6: Three G^- spectra having the same chromaticity but with their XYZ differing by a scale factor. Red curve: G^- spectrum having XYZ = (77.9114, 79.2585, 20.8546). Dotted blue curve: 0.95 x XYZ. Dashed green curve: 0.9 x XYZ. Parameters (α, σ, ϕ) defining these three G spectra are (1.0000, 38.5005, 469.9995), (0.8835, 56.2495, 455.2326) and (0.8922, 74.5022, 436.1658), respectively. Although the three curves appear to intersect at a common point in the plot, they in fact do not.

5.4 Calculating colour descriptors by optimization

Computing the parameters of a wraparound Gaussian that is metameric to a given colour signal is analogous to computing those of the corresponding rectangular metamer, and we have applied the same basic interpolation approach developed by Godau et al. [92] for rectangular metamers. An alternative strategy could be to use a variant of the k-d tree approach of Finlayson et al. [93], which basically uses as a structured look up table without further optimization to get quick, but not necessarily as accurate results. Our implementation is available online. Given a colour signal ϕ_0 under a given illuminant, the KSM coordinates specify a wraparound Gaussian reflectance that is metameric to ϕ_0 under that illuminant.

To determine the KSM colour descriptor corresponding to colour signal, ϕ_0, requires finding (k, σ, μ) minimizing the angular error:

$$E(k, \sigma, \mu) = arccos \frac{\phi_0 . \phi(k, \sigma, \mu)}{|\phi_0||\phi(k, \sigma, \mu)|} \tag{5.3}$$

between ϕ_0 and the colour signal of the wraparound Gaussian specified by (k, σ, μ) under the given illuminant. This at first would appear to require a 3-parameter optimization; however, since the angular error does not depend on the scale factor k, it can be reduced to an optimization involving only two parameters by setting $k = 1$. With only 2 parameters, it becomes possible to build a table relating (σ, μ) pairs to sensor responses $\phi(1, \sigma, \mu)$ that can then be used to find good initial values σ and μ for the optimization. In many cases, these initial values are sufficiently accurate and no further optimization is required. Once σ and μ are determined, the scaling k can be calculated directly as:

$$E(k, \sigma, \mu) = arccos \frac{\phi_0}{\phi(1, \sigma, \mu)} \tag{5.4}$$

As an example of the KSM descriptors, we computed the XYZ under D65 for each pixel in the "Fruits and Flowers" multispectral image obtained from the Joensuu spectral database [94]. The approximate sRGB rendering of this image is shown in Fig. 5.7.a.

Unfortunately, when solving for the parameters of either the inverse Gaussians or the subtractive Gaussians it is not possible to break the three-parameter problem into a two-parameter sub-problem and a one-parameter sub-problem, so the required optimization is much more computationally intensive.

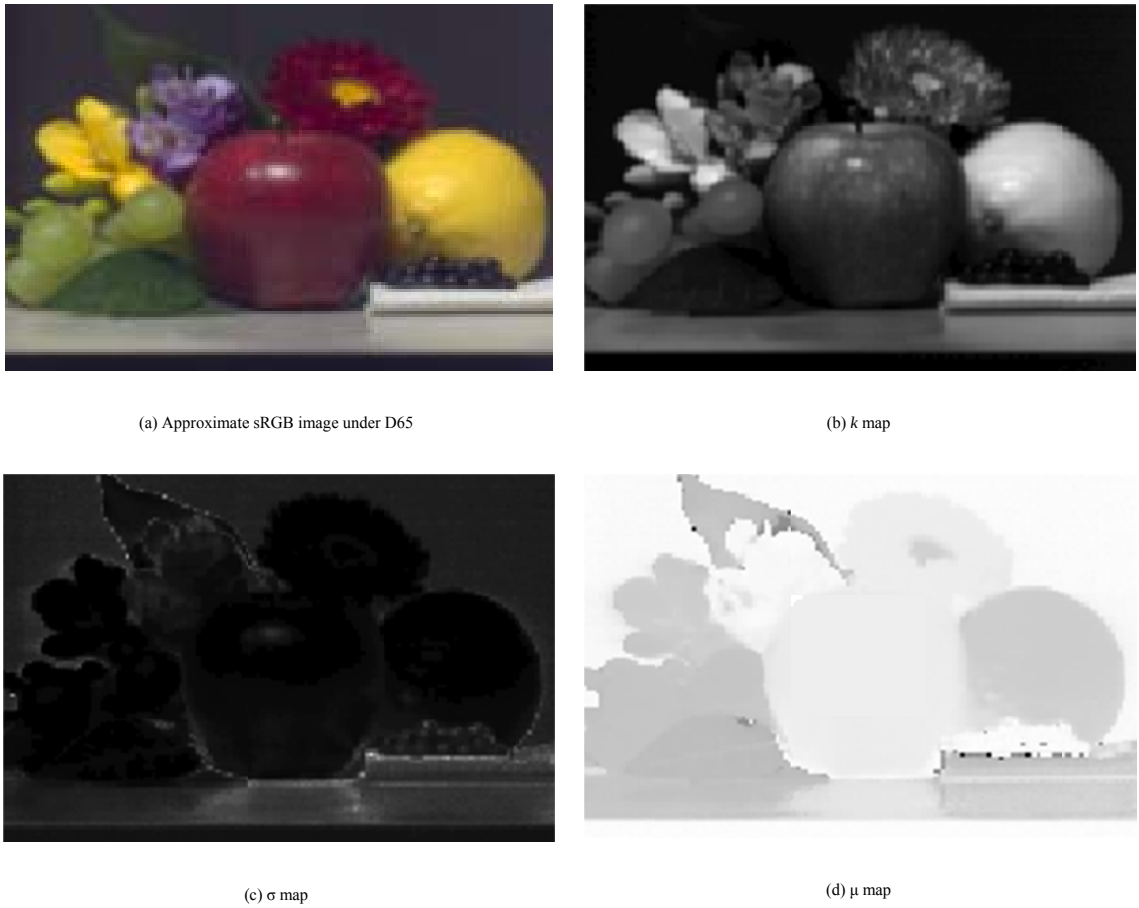

(a) Approximate sRGB image under D65

(b) k map

(c) σ map

(d) μ map

Figure 5.7: KSM colour descriptor (k, σ, μ) maps for the Fruits and Flowers scene under D65. (a) sRGB rendering; (b) map of k values; (c) map of $log(\sigma)$ values; (d) map of μ values. Panel (d) illustrates the correspondence between μ and hue.

5.5 Tests and Results

We address two main questions: How well does the peak wavelength, μ, correlate with hue? And is μ, as a hue descriptor, robust to changes in the illumination? In terms of the first question we compare how well it describes the hues of the Munsell papers, the NCS papers, and the hues Moroney tabulated in a Color Thesaurus [95] that were derived from a large, crowd-sourced, color-naming experiment [96, 97]. In terms of the second question, we compare the shift an illuminant change induces in μ and compare it to the shift it induces in CIECAM02 hue. The results show that μ is an accurate hue descriptor that is more robust relative to the illuminant than CIECAM02 hue.

Note that in what follows, the plots are of hue versus $log(\sigma)$ or hue versus CIECAM02 saturation, but all the analysis is strictly in terms of hue. Possible perceptual correlates of σ will be investigated elsewhere. In the present context, it is simply being used to spread out the hue plots nicely.

5.5.1 Munsell Dataset

As a comparison of KSM μ and CIECAM02 hue correlates, we consider the set of 1600 papers of the Munsell glossy set. This follows a similar analysis by Logvinenko [49] of his ADL hue correlate λ. We synthesized the XYZ tristimulus values of all 1600 papers based on the Joensuu Color Group spectral measurements [94] under the illuminant C using the 2-degree color matching functions and then computed the corresponding KSM (μ), ADL (λ), and CIECAM02 hues. When calculating the CIECAM02 appearance attributes, we adopted the parameters suggested for the "average surround" condition and full adaptation. Figs. 5.8, 5.9, and 5.10 illustrate that qualitatively both KSM μ and CIECAM02 hue appear to correlate quite well with the plotted hues (approximate hues since published version is on an uncalibrated print/display) of the 1600 papers of the Munsell glossy set. The correlation is indicated by the fact that the colors of the same hue align vertically. The plot of ADL λ, on the other hand, shows some intermingling of the reds and yellows. Here and in what follows, the units of λ and μ will be reported in degrees, rather than nanometers for consistency with CIECAM02 for which hue is specified in degrees around the hue circle. The conversion of wavelength ω to degrees d is $d = (\omega - 380)/(780 - 380)x360$.

As a further qualitative comparison, we plot the KSM, ADL, and CIECAM02 hues of the papers of maximal chroma, but varying value, from five pages (10B, 10G, 10Y, 10R,

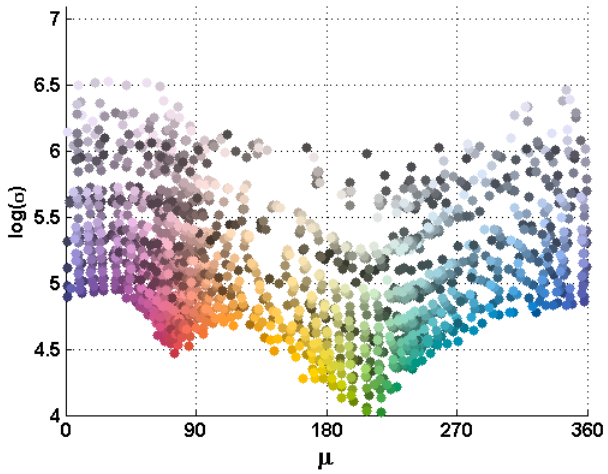

Figure 5.8: Plot of the 1600 papers from the Munsell glossy set as a function of KSM hue descriptors specified in degrees on the hue circle (see text). Each dot color only roughly approximates that of the corresponding Munsell paper under illuminant C.

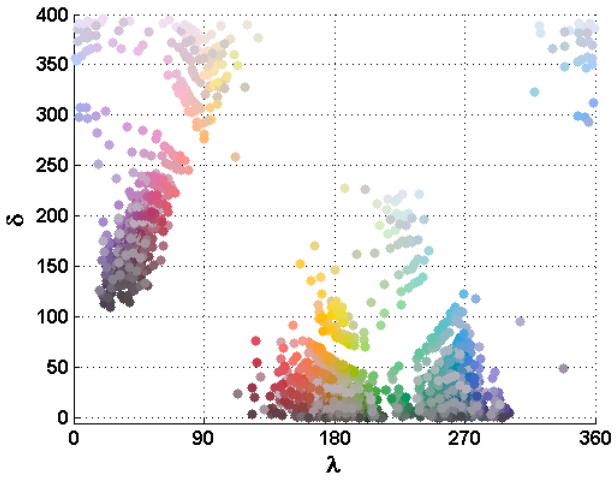

Figure 5.9: Plot of the 1600 papers from the Munsell glossy set as a function of ADL hue descriptors specified in degrees on the hue circle (see text). Each dot color only roughly approximates that of the corresponding Munsell paper under illuminant C.

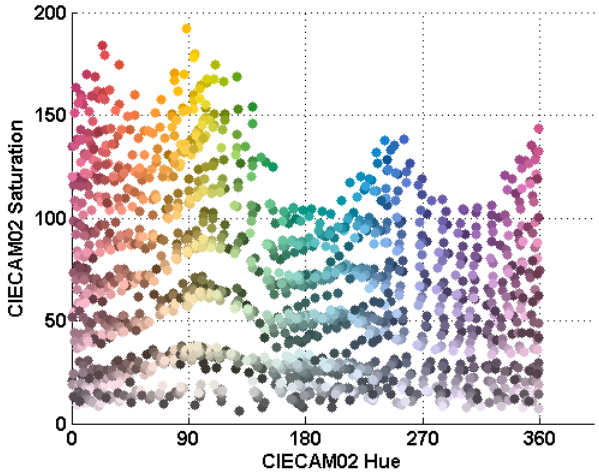

Figure 5.10: Plot of the 1600 papers from the Munsell glossy set as a function of CIECAM02 hue descriptors specified in degrees on the hue circle (see text). Each dot color only roughly approximates that of the corresponding Munsell paper under illuminant C.

and 10PB) of the Munsell Book of Color. As shown in Fig. 5.11, Munsell hue aligns better with the Gaussian KSM coordinate μ and CIECAM02 hue than with the rectangular ADL coordinate λ.

To provide a quantitative measure of how well the three different hue descriptors account for the Munsell hue data, we trained a hue classifier based on genetic algorithm optimization. The problem is defined as finding the optimized hue boundaries that categorize the Munsell papers into 10 main hue groups (R, YR, Y, GY, G, BG, B, PB, P, RP) with the smallest misclassification rate. The misclassification rate then provides a measure of how well the given hue descriptor models Munsell hue. Note that the papers with Neutral Munsell designator have been excluded. These optimized boundaries are found in 3 separate optimizations using the GA optimization strategy [98]. For each optimization, the feature vector (i.e., vector of hues along with corresponding KSM Gaussian peak wavelengths μ, ADL rectangular central wavelengths λ, or CIECAM02 hues) is input to Matlab's ga function from the Matlab Global Optimization Toolbox. The Matlab ga function optimizes the choice of hue boundaries so as to minimize the number of misclassified samples in the given feature vector. The resulting misclassification rates for KSM μ and CIECAM02 hue are low at 7% and 6%, respectively, but higher at 19% for ADL λ.

To evaluate the hues of Munsells papers in more detail, we have used the same genetic

algorithm optimization to determine the optimal hue boundaries for the intermediate Munsell hue classes and measured the corresponding misclassification rates. Fig. 5.12 shows the misclassification rates for the intermediate Munsell hue designators which are red (Munsell hues R, 2.5R, 5R, 7.5R, and 10R) yellow-red (YR, 2.5YR, ...), yellow, green-yellow, green, blue-green, blue, purple-blue, purple, and red-purple papers. The average misclassification rate across all the hues combined is 31% for KSM μ versus 41% for CIECAM02 hue.

5.5.2 NCS Dataset

The Natural Color System (NCS) [99] provides another set of hue data. In the NCS notation hue is defined in terms of the percentage of the distance between the neighboring pairs of the 'elementary' hues red, yellow, green, blue. The two other components of the NCS notation specify the blackness and chromaticness. We carried out a sequence of tests using the NCS data that are similar to those described above using the Munsell data. The plots of the 1950 NCS papers analogous to Figs. 5.8, 5.9, and 5.10 are qualitatively very similar and therefore are not included here. As in the case of the Munsell papers, KSM μ and CIECAM02 hue show a very good correlation with NCS hue, while ADL correlates, but not as unambiguously. Fig. 5.13 plots the NCS papers of NCS hues R, Y50R, Y, G50Y, G, B50G, B, and R50B as a function of the KSM μ, ADL λ and CIECAM02 hue descriptors in a manner analogous to that of Fig. 5.11 for the Munsell papers.

Fig. 5.11 plots Munsell hue versus hue descriptor specified in degrees. The triangle interiors represent the approximate color under illuminant C of the Munsell papers of different Munsell value, each at maximal chroma for the given value, for the five hues 10B, 10G, 10Y, 10R, and 10PB. The triangle boundaries are colored with the maximal chroma for the given Munsell hue. Top left, top right, and bottom plots are of the KSM Gaussian peak wavelength μ, the ADL rectangular central wavelength λ, and CIECAM02 hue. The vertical alignment in the left and right panels shows that papers of the same Munsell hue but differing value are all being assigned the same hue descriptor. In the bottom panel, there is some mingling of the red with the yellow and of the blue with the purple hues.

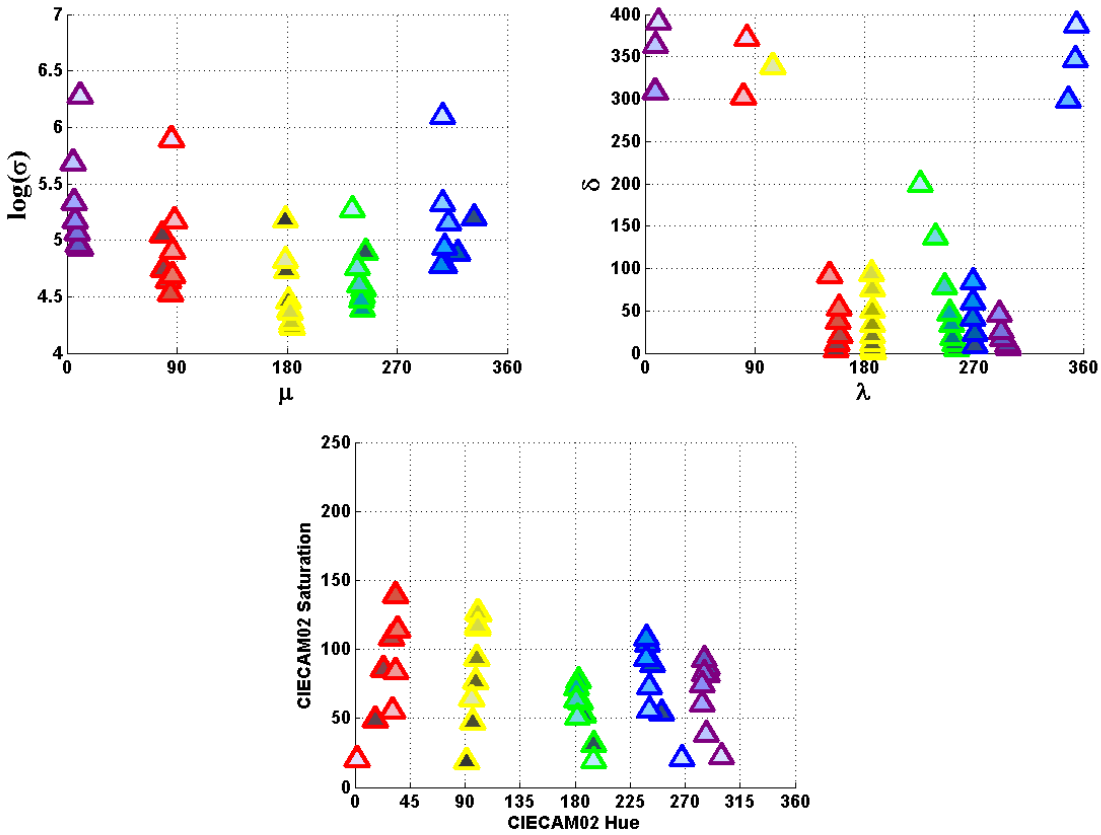

Figure 5.11: Munsell hue versus hue descriptor specified in degrees. The triangle interiors represent the approximate color under illuminant C of the Munsell papers of different Munsell value, each at maximal chroma for the given value, for the five hues 10B, 10G, 10Y, 10R, and 10PB. The triangle boundaries are colored with the maximal chroma for the given Munsell hue. Top left, top right and bottom plots are of the KSM Gaussian peak wavelength μ, ADL rectangular central wavelength λ, and CIECAM02 hue. The vertical alignment in the left and right panels shows that papers of the same Munsell hue but differing value are all being assigned the same hue descriptor. In the bottom panel, there is some mingling of the red with the yellow and of the blue with the purple hues.

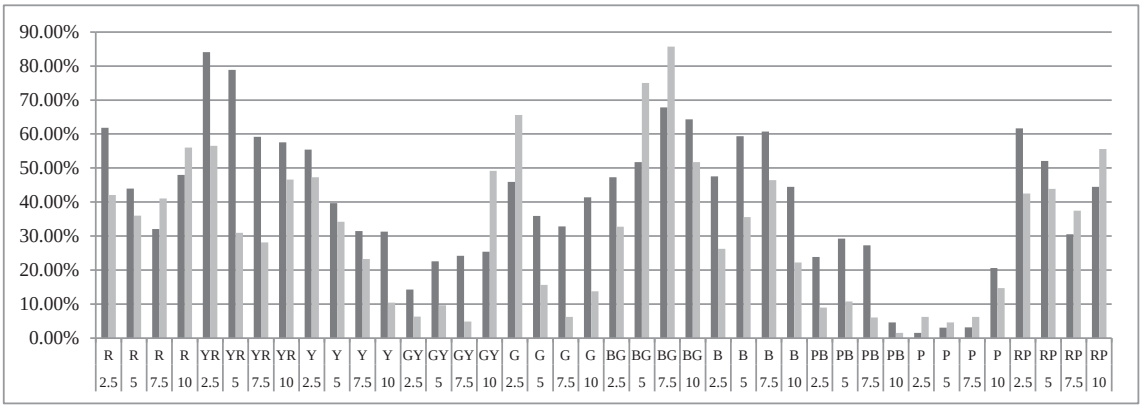

Figure 5.12: Hue misclassification rate for KSM μ (grey) versus CIECAM hue (black) over papers of the intermediate Munsell hues. The average misclassification rate for all the hues combined is 31% for KSM μ versus 41% for CIECAM02 hue.

5.5.3 Thesaurus Hue Names

The issue of color naming is in many ways similar to hue classification. In terms of color naming data, Moroney's color thesaurus summarizes the result of a very large online, crowd-sourced color naming experiment [95, 97]. Subjects were asked to provide unconstrained color names for colors displayed against a uniform grey background viewed on an uncalibrated computer display. The question we ask is: How well do KSM hue and CIECAM02 hue predict the color names found in this color thesaurus? Many of the hue names in the thesaurus are not standard hue names (e.g., 'crimson,' 'sunburst,' 'sea foam'). However, many others like 'fire red' and 'sea green' include a standard hue name as a component of the name. To limit the set of hues to 'standard' ones, the tests described below are based on all the color names from the color thesaurus that included the 8 color names red, green, yellow, blue, brown, purple, pink, and orange from Berlin and Kay [100], excluding black, gray, and white. All the color names that include one of these 8 as a component are extracted from the thesaurus; however, those that include more than one of the 8 names as components are excluded. For example, names such as 'delft blue' and 'sage green' are include under the categories blue and green, but 'blue green' is excluded since it is not clear whether it describes a blue or a green. The result is 8 sets of color names of which there are 22 red, 99 green, 18 yellow, 79 blue, 14 brown, 21 purple, 28 pink, and 14 orange. Each entry in the thesaurus has an associated sRGB color descriptor. This sRGB value is converted to CIECAM02 and KSM [33, 101] coordinates under the assumption that the

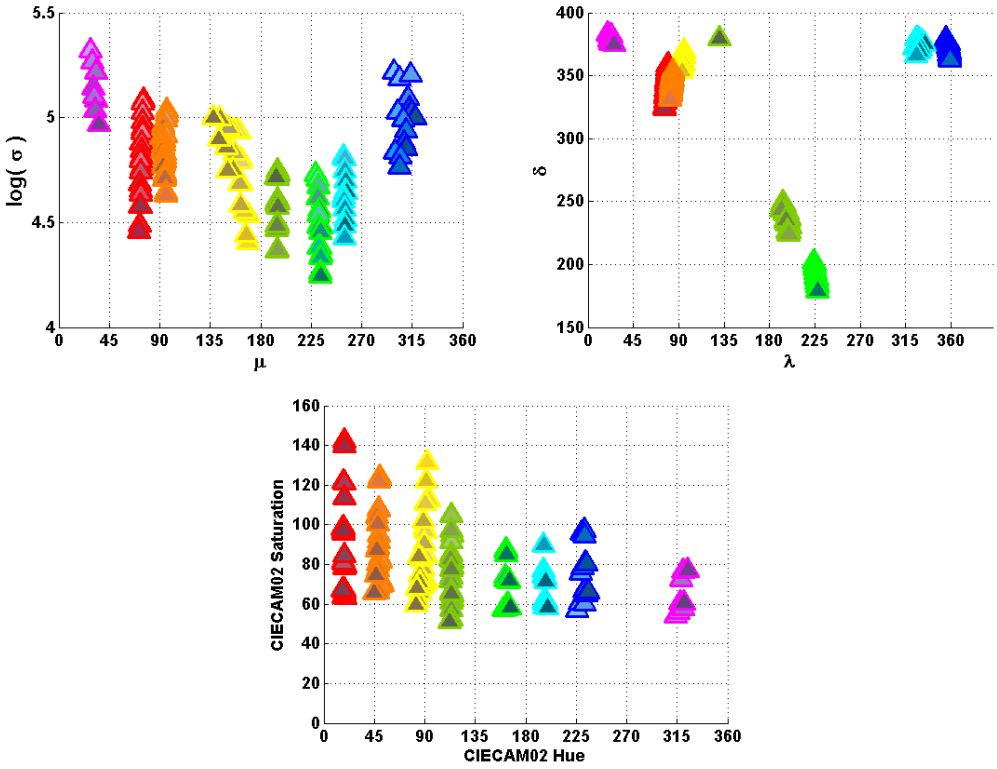

Figure 5.13: NCS hue versus hue descriptor specified in degrees. The triangle interiors represent the approximate color under illuminant C of the NCS papers of hues R, Y50R, Y, G50Y, G, B50G, B, and R50B for chromaticness greater than or equal to 40. The triangle boundaries are colored to indicate the given NCS hue name. Top to bottom the plots are of the KSM Gaussian peak wavelength μ, the ADL rectangular central wavelength λ, and CIECAM02 hue. The vertical alignment in the left and right panels shows that papers of the same NCS hue but differing chromaticness and blackness are all being correctly assigned the same hue descriptor. In the central panel, there is some intermingling of the red, orange and yellow.

display settings and viewing environment are intended to be D65. It should be noted that Logvinenko's color object color atlas describes the colors of objects (surfaces) not lights. Converting sRGB to KSM implies that the sRGB values are recorded from a surface, when in fact in Moroney's experiment they were not, but rather from the light emanating from an emissive display. This might mean that KSM hue will not model displayed colors as well as object colors, but the results below show that it models display colors well in any case. Fig. 5.14 plots the 8 color-name sets in terms of hue and saturation.

As can be seen from Fig. 5.14, KSM hue appears to correlate with the hue names as well or better than CIECAM02 hue in terms of compactness of the hue range along the hue axis, and distinctiveness of the hues from one another. To compare the two hue descriptors quantitatively, we again test their effectiveness in terms of hue classification with class boundaries determined by genetic algorithm optimization. The optimized boundaries are drawn as vertical dashed lines in Fig. 5.14. The misclassification rate for the classifier based on KSM hue is 7%, whereas, for the classifier based on CIECAM02 hue it is 10%.

5.5.4 Robustness of KSM Hue to Illuminant

Thus far KSM μ has been shown to provide a good perceptual correlate of hue. The next question is whether or not this hue descriptor remains relatively consistent under different illuminants.

To determine the relative stability of KSM versus ADL and CIECAM02 hue coordinates under a change in illuminant, we synthesize the XYZ tristimulus values of 1600 Munsell chips under two illuminants (e.g., D65 and A) using the 2-degree observer color matching functions and then determine the corresponding hue coordinates. Table 5.1 provides a quantitative comparison based on circular statistics (since hue is defined on the hue circle) where it can be seen that KSM hue is significantly more stable than either ADL hue or CIECAM02 hue.

It might be argued that one reason KSM hue is more stable than CIECAM02 is that it incorporates knowledge of the full illuminant spectrum. Of course, there is no reason why CIECAM02 could not have been defined to make use of this additional spectral information too since it is readily available in the type of laboratory setting in which CIECAM02 is generally applied. In terms of digital imaging, however, it is often the case that only a 3-channel measurement of the illuminant's "color" is available, so we consider the situation in which the KSM hue calculation is based only on the illuminant XYZ, not its spectrum. For

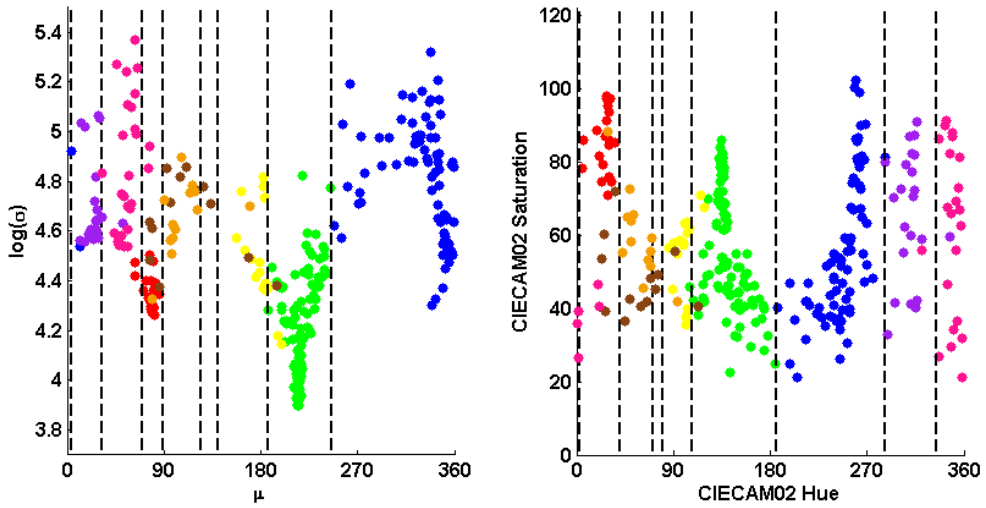

Figure 5.14: The color thesaurus samples from the 8 sets of color names (green, red, blue, yellow, purple, brown, pink and orange) plotted in terms of their KSM μ (left) and CIECAM02 hue (right). A dot's color indicates the corresponding hue set to which the sample belongs. The dashed vertical bars indicate the hue boundaries minimizing the misclassification rate.

	Median	Mean
KSM hue μ	2.10	3.87
ADL hue λ	5.16	9.27
CIECAM02 (full adaptation) hue	4.99	5.69
$(KSM)_2$ hue μ	2.43	3.76

Table 5.1: KSM, ADL AND CIECAM02 Hue Shifts for D65 to A in Degrees

this we follow the procedure proposed by Mirzaei et al. [27] in the context of predicting the change in XYZ induced by a change in illuminant. Given the illuminant XYZ, a metameric wraparound Gaussian illuminant spectrum is found, and then this spectrum is used in the KSM hue calculation in place of the true illuminant spectrum. We will denote this method $(KSM)_2$ since it involves two sets of KSM coordinates: one for the wraparound Gaussian illuminant and the other for the wraparound Gaussian reflectance. The last row of Table 5.1 gives the hue shift using the$(KSM)_2$ approach, which is comparable to the KSM result.

As a further test, we use all non-identical pairings of the different illuminants used by Logvinenko and Tokunaga [9] in their asymmetric color matching experiments. As in the test described above using D65 and A, we first calculate the XYZ tristimulus values of Munsell chips under each of the illuminants and then compute the corresponding KSM and

CIECAM02 hues. The mean and median differences (circular statistics) of the KSM hues, (KSM)2 hues and CIECAM02 hues for the different illuminant pairs are tabulated in the Table 5.2. Clearly, KSM hue μ is significantly more stable than ADL λ and CIECAM02 hues. Surprisingly, there is very little penalty, if any, for using the metameric Gaussian illuminant spectrum in place of the true illuminant spectrum(KSM)$_2$ hue is as stable as KSM hue on average.

5.5.5 Real Images

The tests above show that KSM hue is quite stable with respect to the illuminant, but is it also stable on images of real scenes? As a test, we consider the "Flowers" multispectral image from the University of Columbia spectral database [2] and synthesize the XYZ tristimulus values for it under illuminants CIE D65 and CIE A using the 2-degree observer. For each pixel, we then compute the corresponding KSM μ and CIECAM02 hue and classify each according to the 8 hue ranges shown in Fig. 5.14 that were determined as described above using the Moroney dataset. The results are shown in Fig. 5.15. The upper row shows an approximate sRGB rendering of the image under the illuminant D65, along with KSM μ and CIECAM02 hue classification maps. The pixel colors have been chosen to indicate the hue names (but not the hues themselves). The lower row provides the corresponding results for illuminant A.

Comparing the results in the two rows of Fig. 5.15, we can see, for example, that the CIECAM02 hue class assigned to a large portion of the central flower in the image changes from purple under D65 to pink under A. Fig. 5.16 shows a map of the difference in assigned hue class between the upper and lower rows. Since there are eight classes, and they are defined on the hue circle, the differences range from 0 to 4. It is clear from Fig. 5.16 that the classes defined by KSM μ remain relatively constant, while those of CIECAM02 change. In quantitative terms, the class shift averaged over all distinct colors in the image was 0.07 for μ versus 0.21 for CIECAM02 hue. To avoid large areas of a single color biasing the class shift results, we bin the XYZs and count each bin only once when computing the statistics of hue class shift. Each of the X, Y, and Z ranges is divided into 50 equal intervals so the total number of bins used is 50^3.

As a second example, results of a similar test using the "Oil Painting" multispectral image from the Columbia dataset, along with illuminants D65 and CIE F3 (fluorescent) in place of D65 and A, are shown in Fig. 5.17 and Fig. 5.18. Again, it is clear that KSM μ is

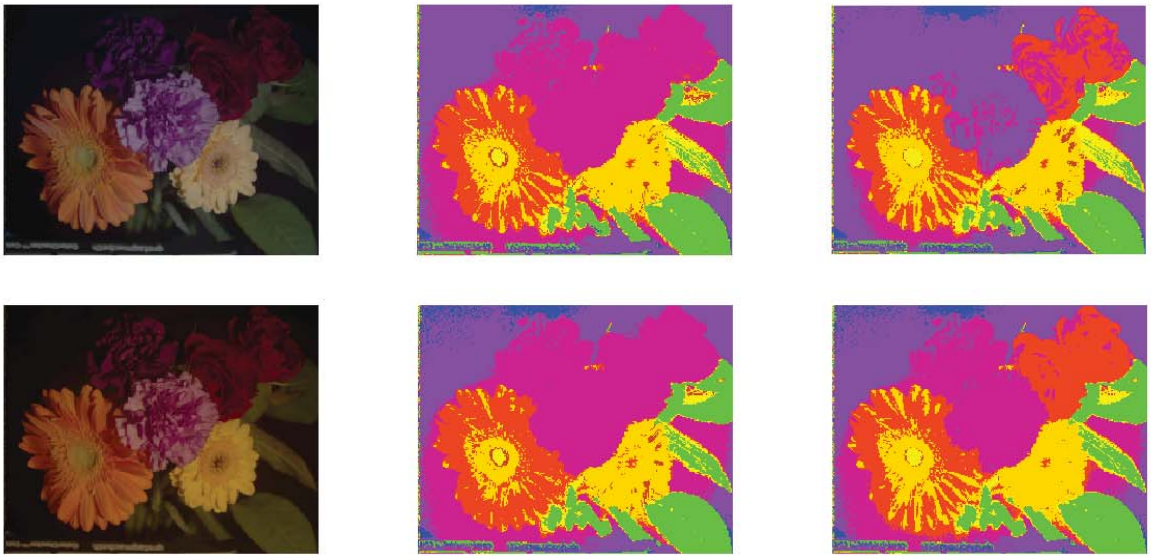

Figure 5.15: Hue classification using KSM μ versus CIECAM02 hue of the Flowers image from the Columbia University spectral database [2]. First and second rows depict the classification results for illuminants D65 and A, respectively. Left panel: Approximate sRGB rendering of the image. Middle: segmentation based on μ. Right: classification based on CIECAM02 hue. Each pixel is colored to roughly represent the hue name assigned to it.

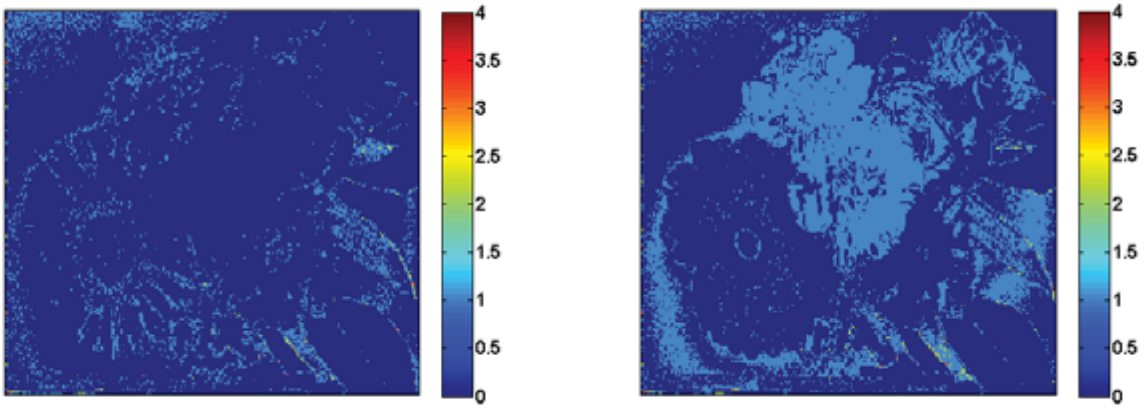

Figure 5.16: Map of hue class shift for μ (left) and CIECAM02 hue (right) when the illuminant is changed from D65 to A. Class shifts can range from 0 to 4.

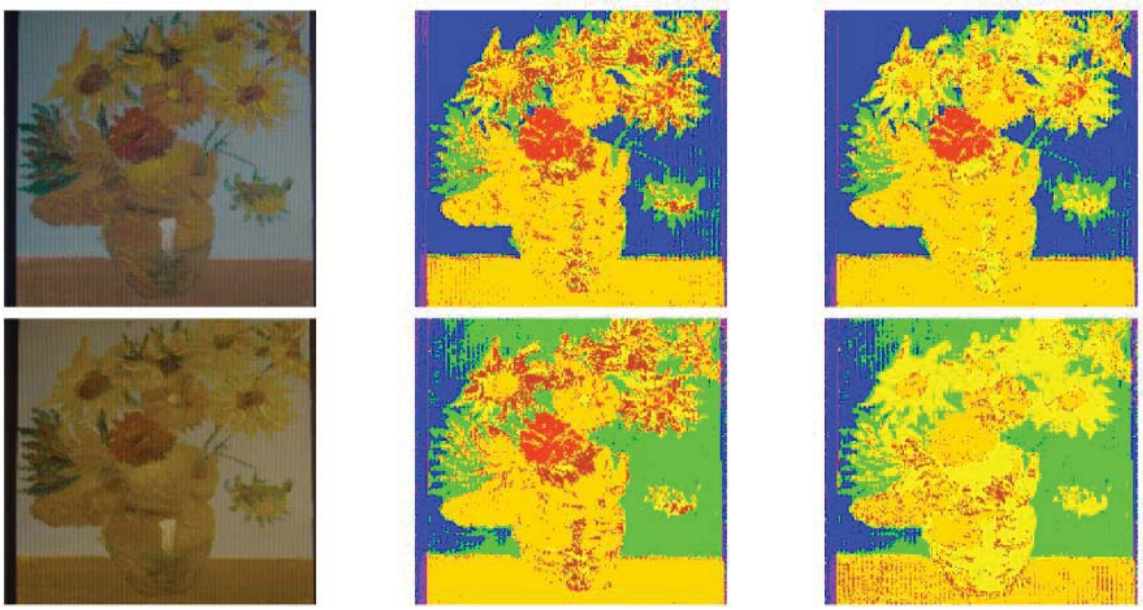

Figure 5.17: Hue classification using KSM μ versus CIECAM02 hue of the Oil Painting image from the Columbia University spectral database [2]. First and second rows depict the classification results for illuminants D65 and F3, respectively. Left panel: Approximate sRGB rendering of the image. Middle: classification based on μ. Right: classification based on CIECAM02 hue. Each pixel is colored to roughly represent the hue name assigned to it.

more stable than CIECAM02 hue. The average class shift is 0.29 for KSM μ versus 0.48 for CIECAM02 hue.

To investigate how hue stability might vary with the illuminant, we consider the "Flowers" image when the illuminant is changed from D65 to each of 10 very different illuminants: G, B, N, Y, R1, R2, CIE F12, CIE F3, and a standard LED light bulb of correlated color temperature 2900^o Kelvin. The average hue class shift for a change from D65 to each of these illuminants, respectively, is plotted in Fig. 5.19.

To investigate how hue stability might vary with the image content, we consider the entire set of images from the Columbia multispectral image dataset. Fig. 5.20 is a bar chart comparing KSM to CIECAM02 for each image for a change in illuminant from D65 to F3. Fig. 5.21 provides a similar plot for a change from D65 to the 2900^o K LED. Although the average shift in hue class varies from image to image, in the significant majority of cases the KSM hue class shift is less than the CIECAM02 hue class shift. This is reflected in the mean and standard deviation of the hue class shift across all the images in the dataset, which for

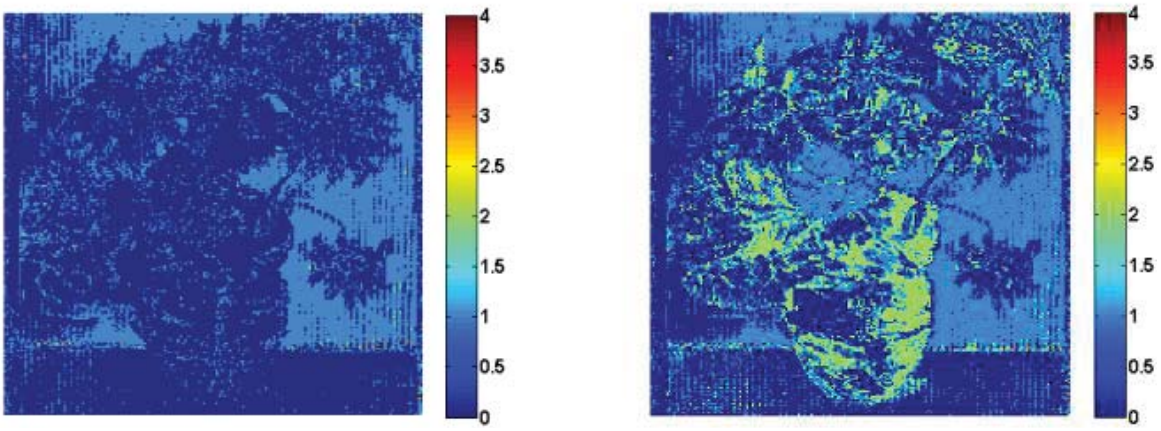

Figure 5.18: Map of hue class shift for KSM μ (left) and CIECAM02 hue (right) when the illuminant is changed from D65 to F3 for the Oil Painting image. Class shifts can range from 0 to 4.

Fig 5.20 are KSM (0.38 mean; 0.10 s.d.) versus CIECAM02 (0.61 mean; 0.21 s.d.); and for Fig 5.21 are KSM (0.14 mean; 0.05 s.d.) versus CIECAM02 (0.18 mean, 0.10 s.d.).

5.6 Conclusion

Hue descriptors based on Gaussian models of spectra in which the peak wavelength of the Gaussian is used as a hue descriptor have been proposed previously by Mizokami [54, 90] and Logvinenko [52]. Mizokami et al. directly model illuminant and reflectance spectral functions as Gaussians. In contrast, Logvinenko considers objects and suggests [52] (but

Illuminants		Median				Mean			
From	To	KSM	$(KSM)_2$	ADL	CIECAM02	KSM	$(KSM)_2$	ADL	CIECAM02
G	B	11.23	13.17	21.79	17.43	22.36	25.77	43.42	27.37
G	N	12.94	15.56	17.71	15.45	14.16	16.66	28.56	20.95
G	Y	12.60	14.67	17.34	15.73	14.40	16.55	30.30	21.42
G	R1	29.25	28.23	50.67	34.24	36.36	31.44	54.39	46.22
B	N	11.83	17.34	36.23	33.77	21.38	25.22	51.19	36.87
B	Y	12.48	17.96	39.21	37.66	23.70	27.14	53.93	40.10
B	R1	32.12	31.59	68.26	61.97	41.22	38.46	69.00	71.28
N	Y	0.90	1.17	2.38	3.54	1.89	2.18	4.51	3.56
N	R1	15.68	11.85	19.43	32.48	24.87	17.98	31.91	36.93
Y	R1	14.93	11.79	18.00	29.38	23.94	17.51	29.01	33.57
Column Means		15.40	16.33	29.10	28.17	22.43	21.89	39.62	33.83

Table 5.2: KSM, ADL AND CIECAM02 Hue Shifts in Degrees for Each Illuminant Pair

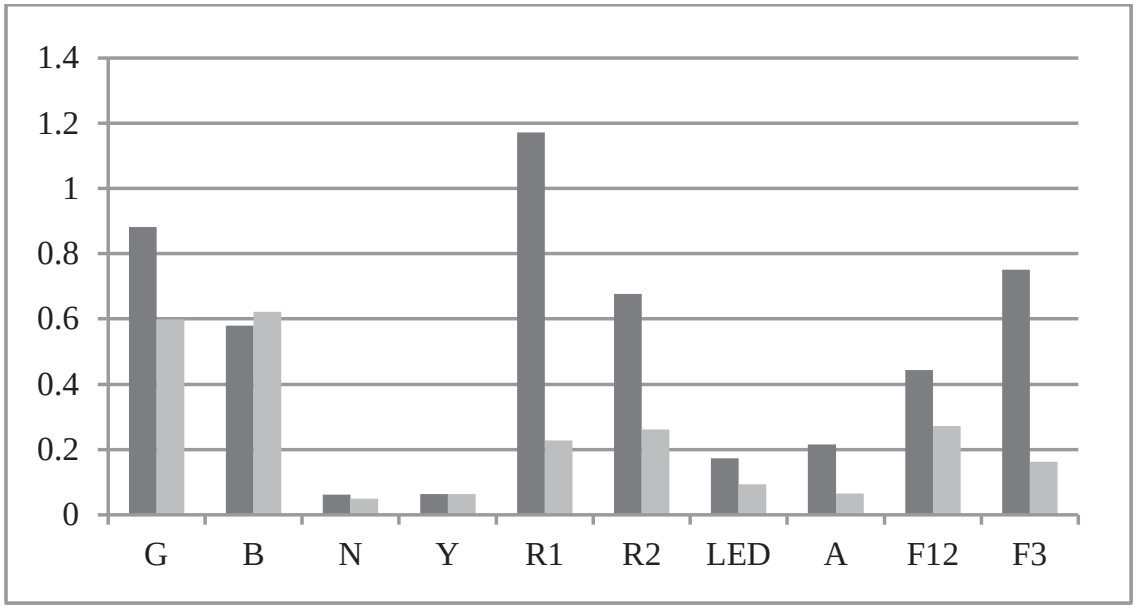

Figure 5.19: Average shift in hue class for KSM hue μ (grey) and CIECAM02 hue (black) for the "Flowers" image for a change in illuminant from D65 to each of 10 other illuminants.

does not test) using Gaussian reflectance functions that are metameric to the observed object color signal (XYZ). In this study, we have investigated both the subtractive Gaussians Mizokami et al. use and the wraparound Gaussians that Logvinenko suggests in terms of three fundamental issues. First, what is the gamut of colors they can represent and is the representation unique? Second, in comparison to CIECAM02 how well does the peak wavelength of the Gaussian correlate with Munsell and NCS hue descriptors, as well as with the color names found in Moroney's Color Thesaurus [95]. Third, in comparison to CIECAM02 how stable is the hue correlate (i.e., Gaussian peak wavelength) across different illuminants? Logvinenko had previously shown [49] that the central wavelength of the rectangular reflectance functions correlated reasonably well with hue so we include tests with those functions for comparison.

In answer to the first issue, we found that the chromaticity gamut of subtractive Gaussians does not cover the entire chromaticity space. Perhaps more importantly, the subtractive Gaussian representation was found to be non-unique in the sense that two metameric subtractive Gaussians with different peak wavelengths exist in many cases. Whether or not the wraparound Gaussians are unique is an open question until a uniqueness proof is

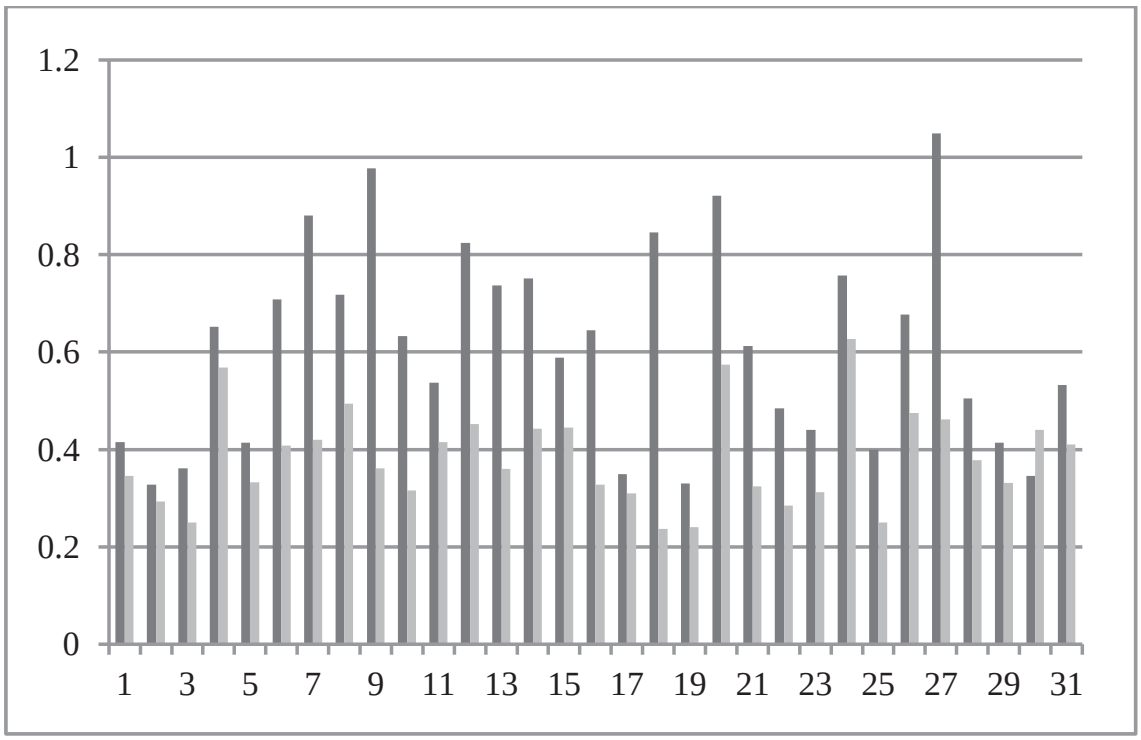

Figure 5.20: Average hue class shift for each image when using KSM hue μ (grey) and CIECAM02 hue (black) for the whole Columbia dataset when the illuminant is changed from D65 to F3. Abscissa: image number. Ordinate: average hue class shift over corresponding image.

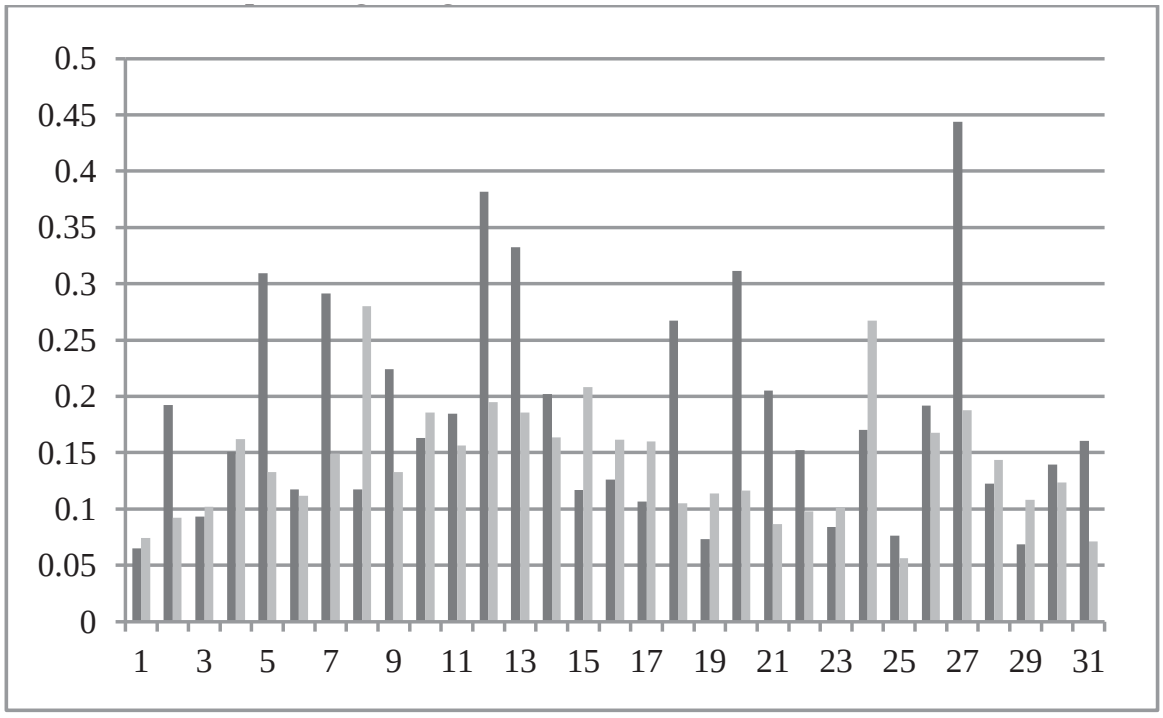

Figure 5.21: Average hue class shift for each image when using KSM hue μ (grey) and CIECAM02 hue (black) over the entire Columbia dataset when the illuminant is changed from D65 to the 2900^{o} K LED. Abscissa: image number. Ordinate: average hue class shift over corresponding image.

provided; however, numerical searching failed to turn up a metameric pair. A uniqueness proof is an important issue for future work.

In terms of the second and third issues, tests with the Munsell, NCS and Moroney data under D65 clearly show that the peak wavelength of the metameric wraparound Gaussian correlates with the different hue descriptors as well as CIECAM02 hue does on average. However, in terms of stability under a widely varied set of illuminants, the Gaussian hue descriptor is significantly more stable than CIECAM02 hue. This was also shown to hold true for $(\mathrm{KSM})_2$ which relies only on the illuminant XYZ, not its full spectrum. The fact that the Gaussian hue descriptor correlates well with hue as defined by the Munsell and NCS color systems as well as the Moroney color naming data supports the hypothesis [54] that Gaussian spectra may in some way underlie hue perception. As demonstrated by the example of classifying the hues in two sample images, the fact that the Gaussian hue descriptor is relatively unaffected by the illuminant shows that it could be advantageous in any image processing application that depends on naming or classifying hues. The fact that in the case of $(\mathrm{KSM})_2$ it was also shown to be stable even when a metameric Gaussian illuminant spectrum is substituted for the actual spectrum of the illuminant is important in the context of image processing when only the illuminant color, not its spectrum, is available.

The chief disadvantage of the KSM hue descriptor is that it is more costly to compute than CIECAM02 hue, a problem that can be easily addressed by appropriate use of lookup tables and kd-trees [93]. Although very important, hue is only one perceptual dimension of color. Future work will involve using the other KSM parameters in modeling dimensions such as purity/saturation.

Chapter 6

Robust Chroma and Lightness Descriptors

6.1 Summary

In an attempt to represent the main dimensions of object colors robustly, Chapter 5 presented a hue descriptor. In this chapter, new descriptors for lightness and chroma are presented that are based on properties of a wraparound Gaussian metameric to the given XYZ tristimulus coordinates. For the 1600 samples of the Munsell glossy set, both descriptors are found to correlate to Munsell value and chroma at least as well as the corresponding CIECAM02 descriptors when the Munsell samples are under the CIE C illuminant. However, when the illuminant is changed the new descriptors were found to be considerably more consistent under the second illuminant than those of CIECAM02. A version of this chapter has appeared in the Color and Imaging Conference, Society for Imaging Science and Technology, 2015 [6].

6.2 Introduction

Object color can be described in terms of three main dimensions, which are often specified as hue, chroma, and lightness [4]. In Chapter 5, we proposed using the peak wavelength of a metameric wraparound Gaussian as a hue descriptor [24, 30] and showed that it correlates as well as CIECAM02 hue does to Munsell hue [94], NCS hue [99], and the hue names in Moroney's color thesaurus [95–97]. The Gaussian-based hue descriptor was also shown to

be more stable than CIECAM02 when the illuminant differs from CIE Standard Illuminant C.

Given a CIE XYZ and the spectrum of the illuminant, the key idea of the hue descriptor is to determine the wraparound Gaussian reflectance function that is metameric (i.e., leads to the same XYZ) under the given illuminant and then base the hue on a property of that reflectance, namely the wavelength at which the Gaussian peaks. This chapter introduces Gaussian-based chroma and lightness descriptors and compares them to CIECAM02 in terms of:

1. How well they each correlate with the chroma and value designators of the 1600 Munsell [94] papers.

2. How stable the respective descriptors are under a change in the illuminant.

Similar to Chapter 5, the new descriptors are defined in terms of the parameters of the wraparound Gaussian function as defined in Equations 2.11, 2.12, 2.13, and 2.14 in page 20. As before, we will refer to triples $k\sigma\mu$ as KSM coordinates, where σ stands for standard deviation, μ for peak wavelength, and k for scaling. Based on these KSM coordinates, we define descriptors for lightness (called KSM lightness) and chroma (called KSM chroma) and compare them to CIECAM02 lightness and saturation. Our tests show two important properties of both KSM lightness and chroma. First, they correlate well with the value and chroma designators of Munsell papers. Second, KSM descriptors are much more stable under a change of illuminant than CIECAM02.

6.3 CIE Lightness

The CIE defines lightness in terms of brightness, where brightness is "a visual perception according to which an area appears to exhibit more or less light." (page 26 of [56]). Lightness is then defined as the brightness of an area judged relative to the brightness of a similarly illuminated reference white (page 26 of [56]).

6.4 KSM Lightness

Given the XYZ coordinates (CIE 1931 2-degree observer) for light reflected from an object illuminated by light of known spectrum, the parameters k, σ, and μ of the metameric

wraparound Gaussian reflectance are determined. Given these KSM parameters, the KSM lightness is defined by:

$$L(k,\sigma,\mu) = 100 \int_{min}^{max} g_{k,\sigma,\mu}(\lambda)\overline{y}(\lambda)d\lambda \tag{6.1}$$

6.5 Chroma and Saturation

Chroma is defined as "the colourfulness of an area judged as a proportion of the brightness of a similarly illuminated reference white" (page 27 of [56]); where colourfulness is defined as "that attribute of a visual sensation according to which an area appears to exhibit more or less chromatic content." (page 26 of [56]). Saturation is defined as "the colourfulness of an area judged in proportion to its brightness" (page 27 of [56]). The distinction is between judging the chromatic content of the object with respect to the brightness of a reference white versus the object's own brightness. Both chroma and saturation are open-ended scales with a zero origin at neutral colors.

6.6 KSM Chroma

Generally, the chromatic content of a wraparound Gaussian will decrease with increasing σ since as σ increases the corresponding wraparound Gaussian reflectance function becomes broader and flatter. Therefore it is natural for KSM chroma to be inversely proportional to σ. However, simply using σ is insufficient in that there is also some dependence on hue. Therefore, KSM Chroma, C, is defined as:

$$C(\sigma,\mu) = \frac{h}{\sigma} \tag{6.2}$$

where h is defined to be $h = 2.4 + |\frac{\mu-\lambda_{min}}{\lambda_{max}-\lambda_{min}} \times 2\pi - t|$, $\lambda_{min} \leq \mu \leq \lambda_{max}$ and offset, t, is determined empirically as $t = 1.15\pi$ for the Munsell dataset. The region around 1.15π corresponds to a greenish yellow hue. As μ departs from t, h increases. Note that the offset of 2.4 is included to avoid zero chroma when we are at t.

6.7 Modeling Munsell Designators Under CIE C

To see how well the Munsell designators are modeled using the KSM lightness and chroma descriptors, we evaluate them on the set of reflectances of the 1600 papers from the Munsell

glossy set. We synthesized the XYZ tristimulus values of all 1600 papers based on the Joensuu Color Group spectral measurements [94] under illuminant C using the CIE 1931 2-degree observer colour matching functions and then computed the corresponding KSM and CIECAM02 lightness descriptors. When calculating the CIECAM02 descriptors, we adopted the parameters suggested for the "average surround" condition and full adaptation.

In the following figures, the Munsell reflectances used are those of the papers of hue 5RR, 5YR, 5YY, 5GY, 5GG, 5BG, 5BB, 5PB, 5PP, and 5RP, chroma 2, 4, 6, 8, 10, and value 5, 6, 7, 8, and 8.5. Figure 6.1 plots a marker encoding the Munsell value for each of these Munsell papers at a location determined by the KSM/CIECAM02 lightness descriptor. It can be seen that lightness descriptors in both systems appear to correlate very well with the Munsell value designator. This is indicated by the fact that the colors of the same Munsell value align horizontally. Note that KSM lightness descriptors $L(k, \sigma, \mu)$, which are originally in [0, 1], have been scaled by 100 for easier comparison to CIECAM02.

One numerical measure of how well the lightness descriptors account for Munsell value is the correlation coefficient between the Munsell value designators and the lightness descriptors. Correlation coefficients for the two lightness descriptors are high: 0.991 (KSM) and 0.995 (CIECAM02). As a second quantitative measure, we trained a lightness classifier based on genetic algorithm optimization. The problem is defined as finding the lightness boundaries that optimally categorize the Munsell papers into 5 Munsell value groups (5, 6, 7, 8, 8.5) with the lowest misclassification rate. The misclassification rate then provides a measure of how well the given descriptor models Munsell value. As can be seen from Fig. 6.1, there is no sample that is misclassified based on either its CIECAM02 lightness or KSM lightness.

A similar test was carried out on the chroma designators of Munsell papers. Fig. 6.2 plots a marker encoding the Munsell chroma for each of the Munsell papers at a location determined by the KSM chroma (upper plot) or CIECAM02 saturation (lower plot) descriptor. The different marker shapes (i.e., upward-pointing triangles, left-pointing triangles, circles, right-pointing triangles, and stars) in the plots correspond to the Munsell chroma of 2, 4, 6, 8, and 10, respectively. The horizontal alignment of similar symbols indicates that KSM chroma and CIECAM02 saturation both correlate well with Munsell chroma.

We are using CIECAM02 saturation rather than CIECAM02 chroma because we found that it correlated better with Munsell chroma. Note that KSM chroma is scaled to match the Munsell chroma range. The correlation coefficient of Munsell chroma designators with

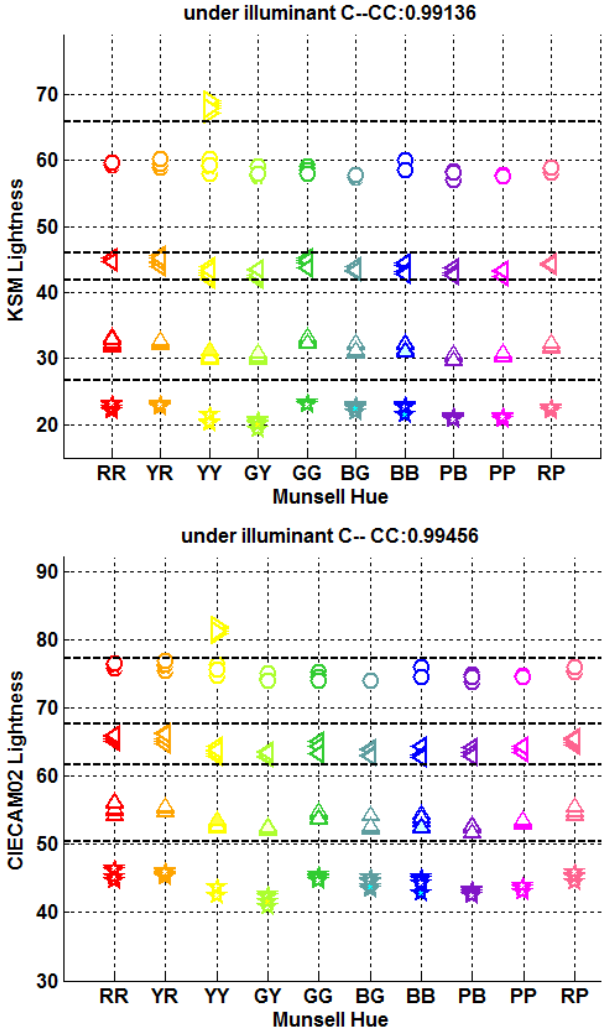

Figure 6.1: Lightness descriptor versus Munsell value for Munsell papers of Munsell hue 5RR, 5YR, 5YY, 5GY, 5GG, 5BG, 5BB, 5PB, 5PP, and 5RP; chroma 2, 4, 6, 8, 10; and value 5, 6, 7, 8, 8.5. The marker shape represents the Munsell value: 5 (star), 6 (upward pointing), 7 (left pointing), 8 (circle), and 8.5 (right pointing). Top and bottom plots are of the KSM and CIECAM02 lightness descriptors, respectively. The horizontal alignment in the panels shows that papers of the same Munsell value but differing chroma and hue are all being assigned the same lightness descriptor. The horizontal dashed lines are the class boundaries as determined by genetic algorithm optimization.

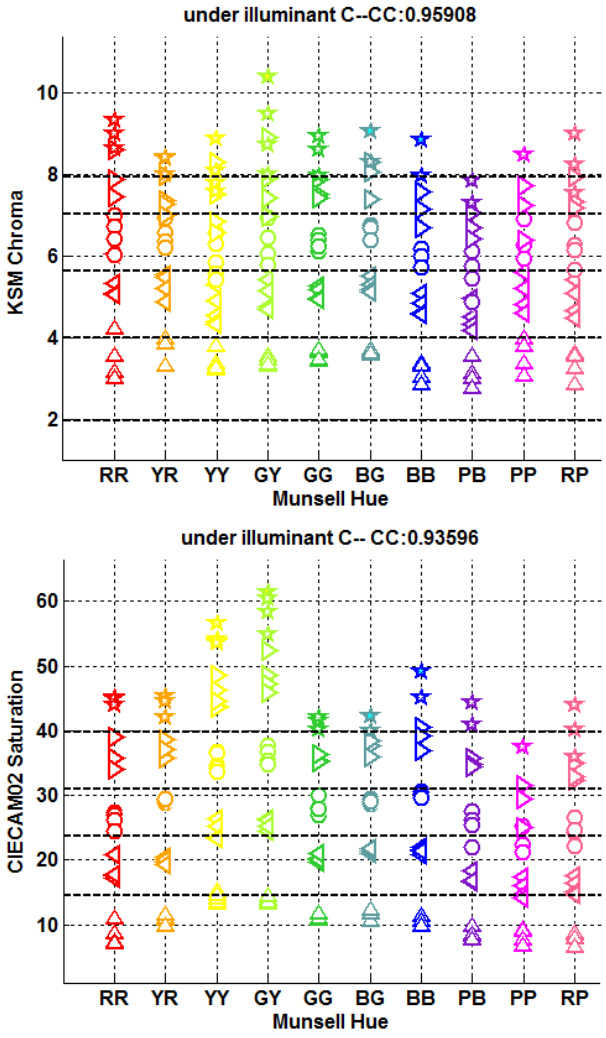

Figure 6.2: Chroma/saturation descriptor versus Munsell chroma for Munsell papers of Munsell hue 5RR, 5YR, 5YY, 5GY, 5GG, 5BG, 5BB, 5PB, 5PP, and 5RP; chroma 2, 4, 6, 8, 10; and value 5, 6, 7, 8, 8.5. The marker shape represents the Munsell chroma: 2 (upward pointing), 4 (left pointing), 6 (circle), and 8 (right pointing), 10 (star). The horizontal alignment in the panels shows that papers of the same Munsell chroma but differing hue and value are all being assigned the same chroma/saturation descriptor. The horizontal dashed lines are the chroma class boundaries as determined by genetic algorithm optimization.

respect to KSM chroma and CIECAM02 saturation are 0.96 and 0.94, respectively. In comparison, the correlation coefficient for CIECAM02 chroma was 0.86. The chroma misclassification rates for a chroma classifier trained using genetic algorithm optimization are 14.4% and 19.3% for KSM chroma and CIECAM02 saturation, respectively.

6.8 Robustness to illuminant change

The tests above have shown that the proposed KSM lightness and chroma descriptors correlate well with the Munsell value and chroma designators. In Chapter 5, we found that the Gaussian-based hue descriptor was more stable with respect to a change of illuminant than CIECAM02 [24, 30]. This leads to the question as to whether the same will be true for KSM lightness and chroma. As we have pointed out, however, any color descriptor–whether CIECAM02, KSM or any other alternative–is limited by the existence of metamer mismatching since a given XYZ under one illuminant can become any of a multitude of possible XYZ within its metamer mismatch volume under the second illuminant; and as shown in Chapter 3 this theoretical metamer mismatch volume can be surprisingly large. However, an advantage of the KSM descriptors over CIECAM02 descriptors under a change of illuminant is that the KSM descriptors are guaranteed to lead to a physically plausible answer since they are based on the properties of a metameric reflectance. In contrast, CIECAM02 updates its descriptors to account for a change in illuminant using a von Kries diagonal transformation, for which there is no guarantee of a physically plausible answer.

To determine the relative stability of the KSM descriptors to those of CIECAM02 under a change in illuminant, we synthesize the XYZ tristimulus values of the 1600 Munsell reflectances under two illuminants (e.g., D65 and A) and then determine the corresponding descriptors. Fig. 6.3 plots the lightness descriptor under A versus the lightness descriptor under D65 for KSM (upper) and CIECAM02 (lower). Fig. 6.4 makes a similar comparison but in terms of chroma/saturation. From the figures it can be seen that, in each case, the CIECAM02 descriptors deviate from the diagonal more than their KSM counterparts. Table 6.1 provides a quantitative comparison based on the coefficient of variation of the root-mean-square error [102] and clearly shows that the KSM descriptors are more stable than the CIECAM02 descriptors.

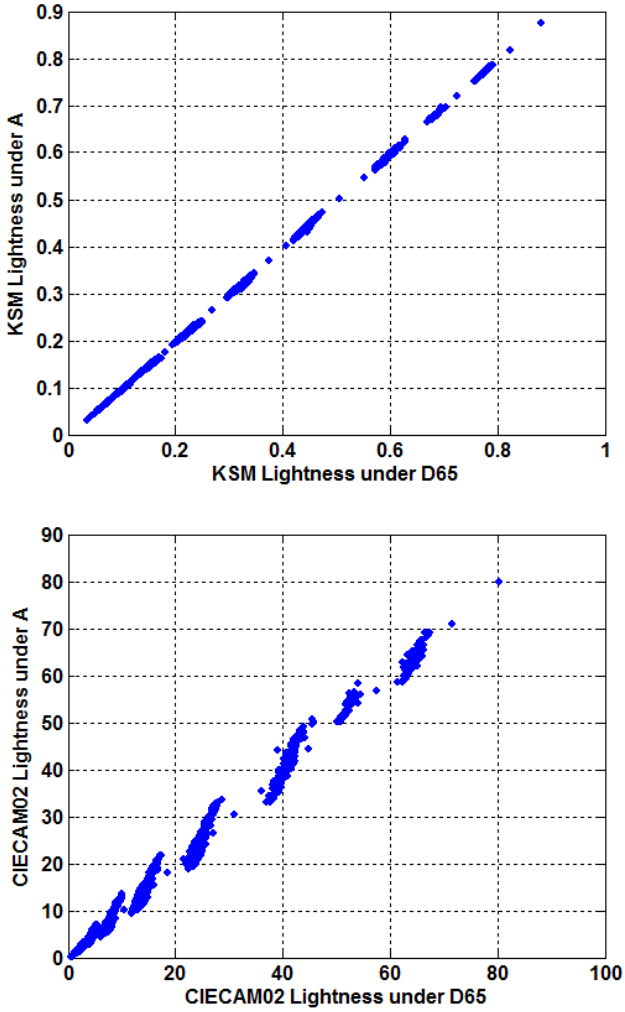

Figure 6.3: KSM (upper) and CIECAM02 (lower) lightness descriptors of the 1600 Munsell papers under illuminants D65 and A. A lightness descriptor that is completely invariant to the illumination will lead to points lying strictly on the diagonal.

	Lightness	Chroma
CIEAM02	3.89	3.98
KSM	0.27	2.21

Table 6.1: Coefficient of variation of the RMSE of the descriptors obtained for the 1600 Munsell papers under illuminant D65 versus illuminant A.

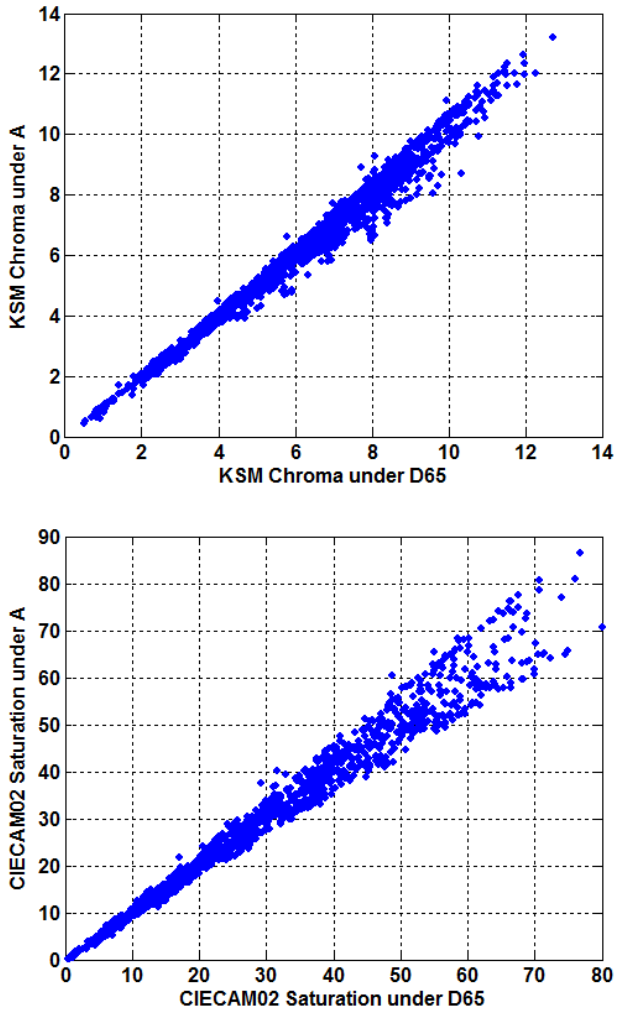

Figure 6.4: KSM chroma (upper) and CIECAM02 saturation (lower) descriptors of the 1600 Munsell papers under illuminants D65 and A. A descriptor that is completely invariant to the illumination will lead to points lying strictly on the diagonal.

6.9 Conclusion

The proposed lightness and chroma descriptors were shown to correlate as well as CIECAM02 descriptors to those of the corresponding Munsell designators, but have the additional advantage that they are more consistent across illuminants. Used in conjunction with the earlier Gaussian-based hue descriptor (chapter 5) [24] they provide a foundation for the specification of the hue, lightness and chroma dimensions of object colors under average viewing surround conditions.

Chapter 7

Object color Signal Prediction using Wraparound Gaussian Metamers

7.1 Summary

In the present chapter, Logvinenko's wraparound Gaussians are used in predicting illuminant-induced colour signal changes. For a given colour signal, his atlas specifies a unique reflectance that is metameric to it under the given illuminant. The method proposed in this chapter is based on computationally 'relighting' that reflectance to determine what its colour signal would be under any other illuminant. The fact that the object colour atlas is complete guarantees that a physically realizable metameric reflectance always exists. Since that reflectance is in the metamer set the prediction is also physically realizable, which cannot be guaranteed for predictions obtained via von Kries scaling. Testing on Munsell spectra and a multispectral image shows that the proposed method outperforms the predictions of both those based on von Kries scaling and those based on the Bradford transform.

Subsequently, an alternative method is proposed that employs metameric Gaussian-like functions to model both illuminant and reflectance spectra. It is unlike the first proposed method that uses the full power spectra of the illuminants. The method's prediction is based on relighting the Gaussian-like reflectance spectrum with the second Gaussian-like illuminant. Tests show that the second proposed method significantly outperforms CIECAT02.

The results presented in this chapter have led to publications in the Journal of Optical Society of America, JOSA A, 2014, and Color and Imaging Conference, Society for Imaging Science and Technology, 2014 [8, 27].

7.2 Introduction

The problem of predicting how the color signal (i.e., cone LMS, CIE XYZ or sRGB) arising in response to light reflected from the surface of an object changes when the lighting changes is a long-standing and important one. It arises in computer vision applications such as color-based object identification and tracking, where it is important to be able to recognize the same object under different illuminants. It also arises in white balancing digital imagery, and when re-rendering printed material for viewing under a second illuminant (e.g., changing from D65 to D50). In this paper, we approach the problem using tools provided by Logvinenko's [49] color atlas. Note that predicting the resulting color signal under a change of illuminant is not equivalent to predicting the resulting color appearance [82]. Also, it is not equivalent to the problem of predicting corresponding colors on displays since then the 'corresponding colors' are the colors of lights, not object colors. In some cases such as part of the Luo et al. LUTCHI dataset [103], corresponding color experiments are performed using objects, but the comparison of the colors is nonetheless made in terms of the XYZ of the light reflected from an object without regard to its reflectance or the spectra of the two illuminants. One exception in this regard is the Spectral Adaptation method proposed by Fairchild [104].

Note also that because of metamerism there is no unique answer to the prediction problem. Since there are many reflectances that can lead to the same color signal under the first light, the set of possible color stimuli that results under the second light forms a volume in color space, often referred to as the metamer mismatch volume. Logvinenko et al. [5] describe how to compute this volume precisely. Since any color signal in the metamer mismatch volume is a possible 'correct' answer, our goal has to be limited to finding the color signal that fits the experimental data best on average. It must be kept in mind that the potential error for any particular color signal prediction is bounded only by the size of the associated metamer mismatch volume of the color signal for the given pair of illuminants.

In this work, we use the wraparound Gaussians as a tool for predicting how a given color signal changes when the lighting changes from illuminant A to illuminant B. Others,

for example Brill [53], Mizokami [54], and McLeod and Golz [55] have also proposed other Gaussian-based models of reflectance, which will be discussed as well.

7.3 Gaussian-Metamer-Based Prediction

A common approach to predicting the color signal under a second illuminant from a color signal under a first illuminant is the von Kries transformation [60] in which each color channel is independently scaled by the ratio of the color signals obtained from an ideal reflector under the two illuminants. This transformation is used as a chromatic adaptation transform, the first step in a color appearance model such as CIECAM02 [82] where the von Kries transformation is applied in a sharpened space [105]. In comparison, the proposed Gaussian Metamer (GM henceforth) method bases the prediction on relighting the wraparound Gaussian reflectance, explained in equations 2.11, 2.12, 2.13, and 2.14, in page 20.

7.3.1 GM Method

In GM method, given a color signal XYZ under a first illuminant there are two steps:

1. compute the corresponding KSM coordinates (i.e., find the metameric wraparound Gaussian reflectance);

2. compute the color signal that will result when that wraparound Gaussian is lit by the second illuminant.

A significant advantage of predicting the new color signal in this way is that it is guaranteed to be in the metamer mismatch volume of the actual object. As Logvinenko points out [49], for the von Kries method there is no such guarantee, which means that, in principle, the von Kries error can be arbitrarily large. The same relighting strategy could be based on the rectangular reflectance functions of Logvinenko's original color atlas, but since those functions contain sharp transitions, they are less likely to model the behavior of typical reflectances found in practice. For this reason, we choose to work with the Gaussian parameterization of his atlas since its functions are smooth while at the same time retaining all the benefits (completeness, uniqueness and illuminant invariance) of the original color atlas.

As discussed previously in section 5.3.1, an important drawback of the inverse and subtractive Gaussians is that in many cases non-physically realizable reflectances are required

in order to create a (theoretical) metamer to a given color signal. Even when it is possible to find a physically realizable metameric inverse or subtractive Gaussian, computing it involves a very slow three-dimensional optimization with a high chance of getting stuck in a local minimum. In comparison, "wraparound Gaussians" are easily computed through a quick lookup followed by a two-dimensional optimization. Given these difficulties in using inverse and subtractive Gaussians, we do not include them in our experimental results.

7.4 Gaussian Reflectance and Illuminant Spectra

The Gaussian Metamer method requires knowledge of the full spectrum of the incident illumination, not just its color signal. To eliminate the need for the full illuminant spectrum, we propose replacing the true illuminant spectrum with a metameric Gaussian spectrum. Although the prediction error increases when using a metameric illuminant, it remains, nonetheless, less than two thirds of the CIECAT02 error. The details are presented below.

Suppose that we have a set of Gaussian-like spectral reflectance functions defined in terms of their scaling, k_m, standard deviation, σ_m, and peak wavelength, μ_m, as defined in equations 2.11, 2.12, 2.13, and 2.14, in page 20.

Now let us consider also the three-parameter set of illuminant functions of the same form defined in terms of their scaling, k_l, standard deviation, σ_l, and peak wavelength, μ_l:

If $\mu_l \leq (\lambda_{min} + \lambda_{max})/2$ we have two cases:

1. For $\mu_l \leq \lambda \leq \mu_l + \Lambda/2$:

$$g_l(\lambda; k_l, \theta_l, \mu_l) = k_l \; exp[-\theta_l(\lambda - \mu_l)^2] \tag{7.1}$$

2. For $\mu_l + (\Lambda/2) \leq \lambda \leq \lambda_{max}$:

$$g_l(\lambda; k_l, \theta_l, \mu_l) = k_l \; exp[-\theta_l(\lambda - \mu_l - \Lambda)^2] \tag{7.2}$$

where $\Lambda = \lambda_{max} - \lambda_{min}$.

On the other hand when $\mu_l > (\lambda_{min} + \lambda_{max})/2$, again we have two cases:

1. For $\lambda_{min} \leq \lambda \leq \mu_l + \Lambda/2$:

$$g_l(\lambda; k_l, \theta_l, \mu_l) = k_l \; exp[-\theta_l(\lambda - \mu_l - \Lambda)^2] \tag{7.3}$$

2. For $\mu_l - (\Lambda/2) \leq \lambda \leq \lambda_{max}$:

$$g_l(\lambda; k_l, \theta_l, \mu_l) = k_l \; exp[-\theta_l(\lambda - \mu_l)^2] \tag{7.4}$$

For the spectral power distributions, the restriction on the scaling is simply $k_l \geq 0$ since the intensity of the light is not limited. We will refer to triples (k_m, σ_m, μ_m) and (k_l, σ_l, μ_l) as the KSM coordinates of the reflectance and light, respectively.

7.4.1 G^{2}M Method

Given the color signal specified in CIE XYZ (or cone LMS) coordinates of light reflected from a surface and the spectra of the first (F) and second (S) illuminants, the first step in the original GM method is to determine the KSM coordinates of the wraparound Gaussian reflectance that is metameric (i.e., of identical XYZ) to the given surface under F. This metameric reflectance spectrum is relit–in other words, multiplied by the full spectrum of S–and the color signal under S is then calculated using the CIE XYZ color matching functions.

The proposed new method models the surface reflectance as well as both illuminants using wraparound Gaussian metamers and will be denoted G^{2}M.

1. determine the KSM coordinates (k_F, σ_F, μ_F), using a fast interpolation method, of the Gaussian illuminant spectrum that is metameric to F.

2. find the KSM coordinates (k_m, σ_m, μ_m) of the Gaussian reflectance that under Gaussian illuminant (k_F, σ_F, μ_F) has the same XYZ as the given surface under F.

3. find the Gaussian illuminant with coordinates (k_S, σ_S, μ_S) that is metameric to S.

4. relight the Gaussian reflectance (k_m, σ_m, μ_m) using the Gaussian illuminant (k_S, σ_S, μ_S) and determine its resulting XYZ color signal.

7.5 Experimental Results

The first step in the GM color prediction process is to compute a KSM descriptor for each XYZ. The speed of calculating the KSM coordinates depends on the required precision. There is a trade-off between precision and speed. Once the interpolation table is built for

To	Method	Median	Mean	95th Percentile
A	GM	0.95	1.18	2.84
	von Kries	3.70	3.70	6.91
	Bradford	1.80	2.01	4.37
F11	GM	1.43	1.75	4.16
	von Kries	2.04	2.62	6.97
	Bradford	1.49	1.87	5.17

Table 7.1: Comparison of color signal prediction accuracy for the 1600 Munsell reflectance spectra using the proposed GM method, von Kries scaling, and the Bradford transform in terms of CIEDE2000 for a change in illuminant from CIE D65 to CIE A and CIE F11.

a given illumination, computing the KSM for an XYZ requires approximately 0.01 seconds on a 2.66 GHz Quad-Core Intel Mac Pro.

7.5.1 GM Color Signal Prediction Results

In order to compare the accuracy of the color signal predictions made by the proposed method to those of von Kries scaling or those involving the Bradford transform, as a first test we synthesize the CIE XYZ tristimulus values of the 1600 Munsell chips [94] under CIE D65 using the CIE 1931 color matching functions [38] and then predict the CIE XYZ values under a second illuminant (CIE F11 or CIE A) using the proposed method, von Kries scaling and the Bradford transform [72]. For the von Kries scaling, the XYZ color signal is first transformed to cone coordinates using the Hunt-Pointer-Estevez transformation [106**?**], and then von Kries scaling is applied. The Hunt-Pointer-Estevez step is part of the RLAB color appearance model [82]. The predictions of the three methods are compared to the computed ground-truth values under the second illuminant (i.e., XYZ of the actual Munsell chip reflectance spectra multiplied by the illuminant spectrum). The results for a change in illuminant from CIE D65 to CIE A and CIE F11 are tabulated in Table 7.1 and show that color signal prediction using Gaussian metamers is better than using either von Kries scaling or the Bradford transform in terms of the CIEDE2000 color difference measure.

Although the lower average prediction errors obtained using GM prediction shown in Table 7.1 are one advantage, a second important advantage, as mentioned above, is that the GM predictions are guaranteed to be within the metamer set so long as the KSM coordinates have $K \leq 1$ since that condition ensures that the resulting wraparound Gaussian is a reflectance function. For a very few color signals the KSM coordinates have $K > 1$. For any

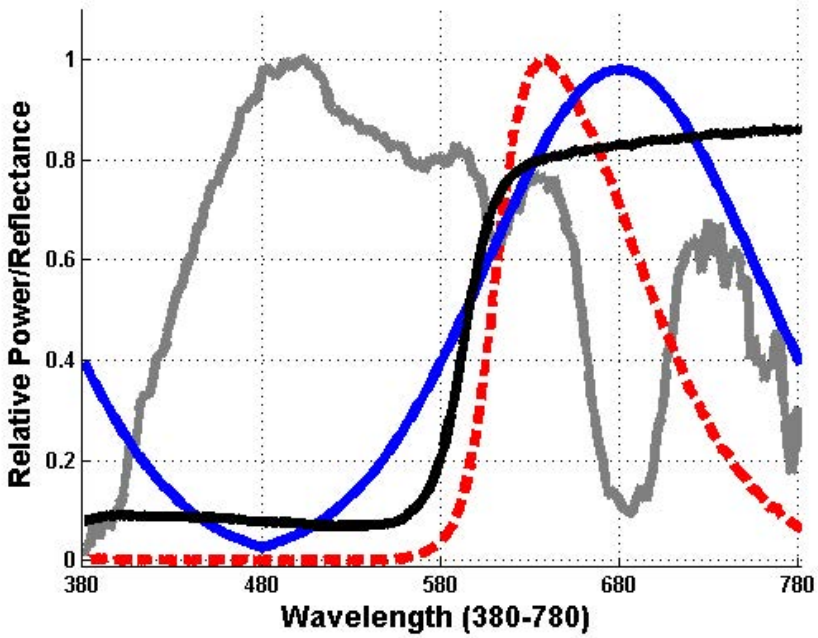

Figure 7.1: Reflectance and illuminant pair example for which von Kries fails. Black curve is the reflectance of Munsell chip 7.5 R 5/16. Blue curve is the corresponding wraparound Gaussian metamer for that Munsell chip. The dashed red curve and the grey curve are the relative spectral power distributions of the first (R2) and second (N) illuminants.

such case, we use a rectangular metamer function from Logvinenko's original object color atlas in place of a wraparound Gaussian. Of the 1600 color signals, the KSM coordinates of only 39 of them had $K > 1$. For these 39 cases, rectangular metamer functions were used in place of wraparound Gaussian functions. Since the atlas is complete, we are guaranteed that there will always be a rectangular reflectance function that is metameric to any given color signal. As a result, all color signal predictions are guaranteed to be feasible in that they lie within the metamer mismatch volume of the given color signal.

In contrast, von Kries scaling can lead to predictions of color stimuli that fall outside the metamer mismatch volume. As an example of the type of large errors von Kries can lead to, consider the illuminant and reflectance spectra shown in Fig. 7.1. The illuminants are Logvinenko and Tokunaga's [9] red (R2) and neutral (N). Under the second illuminant (N) the true XYZ is (34.90, 22.24, 7.30), while von Kries predicts (58.52, 70.03, 10.13), Bradford predicts (71.94, 43.99, 49.62) and GM predicts (39.79, 30.09, 6.20), with corresponding CIEDE2000 errors of 56.51, 26.36, and 14.96 ΔE.

As another test of the proposed GM prediction method versus von Kries and Bradford, similar to Chapter 3, we used the 20 Munsell papers used in the asymmetric matching experiments of Logvinenko et al. [9] under their green and neutral ("white) illuminants. The Munsell designators of the 20 papers are: 5 R 4/14, 10 R 5/16, 5 YR 7/14, 10 YR 7/14, 5 Y 8/14, 10 Y 8.5/12, 5 GY 7/12, 10 GY 6/12, 5 G 5/10, 10 G 5/10, 5 BG 6/10, 10 BG 5/10, 5 B 5/10, 10 B 5/12, 5 PB 5/12, 10 PB 4/12, 5 P 4/12, 10 P 4/12, 5 RP 5/12, 10 RP 5/14.

As another test of GM method of predicting the color signal under a change of illuminant, we considered the problem of predicting what the image of the Fruit and Flowers scene (from [94]) under D65 (see Fig. 5.7.a) would be under illuminants A and F11. In other words, given the XYZ values for each pixel's reflectance under D65, predict what the corresponding XYZ values will be under A and F11. Once again we compare the GM prediction (only 1 pixel had $K > 1$) to that of von Kries and Bradford. Fig. 7.3 shows a pixel-by-pixel map indicating when one of the methods outperforms the other by more than 2 ΔE.

As a final test of GM prediction in comparison to von Kries and Bradford prediction, we used all 30 non-identical pairs of the 6 Logvinenko and Tokunaga's [9] illuminants shown in Fig. 3.2. Table 7.3 lists the mean, median and 95th percentile CIEDE2000 color differences. The Wilcoxon Sign Test [107] finds this performance difference to be significant at the 95% confidence level.

Munsell Paper	GM	Bradford	von Kries
5 R 4/14	9.92	13.52	13.77
10 R 5/16	6.67	18.03	18.62
5 YR 7/14	9.07	21.98	23.35
10 YR 7/14	8.31	14.08	15.16
5 Y 8/14	17.74	6.01	8.22
10 Y 8.5/12	16.39	2.46	7.38
5 GY 7/12	6.51	8.94	10.87
10 GY 6/12	2.65	11.58	13.73
5 G 5/10	1.89	8.64	9.47
10 G 5/10	2.38	9.24	9.63
5 BG 6/10	2.53	10.74	11.35
10 BG 5/10	2.89	7.72	7.86
5 B 5/10	3.08	6.59	7.02
10 B 5/12	2.45	5.74	7.11
5 PB 5/12	2.62	3.49	5.58
10 PB 4/12	3.36	2.97	5.05
5 P 4/12	1.61	4.39	5.65
10 P 4/12	2.42	6.01	6.75
5 RP 5/12	8.92	12.74	12.90
10 RP 5/14	12.23	16.52	16.76
Median	**2.98**	**8.18**	**8.84**
Mean	**5.63**	**8.71**	**9.84**

Table 7.2: Comparison of the color signal predictions made by the GM, Bradford and von Kries methods in terms of the CIEDE2000 error statistics for the 20 chromatic stimulus papers used in Logvinenko's color matching experiment [9] when the illuminant changes from G to N. Paper number corresponds to the order in the sequential list of Munsell designators given in the text.

Because of the potentially large extent of metamer mismatching [31], it is inevitable that GM predictions can be poor some of the time. The illuminant pair and reflectance shown in Fig. 7.4 provide one example. Under the second illuminant this reflectance has XYZ = (123, 53, 0.1), whereas wraparound Gaussian predicts (31, 14, 0.1). This corresponds to a color difference of 37 ΔE between the GM prediction and the true value; however, the von Kries and Bradford prediction differences are even worse at 59 and 55 ΔE, respectively.

7.5.2 Tests Including G^{2}M

We compare the prediction results using GM and G^{2}M to those of CIECAT02, which is a chromatic adaptation transform and the first step in the CIECAM02 color appearance

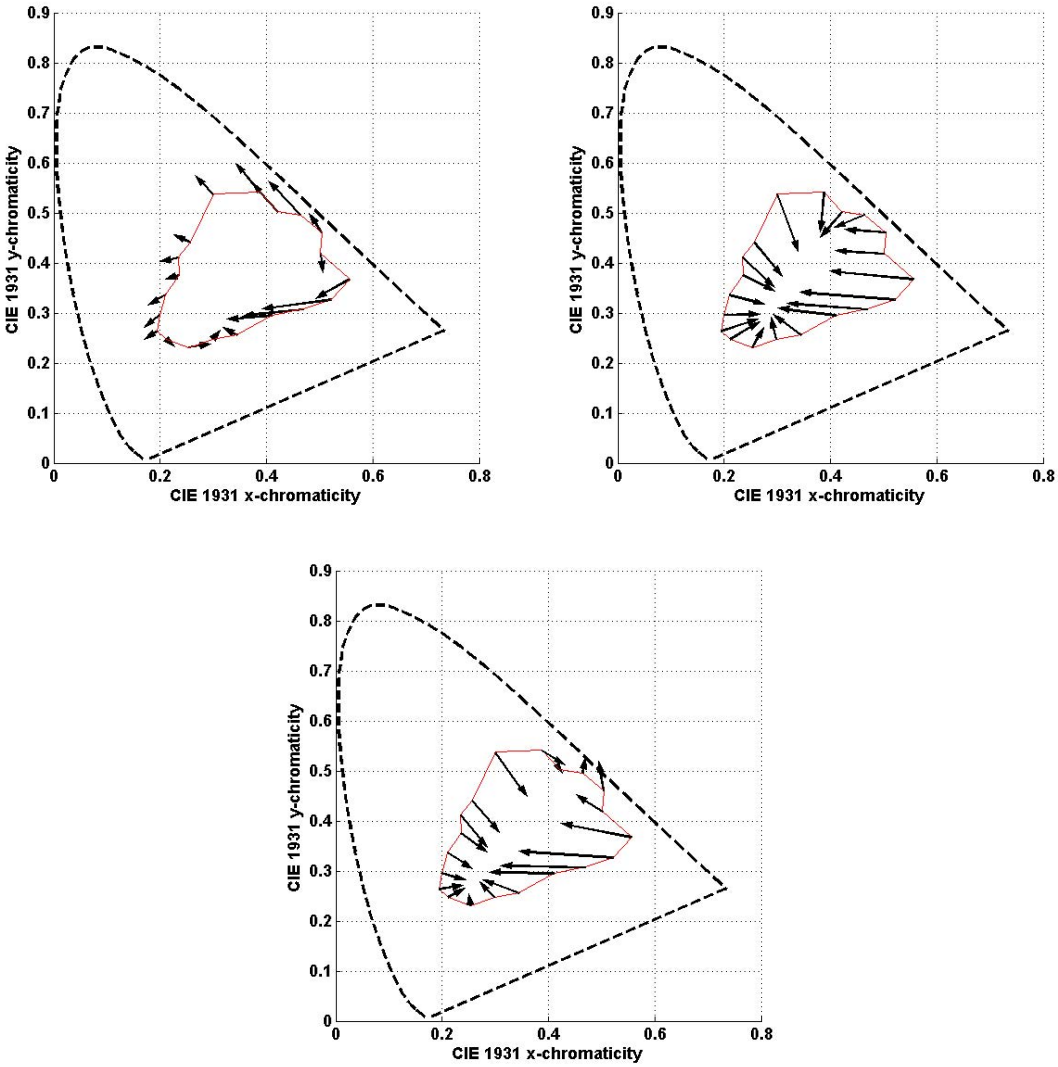

Figure 7.2: Color signal prediction for the 20 Munsell papers when the illuminant is changed from G (green) to N (neutral). Top left GM, top right von Kries, and bottom Bradford. Plot is of CIE xy-chromaticities. An arrow tail indicates the actual chromaticity of the paper under the neutral illuminant and the corresponding arrow head its predicted chromaticity. The red line curve simply links the arrow tails for clarity and is the same in all 3 panels.

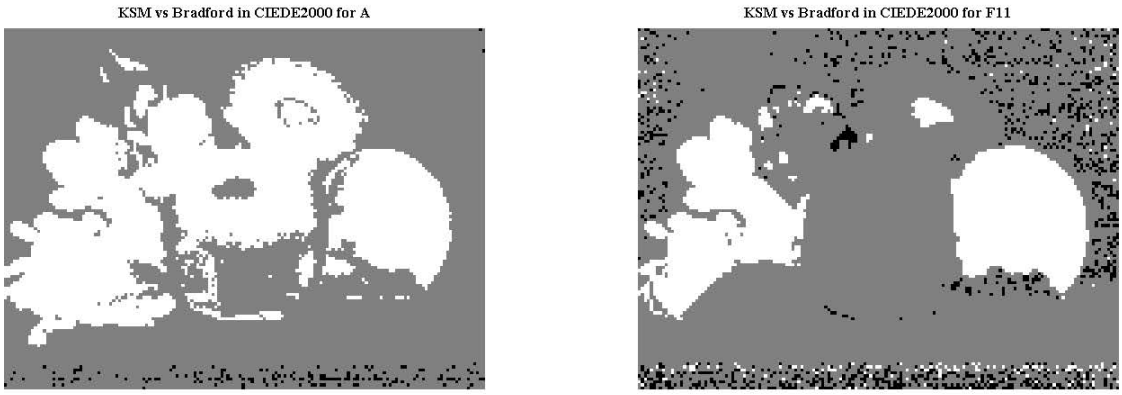

Figure 7.3: Maps of the difference in CIEDE2000 error of the color signals predicted by GM versus Bradford for an illuminant change from CIE D65 to CIE A (left) and to CIE F11 (right). White indicates that the GM error is at least 2 ΔE less than von Kries; grey indicates the absolute error difference between them is less than 2 ΔE; black indicates a von Kries error at least 2 ΔE less than that of GM. Results for von Kries are qualitatively similar to those of Bradford and are not shown here.

Median ΔE			Mean ΔE			95^{th} percentile ΔE		
GM	von Kries	Bradford	GM	von Kries	Bradford	GM	von Kries	Bradford
3.50	9.16	8.08	5.64	12.58	10.91	17.88	35.49	33.82

Table 7.3: CIEDE2000 color difference statistics taken over all Munsell reflectances and 30 illuminant pairs.

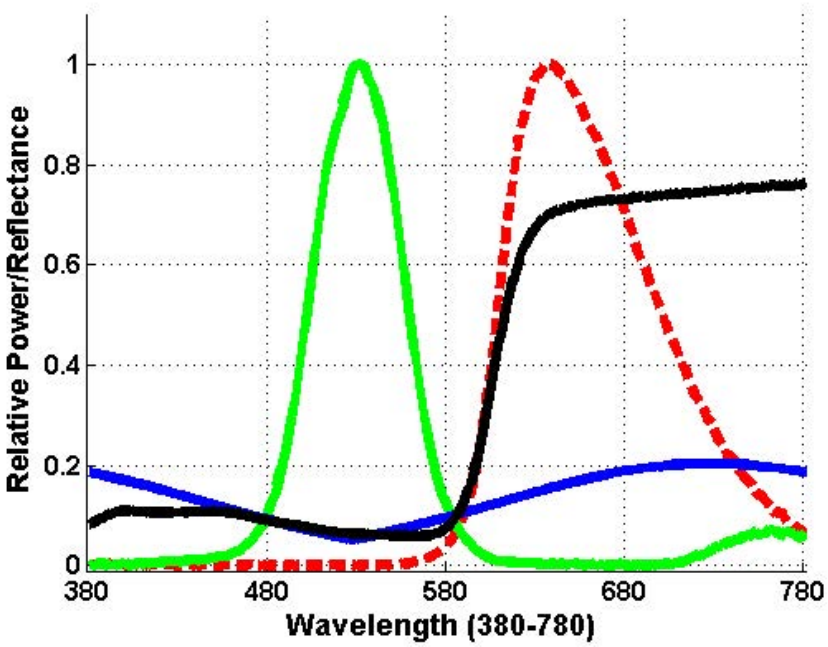

Figure 7.4: Reflectance and illuminant pair for which GM prediction yields a poor result. Black curve is the spectral reflectance of (Munsell 2.5 R 4/14). Green curve is the relative spectral power distribution of G, the first illuminant. Dashed red curve is the second illuminant, R2. Blue curve is the wraparound Gaussian metamer to the reflectance under G.

To	Method	Median	Mean	95th Percentile
A	GM	0.70	0.86	2.06
	G^2M	0.80	0.97	2.22
	CAT02	1.53	1.77	4.04
D65	GM	0.28	0.37	0.98
	G^2M	0.33	0.40	0.99
	CAT02	0.40	0.47	1.08

Table 7.4: CIEDE2000 prediction errors of CIECAT02, GM and G^2M for the case of the 1600 Munsell papers with the illuminant changing from CIE D50 to CIE A and to CIE D65.

model [59]. The three methods' predictions are compared to the computed ground-truth values under the second illuminant (i.e., XYZ of the actual reflectance spectra multiplied by the spectrum of the second illuminant).

7.5.2.1 Munsell Papers under CIE Illuminants

In the first test we consider the set of 1600 Munsell papers [94] under CIE D50 as the first illuminant and CIE A and CIE D65 as two different second illuminants. The accuracy of each color signal prediction is measured in terms of the CIEDE2000 color difference measure. Table 7.4 lists the results where it can be seen that the GM and G^2M predictions are better than those of CIECAT02 using complete adaptation. Although the performance of G^2M is, as expected, slightly worse than that of GM, the difference is surprisingly small given that in G^2M the spectra of both illuminants are replaced with wraparound Gaussians.

Although GM and G^2M make better predictions than CIECAT02, an additional advantage of these methods is that their predictions are guaranteed to be within the metamer set so long as the KSM coordinates have $k_m \leq 1$.Of the 1600 color signals of the Munsell papers under D50, GM found the KSM coordinates of only 44 of them had $k_m > 1$ and G^2M found only 43. For these few cases rectangular metamer functions were used in place of wraparound Gaussian functions.

7.5.2.2 Chromatic Illuminants and Varying Chroma/Value

As a further test of the proposed G^2M method of color signal prediction, we consider the set of illuminants Logvinenko and Tokunaga used in their asymmetric color matching experiment [9]. The spectra of these illuminants are shown in Fig. 3.2.

We considered 20 different hues from the Munsell Book of Color that sample the full hue circle. They are: 5 R, 10 R, 5 YR, 10 YR, 5 Y, 10 Y, 5 GY, 10 GY, 5 G, 10 G, 5 BG, 10 BG, 5 B, 10 B, 5 PB, 10 PB, 5 P, 10 P, 5 RP, and 10 RP. To evaluate the effect of Munsell chroma and value on the predictions, we test the three methods at these hues while varying the chroma over 2, 4, 6, and 8, and value over 5 and 7.

For a change of illuminant from G, B, Y, or R1 to N, Table 7.5 gives the median and average CIEDE2000 error in the predictions taken across the 20 Munsell hues at a given value and chroma. It can be seen that both GM and G^2M methods consistently outperform CIECAT02.

To assess the results visually, consider the example of G to N prediction. Fig. 7.5 plots the GM, G^2M, and CIECAT02 predictions in chromaticity space for the 20 hues at value 7, and chroma 8. The average error over the 20 papers in this case is 8.82 CIEDE2000 for GM, 9.72 for G^2M, and 15.54 for CIECAT02.

In terms of how the prediction error varies with chroma, Fig. 7.6 plots the median error for the same 20 hues at value 7, with the chroma varying over 2, 4, 6, and 8. The illuminant change is from G to N. The error tends to increase with increasing chroma for all three methods; however, the GM and G^2M errors are significantly less than those of CIECAT02 in all cases.

7.6 Discussion

A new method, called the Gaussian Metamer (GM) method, is proposed for predicting what a color signal (e.g., CIE XYZ, camera RGB, or cone LMS) observed from a surface under a first light will be when the same surface is lit instead by a second light. The GM method first determines a metameric wraparound Gaussian reflectance to the color signal under the first light. Second, it computes what the color signal of that metameric reflectance would be under the second light. The color signal determined for the second light is used as its prediction of what the color signal under the first light will be under the second light.

Tests show that the GM method outperforms other existing prediction methods such as von Kries scaling or the Bradford transformation. To be fair, those methods are used as the chromatic adaptation transform step in many color appearance models [82] and their goal is generally to predict the 'corresponding colors' subjects see, and these do not necessarily correspond to the actual color stimuli under the second illuminant that are the

First Illuminant	Munsell Attribute		Median CIEDE2000			Mean CIEDE2000		
	Value	Chroma	GM	G^2M	CAT02	GM	G^2M	CAT02
G	5	2	2.13	2.94	5.89	2.83	4.04	5.99
G	5	4	4.93	5.79	10.31	4.42	6.13	9.90
G	5	6	6.54	7.50	12.55	6.02	7.59	12.38
G	5	8	5.44	8.56	14.22	6.94	8.61	13.89
G	7	2	2.30	2.49	7.18	3.11	3.56	6.33
G	7	4	6.03	5.50	12.14	6.38	7.11	11.13
G	7	6	6.51	6.88	14.81	7.65	8.40	13.30
G	7	8	6.96	7.30	17.62	8.82	9.72	15.54
B	5	2	0.22	0.69	0.57	0.31	0.75	0.71
B	5	4	0.42	1.03	1.10	0.50	1.15	1.19
B	5	6	0.56	1.26	1.45	0.68	1.42	1.51
B	5	8	0.66	1.38	1.87	0.74	1.61	1.83
B	7	2	3.88	6.67	6.57	5.15	6.44	7.63
B	7	4	4.19	9.47	11.35	6.46	9.79	12.67
B	7	6	6.18	11.33	15.69	7.63	11.72	15.44
B	7	8	7.15	12.67	18.74	8.80	13.19	17.87
Y	5	2	2.13	2.94	5.89	2.83	4.04	5.99
Y	5	4	4.93	5.79	10.31	4.42	6.13	9.90
Y	5	6	6.54	7.50	12.55	6.02	7.59	12.38
Y	5	8	5.44	8.56	14.22	6.94	8.61	13.89
Y	7	2	2.30	2.49	7.18	3.11	3.56	6.33
Y	7	4	6.03	5.50	12.14	6.38	7.11	11.13
Y	7	6	6.51	6.88	14.81	7.65	8.40	13.30
Y	7	8	6.96	7.30	17.62	8.82	9.72	15.54
R1	5	2	0.22	0.69	0.57	0.31	0.75	0.71
R1	5	4	0.42	1.03	1.10	0.50	1.15	1.19
R1	5	6	0.56	1.26	1.45	0.68	1.42	1.51
R1	5	8	0.66	1.38	1.87	0.74	1.61	1.83
R1	7	2	3.88	6.67	6.57	5.15	6.44	7.63
R1	7	4	4.19	9.47	11.35	6.46	9.79	12.67
R1	7	6	6.18	11.33	15.69	7.63	11.72	15.44
R1	7	8	7.15	12.67	18.74	8.80	13.19	17.87
Mean	-	-	4.01	5.72	9.51	4.78	6.33	9.21

Table 7.5: The median and average prediction error in CIEDE2000 for the change from each of the 5 different chromatic illuminants to N ('white'). Each row is for papers of the 20 Munsell hues at the specified value and chroma. The last row reports the mean of the values in the corresponding column.

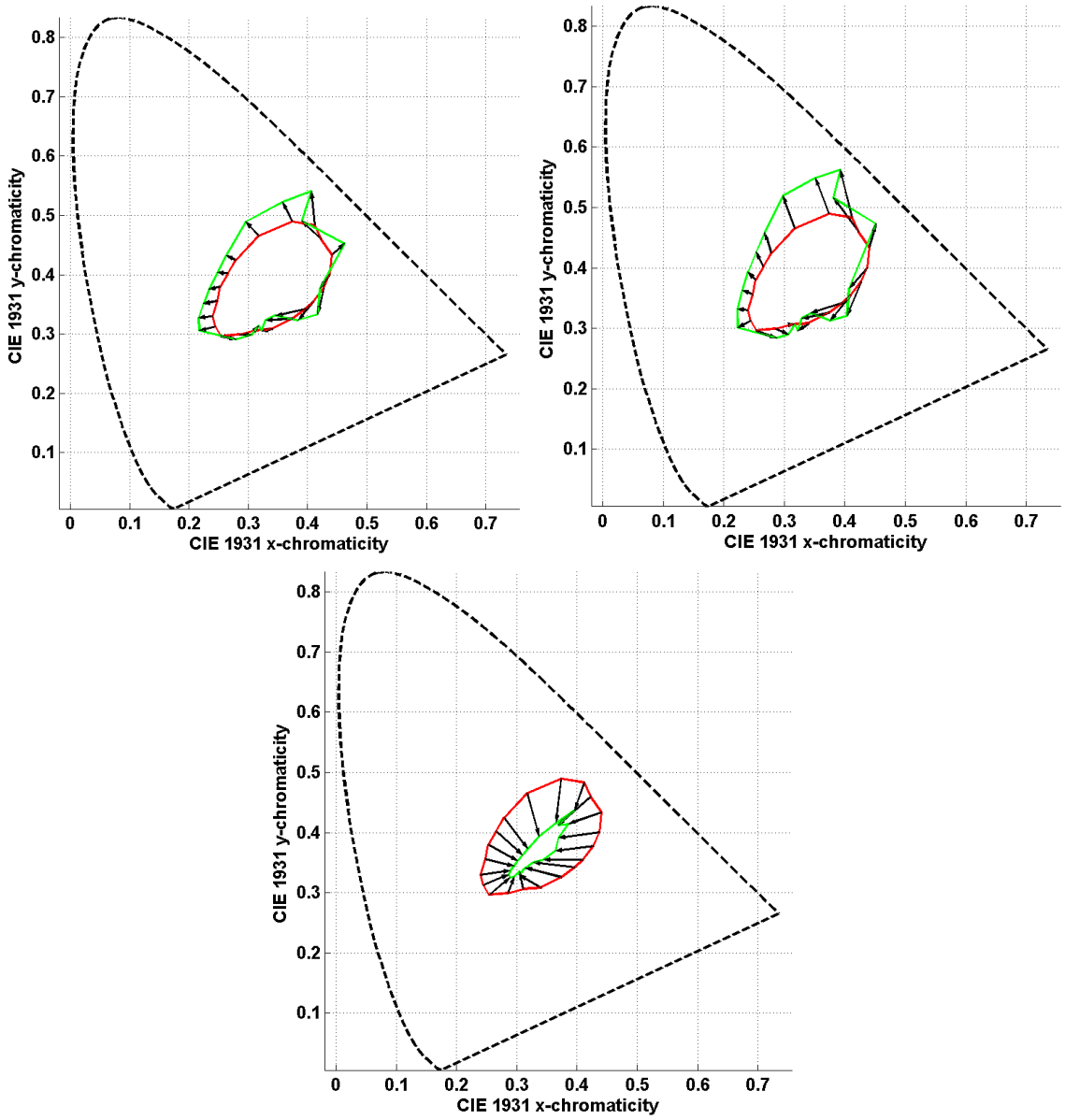

Figure 7.5: color signal prediction for the 20 Munsell papers (of chroma 8 and value 7) when the illuminant is changed from G (green) to N (neutral). Top left GM, right G^2M and bottom CIECAT02. Plot is in CIE xy-chromaticity space. An arrow tail indicates the actual chromaticity of the paper under the neutral illuminant with the corresponding arrow head its predicted chromaticity. The red and green curves simply connect all the arrow tails and arrow heads for clarity. The red curves are the same in all 3 panels.

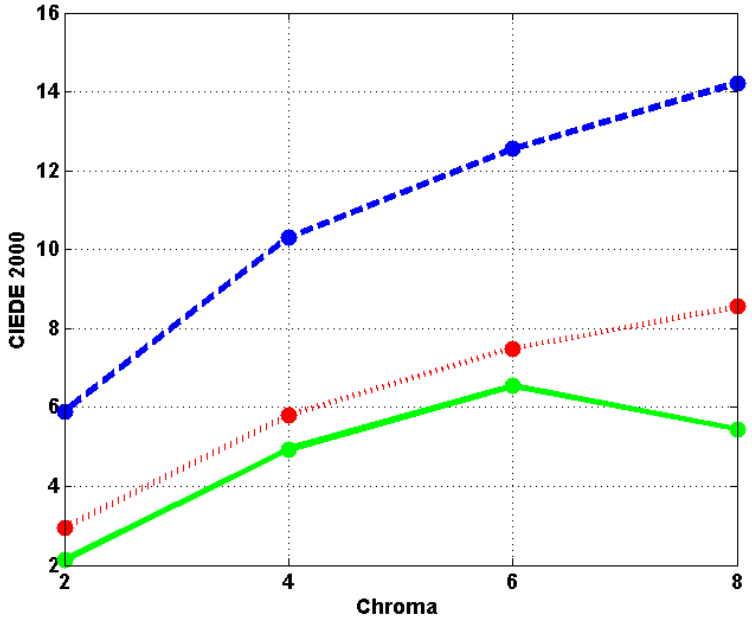

Figure 7.6: Different methods' median CIEDE2000 prediction error as a function of Munsell chroma (2, 4, 6, 8) at value 7 for a change of illuminant from G to N. The GM, G^2M, and CIECAT02 results are plotted in solid green, dotted red, and dashed blue, respectively.

prediction goal discussed here. Fairchild [82, 104] investigated spectral prediction as an alternative chromatic adaption transform with some positive tentative results. However, his method assumes complete knowledge of the reflectance spectrum and both illuminant spectra. A question for further study is to investigate what correlation, if any, there is between corresponding colors and the color stimulus predictions made by the proposed Gaussian metamer method. Unfortunately, this is not as simple a test as it sounds because the existing LUTCHI corresponding color data includes only the tristimulus values of the illuminants, not their complete spectral power distributions.

Underlying the GM method is Logvinenko's object color atlas. The KSM atlas coordinates specify a wraparound Gaussian. For a given surface, the atlas coordinates will be roughly the same under different illuminants. To the extent that they are not the same is due to the unavoidable, metamerism-induced phenomenon Logvinenko [49] terms the color stimulus shift. The proposed GM method relies on the assumption that the color stimulus shift (change in atlas coordinates) will generally be small, and therefore the color signal under the second illuminant can be predicted simply to be the color signal that keeps the KSM atlas coordinates under the second illuminant to be the same as under the first illuminant. The fact that our testing showed that the GM predictions are quite accurate is evidence that this assumption is justified.

Subsequently, the G^2M method was proposed that eliminates the requirement of the previous Gaussian Metamer (GM) method that full spectral power distributions of the two illuminants be known. Although the tests show that the accuracy of G^2M is somewhat less than that of GM, it is still significantly more accurate than CIECAT02 as measured in terms of CIEDE2000 color differences. G^2M shares with GM the fact that, unlike von Kries based prediction methods, all of its predictions are guaranteed to represent a physically realizable change in color signal.

Chapter 8

Conclusion and Future Directions

There are several important areas where this study makes original contributions. In light of metamer mismatching, I carried out a set of experiments, providing the foundation for a larger project titled "Rethinking Colour Constancy" [1] where the impact of metamer mismatching on color constancy is explored. This project proved that metamer mismatching is so huge that undermines the idea of color constancy in its conventional terms. In particular, based on Logvinenko's idea, in some illumination conditions, we found 20 Munsell papers that, under the first illumination, all arise the same color as flat grey, but, under the second illumination, disperse into a wide range of saturated colors *making a full hue circle*.

Later, metamer mismatch volume was proposed to be employed as a measure of color rendering ability of illuminants. With the new definition, illuminants that result in a smaller mismatch volume, when a change is occurred from the given illuminant to the ideal light, will have a better index. The idea behind this new measure is that a good illuminant spectrum must be able to render different reflectance samples faithfully compared to the ideal smooth spectra. With classical color rendering indices that are based on the rendering accuracy of a limited number of reflectance samples, due to metamer mismatching, the light spectrum could be optimized only for those samples to get a better index. However, with the new method, the rendering index is not based on a limited set and cannot be tuned for only those samples. The preliminary results substantiate the effectiveness of the new measure, compared to various measures presented in the literature. However, it is a topic of future research and further experiments.

Returning to the subject of object colors, where the main issue with color description is the illumination variation, we demonstrated that although the common color spaces such as

CIELAB and related spaces in the literature may work well for a fixed illuminant, they can lead to unstable results when the illuminant is changed. To be able to describe the object-colors robustly, we proposed novel hue, chroma, and lightness descriptors that are robust to illumination changes. We defined the new descriptors based on the wraparound Gaussians that Logvinenko suggests and investigated them in three aspects: the gamut of colors these Gaussians can represent, how well these new descriptors correlate with the appearance attributes in different datasets, and how stable the new correlates across different illuminants are. Experiments proved that the new Gaussian based appearance descriptors correlate with the hue descriptors in different datasets as well as or better than CIECAM02 appearance model. In terms of stability under different illuminants, the Gaussian-based descriptors are remarkably more stable than the descriptors defined in CIECAM02 appearance model. These new descriptors provide a foundation for the specification of the hue, lightness and chroma dimensions of object colors under average viewing surround conditions. As a new research direction, a new color difference metric in this three-dimensional color space can be developed.

After developing a robust hue-chroma-value description of colors, in the next step, the problem of predicting how the object-color signal changes when the lighting alters was investigated. A new method, called the Gaussian Metamer (GM) method, was proposed for predicting what a color signal observed from a surface under a first light will be when the same surface is lit instead by a second light. This method is then improved for a more limited case when we only know the color of the illuminants and not their spectral power distribution (G^2M). Although the tests show that the accuracy of G^2M is somewhat less than that of GM, it is still significantly more accurate than CIECAT02 as measured in terms of CIEDE2000 color differences. Perhaps more importantly, for both G^2M and GM, unlike von Kries based prediction methods, predictions are guaranteed to represent a physically realizable change in object-color signal.

In summary, this thesis aimed at first criticizing the conventional approaches of color description, and then laying the foundation to robustly describe the object colors under varying illumination conditions. A robust hue-chroma-value description of object colors was built up, and novel methods to perform the prediction of the colors when lighting alters were developed.

Bibliography

[1] F. Yasuma, T. Mitsunaga, D. Iso, and S.K. Nayar. Generalized Assorted Pixel Camera: Post-Capture Control of Resolution, Dynamic Range and Spectrum. Technical report, Nov 2008. vii, xiv, 6, 91, 92, 93

[2] CIE Colorimetry. Publication no. 15.2. *Bureau Central De la CIE, Vienna*, 1986. vii, 7, 10

[3] Gunter Wyszecki and Walter Stanley Stiles. *Color science*, volume 8. Wiley New York, 1982. vii, 7, 8, 10, 17, 73, 99

[4] Alexander D Logvinenko, Brian Funt, and Christoph Godau. Metamer mismatching. *Image Processing, IEEE Transactions on*, 23(1):34–43, 2014. vii, 1, 13, 14, 15, 16, 29, 39, 63, 65, 110

[5] Hamidreza Mirzaei and Brian Funt. Robust chroma and lightness descriptors. In *Color and Imaging Conference*, volume in press. Society for Imaging Science and Technology, 2015. viii, 4, 21, 99

[6] Alexander D Logvinenko and Rumi Tokunaga. Colour constancy as measured by least dissimilar matching. *Seeing and perceiving*, 24(5):407–452, 2011. viii, 23, 25

[7] Hamidreza Mirzaei and Brian Funt. Object-color-signal prediction using wraparound gaussian metamers. *JOSA A*, 31(7):1680–1687, 2014. xii, 4, 21, 75, 110

[8] A. D. Logvinenko and Rumi Tokunaga. Colour constancy as measured by least dissimilar matching. *Seeing and Perceiving*, 24:407–452, 2011. xviii, xix, 30, 42, 44, 90, 116, 117, 121

[9] Kevin AG Smet, Wouter R Ryckaert, Michael R Pointer, Geert Deconinck, and Peter Hanselaer. Memory colours and colour quality evaluation of conventional and solid-state lamps. *Optics Express*, 18(25):26229–26244, 2010. xviii, 64, 67, 70

[10] Wendy Davis and Yoshi Ohno. Color quality scale. *Optical Engineering*, 49(3):033602–033602, 2010. xviii, 70

[11] Jie Yang, Rainer Stiefelhagen, Uwe Meier, and Alex Waibel. Visual tracking for multimodal human computer interaction. In *Proceedings of the SIGCHI conference on Human factors in computing systems*, pages 140–147. ACM Press/Addison-Wesley Publishing Co., 1998. 1

[12] Theo Gevers and Arnold WM Smeulders. Pictoseek: Combining color and shape invariant features for image retrieval. *Image Processing, IEEE Transactions on*, 9(1):102–119, 2000.

[13] Mark D Fairchild. *Color appearance models*. John Wiley & Sons, 2013. 1, 2

[14] Kobus Barnard. *Practical colour constancy*. PhD thesis, Simon Fraser University, 1999. 2

[15] Lawrence E Arend Jr, Adam Reeves, James Schirillo, Robert Goldstein, et al. Simultaneous color constancy: papers with diverse munsell values. *JOSA A*, 8(4):661–672, 1991. 2

[16] P. B. Delahunt and D.H. Brainard. Does human color constancy incorporate the statistical regularity of natural daylight? *Journal of Vision*, 4:57–81, 2004.

[17] David H Foster. Color constancy. *Vision research*, 51(7):674–700, 2011.

[18] David H Brainard, James M Kraft, and Philippe Longere. Color constancy: Developing empirical tests of computational models. *Colour perception: From light to object*, pages 307–334, 2003. 2

[19] D. H. Foster. Does colour constancy exist? *Trends in Cognitive Science*, 7:439–443, 2003. 2, 11

[20] David H. Foster. Color constancy. *Vision Research*, 51:674–700, 2011. 2

[21] Alexander Logvinenko, Brian Funt, Hamidreza Mirzaei, and Rumi Tokunaga. Rethinking colour constancy. *PLOS ONE*, In Press, 2015. 2, 4, 29, 30, 62, 73, 127

[22] Lorne A Whitehead and Michele A Mossman. A monte carlo method for assessing color rendering quality with possible application to color rendering standards. *Color Research & Application*, 37(1):13–22, 2012. 3, 64

[23] Xiandou Zhang, Brian Funt, and Hamidreza Mirzaei. Metamer mismatching in practice versus theory. *JOSA A*, 33(3):A238–A247, 2016. 4, 30

[24] Hamidreza Mirzaei and Brian Funt. Gaussian-based hue descriptors. *IEEE Transactions on Pattern Analysis & Machine Intelligence*, (1):1–1. 72, 73, 99, 105, 108

[25] Hamidreza Mirzaei and Brian Funt. Metamer mismatching as a measure of the color rendering of lights. 2015. 63

[26] Xiandou Zhang, Brian Funt, and Hamidreza Mirzaei. Metamer mismatching and its consequences for predicting how colours are affected by the illuminant. In *Proceedings of the IEEE International Conference on Computer Vision Workshops*, pages 1–7, 2015. 30

[27] Hamidreza Mirzaei and Brian Funt. Gaussian illuminants and reflectances for colour signal prediction. In *Color and Imaging Conference*, volume 2014, pages 212–216. Society for Imaging Science and Technology, 2014. 21, 90, 110

[28] Brian Funt, Hamidreza Mirzaei, and Alexander D Logvinenko. Metamer mismatch volumes of flat grey. In *Color and Imaging Conference*, volume 2014, pages 240–241. Society for Imaging Science and Technology, 2014. 30

[29] Hamidreza Mirzaei and Brian Funt. Hue correlate stability using a gaussian versus rectangular object colour atlas. In *AIC 2013, 12th International Colour Congress, International Colour Association*, pages 1133–1136, 2013. 72, 73

[30] Hamidreza Mirzaei and Brian Funt. A robust hue descriptor. In *Color and Imaging Conference*, volume 2013, pages 75–78. Society for Imaging Science and Technology, 2013. 72, 73, 99, 105

[31] AD Logvinenko, BV Funt, and H Mirzaei. The extent of metamer mismatching. *Proc. 12th Congr. AIC*, pages 507–510, 2013. 30, 117

[32] Hamidreza Mirzaei and Brian Funt. Gaussian-metamer-based prediction of colour signal change under illuminant change. *AIC*, 2011.

[33] Brian Funt and Hamidreza Mirzaei. Intersecting color manifolds. In *Color and Imaging Conference*, volume 2011, pages 166–170. Society for Imaging Science and Technology, 2011. 4, 87

[34] Sabine Süsstrunk. Computing chromatic adaptation. Technical report, University of East Anglia, 2005. 9

[35] Steven A Shafer. Using color to separate reflection components. *Color Research & Application*, 10(4):210–218, 1985. 9, 11

[36] Edwin H Land et al. *The retinex theory of color vision*. Scientific America., 1977. 11

[37] Ron Gershon, Allan D Jepson, and John K Tsotsos. From [r, g, b] to surface reflectance: Computing color constant descriptors in images. In *IJCAI*, pages 755–758, 1987. 11

[38] G. Wyszecki and W. S. Stiles. *Color Science: Concepts and Methods, Quantitative Data and Formulae*. John Wiley and Sons, New York, 2nd edition, 1982. 11, 12, 14, 33, 39, 114

[39] A. D. Logvinenko and V. L. Levin. Foundations of colour science. 2015. 12, 14

[40] Graham D Finlayson and Peter Morovic. Metamer sets. *JOSA A*, 22(5):810–819, 2005. 12, 13

[41] F. J. M. Schmitt. A method for the treatment of metamerism in colorimetry. *Journal of the Optical Society of America*, 66:601–608, 1976. 12

[42] GÜNTER WYSZECKI. Evaluation of metameric colors. *JOSA*, 48(7):451–452, 1958. 12

[43] Jozef B Cohen and William E Kappauf. Metameric color stimuli, fundamental metamers, and wyszecki's metameric blacks. *The American journal of psychology*, pages 537–564, 1982. 12

[44] Jozef B Cohen and William E Kappauf. Color mixture and fundamental metamers: Theory, algebra, geometry, application. *The American journal of psychology*, pages 171–259, 1985. 12

[45] Scott A Burns, Jozef B Cohen, and Edward N Kuznetsov. Multiple metamers: preserving color matches under diverse illuminants. *Color Research & Application*, 14(1):16–22, 1989. 12

[46] K. Takahama and Y. Nayatani. New method for generating metameric stimuli of object colors. *Journal of the Optical Society of America*, 62:1516–1520, 1972. 13

[47] N. Ohta. Generating metameric object colors. *Journal of the Optical Society of America*, 65:1081–1082, 1975. 13

[48] Philipp Urban and Rolf-Rainer Grigat. Metamer density estimated color correction. *Signal, image and video processing*, 3(2):171–182, 2009. 13

[49] Alexander D Logvinenko. An object-color space. *Journal of Vision*, 9(11):5, 2009. 14, 17, 18, 21, 73, 82, 95, 110, 111, 126

[50] Erwin Schrödinger. Theorie der pigmente von grösster leuchtkraft. *Annalen der Physik*, 367(15):603–622, 1920. 14

[51] V. V. Maximov. *Transformatsii tsveta pri izmenenii osvescheniya*. Nauka, Moscow, 1984. 14

[52] A. D. Logvinenko. Object-colour manifold. *International Journal of Computer Vision*, 101(1):143–160, 2013. 17, 19, 20, 30, 73, 94

[53] Michael H Brill and Graham Finlayson. Illuminant invariance from a single reflected light. *Color Research & Application*, 27(1):45–48, 2002. 20, 73, 74, 111

[54] Yoko Mizokami and Michael Webster. Are gaussian spectra a viable perceptual assumption in color appearance? *Journal of Vision*, 10(7):399–399, 2010. 73, 74, 78, 94, 98, 111

[55] Donald IA MacLeod and Jürgen Golz. A computational analysis of colour constancy. *Colour perception: Mind and the physical world*, pages 205–242, 2003. 20, 73, 74, 111

[56] Ming Ronnier Luo and Changjun Li. Ciecam02 and its recent developments. In *Advanced Color Image Processing and Analysis*, pages 19–58. Springer, 2013. 21, 100, 101

[57] M Ronnier Luo, Guihua Cui, and B Rigg. The development of the cie 2000 colour-difference formula: Ciede2000. *Color Research & Application*, 26(5):340–350, 2001. 22

[58] MR Luo and RWG Hunt. The structure of the cie 1997 colour appearance model (ciecam97s). *Color Research & Application*, 23(3):138–146, 1998. 22

[59] Nathan Moroney, Mark D Fairchild, Robert WG Hunt, Changjun Li, M Ronnier Luo, and Todd Newman. The ciecam02 color appearance model. In *Color and Imaging Conference*, volume 2002, pages 23–27. Society for Imaging Science and Technology, 2002. 22, 73, 121

[60] Johannes von Kries. Chromatic adaptation. *Festschrift der Albrecht-Ludwigs-Universität*, pages 145–158, 1902. 24, 111

[61] David H Brainard and Brian A Wandell. Asymmetric color matching: how color appearance depends on the illuminant. *JOSA A*, 9(9):1433–1448, 1992. 24

[62] Gerhard West and Michael H. Brill. Necessary and sufficient conditions for von kries chromatic adaptation to give color constancy. *Journal of Mathematical Biology*, 15:249–258, 1982.

[63] Graham Finlayson, Mark Drew, and Brian Funt. Color constancy: Generalized diagonal transforms suffice. *Journal of the Optical Society of America A,*, 11(11):3011–3020, 1994. 26

[64] James A Worthey and Michael H Brill. Heuristic analysis of von kries color constancy. *JOSA A*, 3(10):1708–1712, 1986. 24, 26

[65] Gerhard West and Michael H Brill. Necessary and sufficient conditions for von kries chromatic adaptation to give color constancy. *Journal of Mathematical Biology*, 15(2):249–258, 1982.

[66] Michael H Brill. Minimal von kries illuminant invariance. *Color Research & Application*, 33(4):320–323, 2008. 26

[67] Graham Finlayson, Mark Drew, and Brian Funt. Spectral sharpening: Sensor transformations for improved color constancy,. *Journal of Optical Society of America A*, 11(5):1553–1563, May 1994. 26, 73

[68] Graham D Finlayson and Brian V Funt. Coefficient channels: Derivation and relationship to other theoretical studies. *Color Research & Application*, 21(2):87–96, 1996.

[69] Kobus Barnard, Florian Ciurea, and Brian Funt. Sensor sharpening for computational color constancy. *JOSA A*, 18(11):2728–2743, 2001. 26

[70] Graham D Finlayson, Mark S Drew, and Brian V Funt. Color constancy: Enhancing von kries adaptation via sensor transformation, spie. 1993. 26

[71] Mark D Fairchild. A revision of ciecam97s for practical applications. *Color Research & Application*, 26(6):418–427, 2001. 26

[72] KM Lam. *Metamerism and colour constancy.* PhD thesis, University of Bradford, 1985. 114

[73] Changjun Li, M Ronnier Luo, Bryan Rigg, and Robert WG Hunt. Cmc 2000 chromatic adaptation transform: Cmccat2000. *Color Research & Application*, 27(1):49–58, 2002. 26

[74] Graham D Finlayson, Steven D Hordley, Cheng Lu, and Mark S Drew. On the removal of shadows from images. *Pattern Analysis and Machine Intelligence, IEEE Transactions on*, 28(1):59–68, 2006. 27

[75] Mark S Drew, Graham D Finlayson, and Steven D Hordley. Recovery of chromaticity image free from shadows via illumination invariance. In *IEEE Workshop on Color and Photometric Methods in Computer Vision, ICCV03*, pages 32–39, 2003.

[76] Graham D Finlayson, Mark S Drew, and Cheng Lu. Intrinsic images by entropy minimization. In *Computer Vision-ECCV 2004*, pages 582–595. Springer, 2004. 27

[77] Graham D Finlayson, Steven D Hordley, and Mark S Drew. Removing shadows from images. In *Computer VisionECCV 2002*, pages 823–836. Springer, 2002. 27

[78] A. D. Logvinenko, B. Funt, and C. Godau. Metamer mismatching. *IEEE Trans. on Image Processing*, 23(1):34 – 43, 2014. 30, 39

[79] Johannes Von Kries. Influence of adaptation on the effects produced by luminous stimuli. In David L. MacAdam, editor, *Sources of color science*, pages 120–126. MIT Press, Cambridge, MA, 1970. 43

[80] R. W. G. Hunt and M. R. Pointer. A colour-appearance transform for the 1931 standard colorimetric observer. *Color Research and Application*, 10:165–179, 1985. 43

[81] R. W. G. Hunt. *The reproduction of colour*. John Wiley and Sons, Ltd, Chichester, England, sixth edition edition, 2004. 43

[82] Mark D. Fairchild. *Color Appearance Models*. Wiley publication in Imaging Science and Technology. Wiley, Chichester, UK, 2 edition, 2005. 43, 110, 111, 114, 122, 126

[83] Albert Henry Munsell. *The Munsell book of color glossy edition*. X-rite Inc., Grand Rapids, MI. 54

[84] CIE. Method of measuring and specifying colour rendering properties of light sources. *CIE Publication*, 3(13), 2011. 63

[85] Deane B Judd. A flattery index for artificial llluminants. 1967. 64

[86] WA Thornton. A validation of the color-preference index. *Journal of the Illuminating Engineering Society*, 4(1):48–52, 1974. 64

[87] K. Smet and P. Hanselaer. Memory and preferred colours and the colour rendition evaluation of white light sources. *Lighting Research and Technology.*, 2015. 64

[88] KAG Smet, WR Ryckaert, Michael R Pointer, Geert Deconinck, and Peter Hanselaer. A memory colour quality metric for white light sources. *Energy and Buildings*, 49:216–225, 2012. 70

[89] Kevin AG Smet, Janos Schanda, Lorne Whitehead, and Ronnier M Luo. Cri2012: A proposal for updating the cie colour rendering index. *Lighting Research and Technology*, page 1477153513481375, 2013. 71

[90] Y. Mizokami, J. S. Werner, M. A. Crognale, and M. A. Webster. Nonlinearities in color coding: Compensating color appearance for the eye's spectral sensitivity. *Journal of Vision*, 6:996–1007, 2006. 73, 78, 94

[91] Sean F ONeil, Kyle C McDermott, Yoko Mizokami, John S Werner, Michael A Crognale, and Michael A Webster. Tests of a functional account of the abney effect. *JOSA A*, 29(2):A165–A173, 2012. 73, 78

[92] Christoph Godau and Brian Funt. Xyz to adl: calculating logvinenko's object color coordinates. In *Color and Imaging Conference*, volume 2010, pages 334–339. Society for Imaging Science and Technology, 2010. 80

[93] Graham D Finlayson, Michal Mackiewicz, and Anya Hurlbert. Making the calculation of logvinenko's coordinates easy. In *Color and Imaging Conference*, volume 2012, pages 264–269. Society for Imaging Science and Technology, 2012. 80, 98

[94] U. of Joensuu Color Group. Joensuu color group spectral database. http://spectral.joensuu.fi/. Accessed 2010. 80, 82, 99, 100, 102, 114, 116, 121

[95] N Moroney. The color thesaurus. *magcloud. com, June*, 2008. 82, 87, 95, 99

[96] N Moroney. http://www.hpl.hp.com/personal/nathan-moroney/. Accessed March. 2013. 82

[97] Nathan Moroney. Unconstrained web-based color naming experiment. In *Electronic Imaging 2003*, pages 36–46. International Society for Optics and Photonics, 2003. 82, 87, 99

[98] Andrew R Conn, Nicholas IM Gould, and Philippe Toint. A globally convergent augmented lagrangian algorithm for optimization with general constraints and simple bounds. *SIAM Journal on Numerical Analysis*, 28(2):545–572, 1991. 84

[99] Anders Hård and Lars Sivik. Ncsnatural color system: a swedish standard for coloer notation. *Color Research & Application*, 6(3):129–138, 1981. 85, 99

[100] Brent Berlin and Paul Kay. *Basic color terms: Their universality and evolution*. Univ of California Press, 1991. 87

[101] Christoph Godau and Brian Funt. The logvinenko object color atlas in practice. *Color Research & Application*, 37(2):117–125, 2012. 87

[102] Rob J Hyndman and Anne B Koehler. Another look at measures of forecast accuracy. *International journal of forecasting*, 22(4):679–688, 2006. 105

[103] M Ronnier Luo, Anthony A Clarke, Peter A Rhodes, André Schappo, Stephen AR Scrivener, and Chris J Tait. Quantifying colour appearance. part i. lutchi colour appearance data. *Color Research & Application*, 16(3):166–180, 1991. 110

[104] Mark D Fairchild. Spectral adaptation: A reason to use the wavenumber scale. In *Color and Imaging Conference*, volume 2006, pages 314–319. Society for Imaging Science and Technology, 2006. 110, 126

[105] Graham D Finlayson, Mark S Drew, and Brian V Funt. Spectral sharpening: sensor transformations for improved color constancy. *JOSA A*, 11(5):1553–1563, 1994. 111

[106] Robert William Gainer Hunt. *The reproduction of colour*. John Wiley & Sons, 2005. 114

[107] Robert V Hogg and Elliot A Tanis. *Probability and statistical inference*, volume 993. Macmillan New York, 1977. 116